Master's Theses   Master's Theses and Graduate Research

2000

Wirebond integrity for ultra fine pitch devices

Jae-Eun Song
San Jose State University

INFORMATION TO USERS

This manuscript has been reproduced from the microfilm master. UMI films the text directly from the original or copy submitted. Thus, some thesis and dissertation copies are in typewriter face, while others may be from any type of computer printer.

The quality of this reproduction is dependent upon the quality of the copy submitted. Broken or indistinct print, colored or poor quality illustrations and photographs, print bleedthrough, substandard margins, and improper alignment can adversely affect reproduction.

In the unlikely event that the author did not send UMI a complete manuscript and there are missing pages, these will be noted. Also, if unauthorized copyright material had to be removed, a note will indicate the deletion.

Oversize materials (e.g., maps, drawings, charts) are reproduced by sectioning the original, beginning at the upper left-hand corner and continuing from left to right in equal sections with small overlaps.

Photographs included in the original manuscript have been reproduced xerographically in this copy. Higher quality 6" x 9" black and white photographic prints are available for any photographs or illustrations appearing in this copy for an additional charge. Contact UMI directly to order.

UMI®

WIREBOND INTEGRITY FOR ULTRA FINE PITCH DEVICES

A Thesis

Presented to

The Faculty of the Department of Chemical and Materials Engineering

San Jose State University

In Partial Fulfillment

of the Requirements for the Degree

Master of Science

By

Jae-Eun Song

August 2000

UMI®
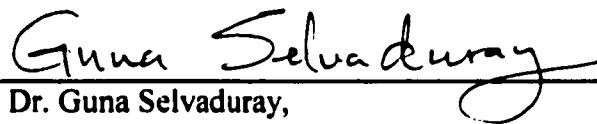
APPROVED FOR
THE DEPARTMENT OF CHEMICAL AND MATERIALS ENGINEERING

Dr. Guna Selvaduray,
Department of Chemical and Materials Engineering

Dr. Manfred Cantow,
Department of Chemical and Materials Engineering

Dr. Luu Nguyen, National Semiconductor Corporation

APPROVED FOR THE UNIVERSITY

ABSTRACT

Wirebond Integrity for Ultra Fine Pitch Devices

By Jae-Eun Song

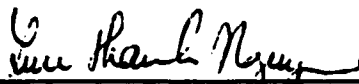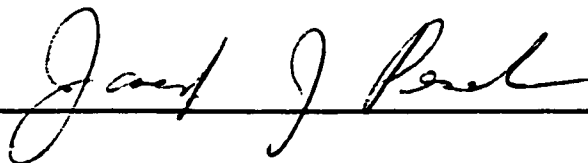The reliability merits measured in ultra fine pitch wirebonding with two different processes, namely, standard wirebonding vs. "encapsulated wirebonding", were compared. The latter, developed internally at National Semiconductor, involved the use of specially tailored capillaries that allowed ultra fine pitch bonding on conventional wirebonder platforms. The effects of varying wirebonding process parameters on the bond integrity for aluminum metal-based devices were investigated. For reliability evaluation, the bond pull and ball shear strengths were measured and metallographic examinations were performed. The formation of gold-aluminum intermetallic compounds during ball bonding and the growth of the intermetallic layer with high temperature aging were examined and correlated with bond integrity. The results showed that the reliability of "encapsulated wirebonding" was comparable to standard wirebonding, for devices with Al metallurgy.

ACKNOWLEDGMENTS

TABLE OF CONTENTS

LIST OF FIGURES

LIST OF TABLES

CHAPTER 1

Introduction

As electronics products become smaller, more portable, cheaper, and higher in performance, efforts have been made to reduce the die size. To achieve this reduction, microelectronic packages have been developed reducing package size, increasing interconnect density and speed for high power. These trends are shown in Table 1.[1] For example, in 1998, the feature size was 0.25 μm and the number of I/O terminals was limited to 1,500. However, a reduction in the feature size of 28% and an increase of approximately 33% in the number of I/O terminals are expected by 2001. Increases in the chip size of logic/unprocessor and DRAM are also expected with a slight decrease in the wafer processing cost compared to those for 1998.

Table 1. Semiconductor Evolution.[1]

	1992	1995	1998	2001	2004	2007
Feature size (μm)	0.5	0.35	0.25	0.18	0.12	0.10
Chip size (mm^2)						
Logic/unprocessor	250	400	600	800	1000	1250
DRAM	132	200	320	500	700	1000
Wafer processing cost ($/cm^2)	4.00	3.90	3.80	3.70	3.60	3.50
Wafer diameter (mm)	200	200	200-400	200-400	200-400	200-400
No. I/Os	500	750	1500	2000	3500	5000
Maximum power (w/ die)						
High performance	10	15	30	40	40-120	40-200
Performance (MHz)						
On chip	120	200	350	500	700	1000
Off chip	60	100	175	250	350	500

One area of the research that has been vigorously investigated to meet these packaging requirements is interconnect technology. An "interconnect" is defined as the

means by which the chip is connected to the package to provide the electrical path for power and signal distribution.[2] The interconnection between the chip and the package is generally provided by one of three technologies: wirebonding, flip chip, or tape automated bonding (TAB).

The wirebonding technique employs a fine diameter wire which is attached between the input/output (I/O) terminals and their corresponding package pins to create an electrical path. There are three different types of wirebonding methods: thermocompression bonding, ultrasonic wedge bonding, and thermosonic ball and wedge bonding.[1,2,3]

The history and the description of the three different types of wirebonding methods are as follows. Thermocompression wedge and ball bonding was introduced in 1957 and used until ultrasonic wedge bonding replaced it as the primary bonding method in the mid 1960s. This technique requires a high force and a high interface temperature to plastically deform the welding elements so that intimate contact can be made between cleansed surfaces. The major process variables involved in this technique are time, temperature, and deformation. The average temperature used for the bonding is approximately 300°C. Thermocompression bonding is seldom used today because of its sensitivity to surface contaminants and its need for high interface temperatures.

Ultrasonic wedge bonding was developed in 1960 and widely used in the microelectronics industry eventually replacing thermocompression bonding. The chief advantage of this method was that bonding is performed at room temperature. Application of ultrasonic energy with a resonating transducer tool and a clamping force

2

eliminates the need for the higher temperatures used in thermocompression bonding. The primary use of ultrasonic bonding is to bond large-diameter (0.5 ~ 0.75 mm) Al wire to either Au or Al bond pads. The ultrasonic energy required for the process is relatively high, ranging up to approximately 25 watts. In addition, the package or transducer needs to be mechanically aligned for each wire. This slows down the process and reduces its yield.

Thermosonic bonding combines ultrasonic and thermocompression bondings. It was developed in 1970 by combining ultrasonic energy with heat, to enhance the bonding process. This bonding method became dominant in device production, replacing ultrasonic wedge bonding. Thermosonic bonding is most often used with gold or copper wire for interconnections to integrated circuits. The bonding is affected by the amount of energy applied through heat, ultrasonic energy, and time. Thus, the bond strength is affected by the combined ultrasonic and heat energies which are applied for a given time.[3] Typical bonding temperatures range from 125°C to 220°C with bonding times from 5 ms to 20 ms. This bonding method helps minimize various types of damage, such as cratering, that occur on the semiconductor chip.

The general procedures for thermosonic gold ball bonding are illustrated in Figure 1.[3] Wirebonding is performed following attachment of the chip to the package. For ball bonding, the bonding wire is threaded through a capillary tool and an electronic discharge or electronic flame off (EFO) spark melts the wire tip and forms a ball at the bottom of the tool. The bond is made by pressing the ball against the heated bond pad on the die, as shown in Item 3 in Figure 1. When the bonding process is complete, the capillary is

raised and repositioned over the bond finger or bond pad of the package substrate. The second bond is made when the wire is deformed against the bond pad by capillary pressure. After the second bond is formed, the capillary tool is raised, thus breaking the wire. These procedures are repeated for all subsequent bonds.
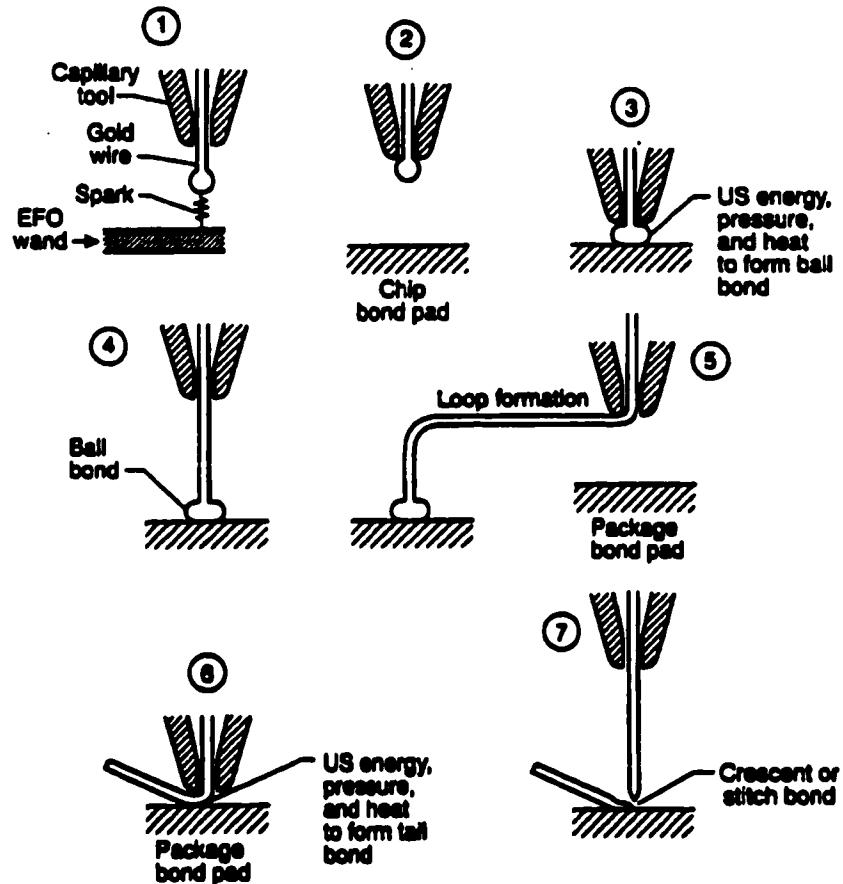
Figure 1. Thermosonic Ball Bonding Procedures.[3]

Wirebonding is the most widely used method of chip interconnection.[2] Compared to other bonding technologies such as flip chip and TAB, wirebonding is more flexible and cost effective. Modifications in wiring and bonding programs can be easily done without the need for expensive tooling and material changes. It also provides

4

thermal dissipation by die bonding to the substrate. So far, the wirebonding process has been more reliable than flip chip and TAB technologies. All these benefits became the driving forces for developing wirebonding technology for fine pitch applications, which are essential for satisfying the demand for high numbers of I/Os. Fine pitch in wirebonding technology is achieved by using smaller-diameter wire and/or modified capillary tools such as bottleneck capillaries to obtain smaller ball sizes.[3]

National Semiconductor developed a fine pitch wirebonding method, called "encapsulated wirebonding", which allows the use of large diameter wire and cost savings with minimal modification of standard wirebonding equipment. In addition, this technology enables low temperature wirebonding. This enhanced process can be incorporated into existing wirebonding machines with only the addition of a modified capillary and an upgraded software package. As shown in Figure 2, "encapsulated wirebonding" has an advantage over the standard process by reducing the ball size, which is essential for the fine pitch application.

This study was undertaken to investigate and compare the reliability achieved in ultra fine pitch wirebonded packages built with two different processes, standard wirebonding and "encapsulated wirebonding". Since most wirebond reliability problems can be attributed to the alloying reactions occurring at the interface between the gold wire and the aluminum bond pad, Au-Al intermetallic compound formation during ball bonding and the growth of the intermetallic layer with high temperature aging were examined and correlated with bond integrity.

(a)   (b)

(c)   (d)
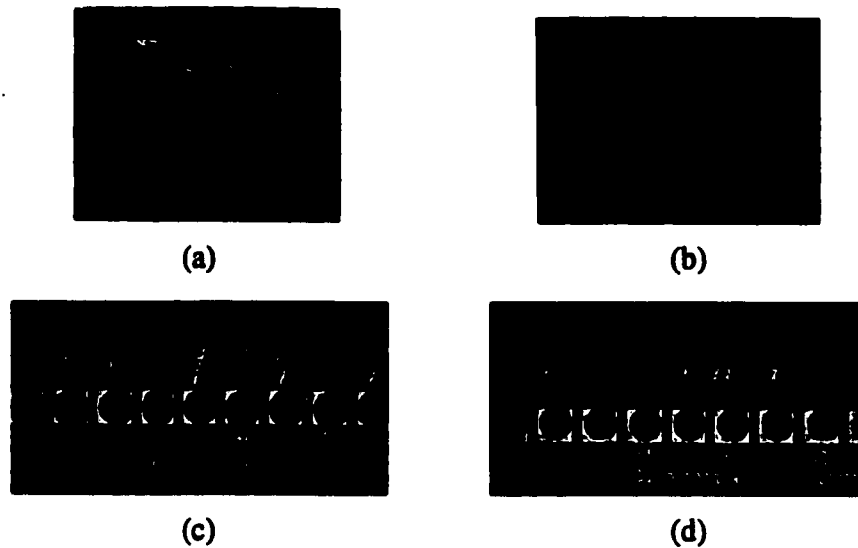
Figure 2. Ball shape in standard (a) vs. "encapsulated" (b) process; Examples of wirebonds on 70 µm in-line pitch Daisy Chain Test Chip with (c) standard process and (d) encapsulated process (25.4 µm thick Au wire was used.).[4]

A review of Au-Al intermetallic compound formation in various Au-Al alloy systems, kinetics of the intermetallic compound formation, and Kirkendall voids induced by the formation of intermetallic compounds is presented in Chapter 2. In this chapter, the intermetallic compound formation and growth are discussed from the thermosonic wirebonding perspective. The research objectives are stated in Chapter 3, followed by the experimental approach in Chapter 4. The results obtained in this study are presented and discussed in Chapter 5. Conclusions, recommendations for future research, and references are presented in Chapters 6, 7, and 8, respectively.

CHAPTER 2

Intermetallic Compound Formation in Au-Al Alloy Systems

In this chapter, various aspects of Au-Al intermetallic compounds are discussed. The general formation mechanism and properties of Au-Al intermetallic compounds are discussed in Section 2.1. A review of early studies for the formation and growth of the intermetallic compounds in various Au-Al alloy systems is presented in Section 2.2. The kinetics of Au-Al intermetallic compounds and the formation of Kirkendall voids are discussed in Sections 2.3 and 2.4, respectively.

2.1 Au-Al Intermetallic Compound Formation and Properties

When pure Au and Al are welded, intermetallic compounds form at the interface. Intermetallic compounds are defined as stoichiometric compounds, which form at fixed ratios of each pure metal in the binary alloy system.[5] Intermetallic compounds have unique crystal structures and physical properties that are distinguished from those of the elemental components.[5,6,7]

Atomic diffusion in the Au-Al binary alloy system is based on the vacancy mechanism, which is the dominant diffusion mechanism in FCC (face-centered cubic) metals and alloys.[6] At high temperatures, interdiffusion between Au and Al can induce the Kirkendall effect, the movement of interfaces between different phases, in any binary alloy system, due to the high temperature interdiffusion. This phenomenon occurs when one species diffuses out of one region faster than the other species can diffuse into the region, due to the difference in diffusion rates.[6,7] Since it is generally found that, in any

7

given couple, elements with the lower melting point have the higher diffusivity, Al is expected to have higher diffusivity than Au in Au-Al alloy systems.[7]

Interdiffusion between Au and Al occurs to produce a decrease in the Gibbs free energy of the system.[7] The most stable state is formed when the free energy is the lowest. The state of each component in a binary solution is described by activity, which is defined as a measure of the tendency of an atom to escape a solution.[7] The difference in activity provides the driving force for diffusion and activity determines the direction of diffusion in a system.[8] Diffusion ceases when the system reaches equilibrium, i.e., when the chemical potential of the species are the same in the different phases. In the case of Au-Al diffusion couples, the formation of multiple phases is probable, as shown in Figure 3. For example, if there are two different phases present in the Au-Al diffusion couple at a specific condition of interest, a local equilibrium is expected at the interface of the two phases satisfying the equilibrium condition that the activities of each component in the two phases are the same. However, each interface in the diffusion couple is expected to move as diffusion continues, until the final equilibrium state is reached.[7]

Based on the phase diagram shown in Figure 3[9], the intermetallic compounds in the binary alloy system of gold (Au) and aluminum (Al) are $AuAl_2$, $AuAl$, Au_2Al, Au_5Al_2, and Au_4Al. All five compounds have different compositions and physical properties. In Figure 3, the $AuAl_2$ and Au_2Al phases are shown to have melting temperature maxima, which indicate that they form congruently. Peritectic reactions can be found in the formations of the three other intermetallic compounds. The melting points of all intermetallic compounds show that they are stable at temperatures up to at least

8

500°C. The compositions and melting points of each intermetallic compound and the pure components are summarized in Table 2.
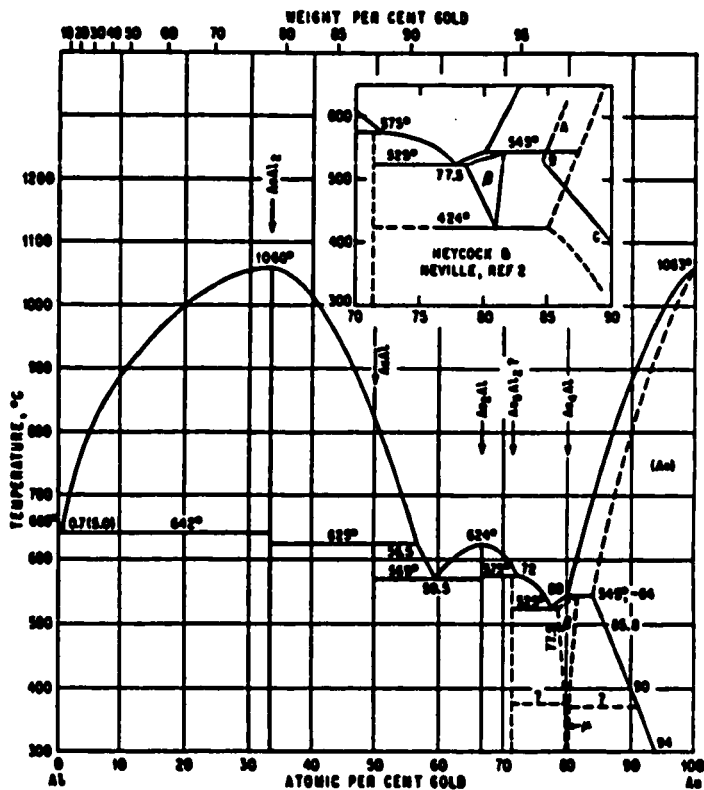
Figure 3. Binary phase diagram of Al and Au alloy system.[9]

Table 2. Compositions and melting points of Au-Al intermetallic compounds.[9]

Compound	Melting Point (°C)	Composition
Al	660	
AuAl$_2$	1060	78.52 wt. % Au
AuAl	625	87.97 wt. % Au
Au$_2$Al	624	93.60 wt. % Au
Au$_5$Al$_2$	575	94.82 wt. % Au
Au$_4$Al	545	95.64 wt. % Au
Au	1063	

The solid solubility of Al in Au has been determined parametrically at various temperatures between 300°C and 570°C and are listed in Table 3.[9] As summarized in Table 3, Al is most soluble in Au at 530°C, which is close to the peritectic temperature of 545°C. In contrast, the solid solubility of Au in Al is extremely small, below 1 wt. % (0.2 at. %) Au at the eutectic temperature of 642°C. Based on the mutual solid solubilities of Au and Al, Al is expected to have a higher diffusivity than Au in Au-Al binary systems.

Table 3. The solid solubility of Al in Au at various temperatures.[9]

Temperature (°C)	Solubility of Al in Au (%Al)
300	0.85 wt.% (6.0 at.%)
350	1.15 wt.% (8.0 at.%)
400	1.50 wt.% (10.0 at.%)
450	1.85 wt.% (12.0 at.%)
500	2.20 wt.% (14.2 at.%)
530	2.45 wt.% (15.5 at.%)
570	2.30 wt.% (14.7 at.%)

Unique features of the intermetallic compounds are also found in their crystal structures. Compared to the face-centered cubic (FCC) structure that Au and Al have, Au-Al intermetallic compounds have various crystal structures. $AuAl_2$ has the CaF_2 structure.[9-11] AuAl has been reported to have a distorted MnP type structure.[10] Au_5Al_2 has a structure similar to γ-brass but distorted into a hexagonal cell.[9-11] Au_4Al has a structure of β-Mn.[9-11] Au_2Al has been reported to have three different phases depending on temperature.[10] It has a structure similar to $MoSi_2$ type at temperatures above 550°C. The other two phases have an orthorhombically deformed $MoSi_2$ type substructure.

Crystal structure types and the corresponding lattice constants for the specific intermetallic compounds are summarized in Table 4. Generally, the lattice constants of the intermetallic compounds are larger than those of the pure components.

Each Au-Al intermetallic compound also has a specific color.[12] The gold-rich phases, Au_4Al, Au_5Al_2, and Au_2Al, are tan in color. AuAl is reported to be white with a gray hue. The aluminum-rich $AuAl_2$ phase, which is widely known as "purple plague,"[2] is purple in color. All other properties of the specific Au-Al intermetallic compounds, including resistivity, hardness, and coefficient of thermal expansion (CTE), are summarized in Table 4. As can be seen in Table 4, Au-Al intermetallic compounds are harder and have higher resistivities than pure Au and Al.

Table 4. Properties of Au-Al Intermetallic Compounds.[9-12]

Compound	Color	Structure Type	Lattice Constant (Å)	Vicker's Hardness (5 Kg)	CTE (10^{-6}/K)	Resistivity (10^6 Ω-cm)
Au	Yellow	FCC	4.08	60-90	14.2	2.3
Au_4Al	Tan	Cubic β-Mn	6.92	334	12.0	37.5
Au_5Al_2	Tan	γ-Brass	Unknown	271	14.0	25.5
Au_2Al	Tan	$MoSi_2$	Unknown	130	13.0	13.1
AuAl	White/ Gray	MnP Type	6.05	249	12.0	12.4
$AuAl_2$	Purple	FCC CaF_2	6.00	263	9.4	7.9
Al	White	FCC	4.05	20-50	23.0	3.2

2.2 Au-Al Intermetallic Compounds in Early Studies

Although the formation of five Au-Al intermetallic compounds is theoretically possible in any Au-Al binary system in equilibrium, the number of intermetallic compound(s) formed varies from system to system. This variation can be caused by differences in sample preparation, in experimental conditions, or in the environments to which Au-Al samples are exposed. Since the mid 1960s, many efforts have been made to investigate the formation of intermetallic phases in Au-Al binary systems, as related to the performance of microelectronic devices. Au-Al specimens subjected to various thermal conditions have been investigated. In this section, the studies carried out between the mid 1960s and late 1990s are reviewed. For this review, about 100 articles were obtained as a result of a search of the following databases: Compendex, Inspec, and Metadex. However, most articles focused on the effects of Au-Al intermetallic compounds on device performance rather than the formation and growth of the intermetallic compounds themselves. This review is based on 10 articles and focused primarily on the intermetallic compound formation and growth. The results of these studies are discussed in relationship to the current study of Au-Al fine pitch wire bonding.

Definite investigations of the intermetallic compound formation and its effects on Au-Al alloy systems started with Kashiwabara et al.[11] in 1969. Their research mainly focused on the electrical resistance change as related to the formation of intermetallic compounds in ultrasonic Al and Au wire bonding systems. Samples used for the study were 0.3 mm thick 99.99 % pure Al wire and 0.4 mm thick 99.99 % pure Au ribbon, to

which the Al wire was ultrasonically bonded. The samples were thermally aged at 337°C for 98 hours and at 450°C for 5 hours, in air in both cases. Identification of intermetallic compounds was made using an X-ray probe microanalyzer. Calculated Al K_α X-ray intensity values from standard samples were compared with the actual values obtained from the samples for the identification.

They reported seeing three intermetallic phases, $AuAl_2$, $AuAl$, and Au_2Al, after aging at the two different temperatures and times. They visually identified three different layers with two different colors, purple and gray, from the cross-sectioned sample. They found that three different intermetallic phases, $AuAl_2$, $AuAl$, and Au_2Al, were formed in sequence from the Al wire side to Au ribbon. The purple colored phase was identified as being $AuAl_2$ and other gray colored intermetallic compounds were identified as $AuAl$ and Au_2Al.

Kashiwabara et al. introduced a methodology suitable for the study of intermetallic compounds. Even though they had success in identifying specific intermetallic compounds under high temperature storage conditions, their results are not directly applicable to the current wirebonding study due to the differences in specimen type, thermal aging conditions, and wirebonding technology. For example, the thicknesses of their Au and Al specimens, 0.4 mm and 0.3 mm, respectively, are much larger than those for the Au and Al specimens used in the current wirebonding study, 0.025 mm and 0.002 mm, respectively. Though the wedge size was not specified in their report, the relative dimensions of the bond area can be estimated based on the Al wire and Au plate sizes. Since the diameter of the Al wire, 0.3 mm, was about 10 times bigger

than the size of Au wire used in thermosonic wirebonding, the bonding area between the Al wire and Au ribbon is expected to be greater than the ball bonding area produced by current wirebonding techniques. The difference not only in the bonding wire diameter, but also in the wirebonding methods, i.e., thermosonic ball bonding as opposed to Al ultrasonic wedge bonding, is expected to influence the types of intermetallic compounds formed. In contrast to ultrasonic bonding that supplies a limitless amount of Al, the amount of Al available during Au wire thermosonic bonding is restricted. In addition, the aging temperatures were higher than the 150°C and 175°C in the current study. These deviations in specimen types and aging condition make it hard to apply the results directly to the current wirebonding study, which is based on thermosonic bonding with low bonding and aging temperatures. However, the study done by Kashiwabara et al. gives a good guide for analysis of the results.

Philofsky[12] performed an extensive study to clarify the conflicting results of earlier studies[13-17] of Au-Al formation. He employed Au-Al butt-welded diffusion couples, thermal aging conditions ranging from 200°C to 460°C, and aging times up to 97 hours. All five intermetallic compounds were reported to have formed in the bulk Au-Al diffusion couples. Identification of the intermetallic phases was performed using an electron microprobe. Formation of specific intermetallic phases was found to vary depending on the thermal aging conditions.

The observations on each specific intermetallic compound can be summarized as follows. A gold rich phase, Au_5Al_2, was the main intermetallic compound formed, regardless of time or temperature. A small amount of the $AuAl_2$ phase was observed to

form with a slow growth rate. AuAl appeared at long times and low temperatures and grew into the $AuAl_2$ phase. In the case of Au_2Al, it was found to nucleate slowly but grow fast once initiated. The Au_4Al phase was found to be present in most specimens even though it showed a very slow rate in growth. $AuAl_2$ was reported as a prominent phase present in samples aged at temperatures above 250°C, and the amount was found to increase with aging time. In the temperature range between 200°C and 250°C, however, only small amounts of $AuAl_2$ were reported to form after 97-hour aging. Overall, the Au_5Al_2 phase was found to make up the most of intermetallic compounds formed in the temperature and time range investigated.

Philofsky's extensive study of Au-Al butt-welded diffusion couples gives general ideas about the formation and growth of the specific Au-Al intermetallic phases, as related to thermal aging conditions. Although the study covers a wide range of aging temperatures, from 200°C to 460°C, there is a lack of prolonged aging times, which are essential for the reliability test of wirebonds used in current microelectronic devices. Furthermore, the study was designed such that an unlimited supply of Au and Al would be available for intermetallic compound formation; this, however, is not the case in actual wirebonding.

Sinha[18] investigated the formation of intermetallic compounds in the Au-Al thermocompression wirebonding system. Intermetallic compound formation at the interface between the Au wire and the Al bond pad was reported, but the stoichiometry of intermetallic compounds was not identified.

His report contains some flaws, which brings the quality of the work into question. First, there was no description of the specimens employed for the experiment. Second, no specifics about high temperature storage conditions, such as the stabilization bake, burn-in and thermal cycling, have been described. In addition, details about temperature range, rate of thermal cycle, and baking time were also missing in the experimental section. Third, general statements related to the intermetallic compound formation were made, without provision of any supporting data. For example, the author made a statement saying that the purple phase, assumed to be $AuAl_2$, can be formed only when the operating temperature exceeds 200°C. This is in contradiction to the observation made by Philofsky,[12] which indicated that $AuAl_2$ can be formed when stored at low temperature for a long period of time. Another statement from the report, "the weakest boundary is the intermetallic interface,"[18] can be misleading without giving sufficient evidence or data. In addition, the author showed two SEM micrographs to illustrate the presence of intermetallic compounds at the bond interface and microcracks within the intermetallic compounds. However, the intermetallic phases assumed by the author in his report were not identified using any analytical tools. The author also stated that plastic packages were not suitable for devices operated at temperatures higher than 200°C. This can be misleading without providing any supporting data for the comparison between plastic and ceramic packages in terms of reliability merits. Overall, Sinha did not cite references properly when he made statements based on various observations and studies pursued by early researchers, such as Philofsky.[12]

In the late 1970s, a different approach was tried, to investigate the intermetallic compound formation and growth in Au-Al systems. A representative work was done by Galli et al.[19] in 1979. For the study of the kinetics of the intermetallic compound formation and the mechanism responsible for the growth, Au-Al thin film diffusion couples were used. Au and Al films were deposited on oxidized Si single crystals in a high vacuum oil-free system using an electron gun. The thickness of the Au and Al films was varied from 1000Å to 3000Å, and thermally annealed after deposition in a vacuum furnace at temperatures ranging from 50°C to 500°C. X-ray diffraction and He^+ Rutherford backscattering were employed for identification of the intermetallic compounds and thickness measurements, respectively.

The formation of the Au_5Al_2 phase after aging at an unspecified "low" temperature was reported. The Au_2Al phase was reported to form as the heat treatment continued. Corresponding temperatures and times for the heat treatment were not specified. Different kinds of the intermetallic compounds were found to form, depending on the thickness of the starting metals, Au and Al. For instance, when the amount of Au was much larger than that of Al, Au_4Al was formed. In the case when a large amount of Al, compared to Au, was present in the sample, $AuAl_2$ formed as the end phase. When the same amounts of Au and Al were supplied, the end phase came out as AuAl. They also found that $AuAl_2$ started to form when all of the Au was consumed. In the case of Au_4Al, the compound started to form after complete consumption of Al. AuAl was formed only when both Au and Al were consumed. In the cases of Au_5Al_2 and Au_2Al, they resulted as end phases only when the exact atomic ratios of Au/Al were chosen as

17

5/2 and 2/1, respectively. They reported that all the end phases were found to be stable at temperatures up to 500°C.

Galli and his coworker further studied the change of intermetallic compounds along with temperature and time by preparing a sample with 1500Å thick Au and 1400Å thick Al. At room temperature the Au_5Al_2 phase formed. When the sample was thermally annealed at 247°C for 5 minutes, Au_2Al and $AuAl_2$ were formed from the previous phase, Au_5Al_2. Further annealing at the same temperature for 15 minutes induced the formation of AuAl. After 120 minutes, the Au_2Al and $AuAl_2$ were nearly all converted to AuAl.

For the formation of Au_5Al_2, they specified the annealing temperature, which was room temperature, but did not specify aging times. No further information about thermal annealing was provided in their paper for the formation of Au_2Al and other intermetallic compounds, which were observed in the specimens with large amounts of Au or Al.

Based on their findings, Au_4Al is expected to be the end phase in the case of Au-Al thermosonic wirebonding, where the supply of Al is limited. Overall, they reported seeing all five intermetallic compounds predicted by the phase diagram in their thin film couples.

A further study, employing the same kind of Au-Al diffusion film couples, was performed and reported by Majni et al.[10] in a subsequent article published in 1981. Majni et al. continued to investigate the sequence of intermetallic phase formation by observing diffusion interactions between Au and Al thin films. This study was more detailed and systematic than the previous study performed by Galli et al.[19]

Temperatures employed for the study ranged between 25°C and 500°C, with thermal aging times between 15 minutes and one month. The samples used for the study were Au and Al films deposited on thermally oxidized Si, identical to the samples used by Galli et al. with the same film deposition procedures as Galli et al. as well. Based on the phase diagram, exact atomic ratios of Au and Al, i.e., 1/2, 1/1, 2/1, 5/2, and 4/1, were employed, and the final thickness of intermetallic compound layers was measured. The intermetallic compounds were identified using x-ray diffraction (XRD).

Manji et al. reported the identification of all five intermetallic phases in their specimens. First, they found Au_5Al_2 as the first phase, which formed in all samples when aged at room temperature for one month. Au_2Al was found to be the second phase formed in all samples after thermal aging at 80°C for 15 minutes. After the Au_2Al phase was formed, various phases nucleated at the expense of existing phases, as shown in Figure 4. It was found that a new intermetallic phase nucleated and grew at the interface of two others. For example, the Au_5Al_2 phase formed at the interface of Au and Al and then the Au_2Al phase nucleated at the interface of Au_5Al_2 and Al through an interaction between the gold rich Au_5Al_2 phase and non-reacted Al. As a result, a more stable phase resulted at a given aging condition.

Worth noticing among the phase formation results from various samples is the one obtained from a sample consisting of a large amount of Au. When the amount of Au was much more than that of Al in the sample, Au_5Al_2 was reported to appear as the intermediate phase and react with non-reacted Au to form the end phase, Au_4Al. Based on the result, Au_4Al is expected to form as the final phase in the case of wirebonds in
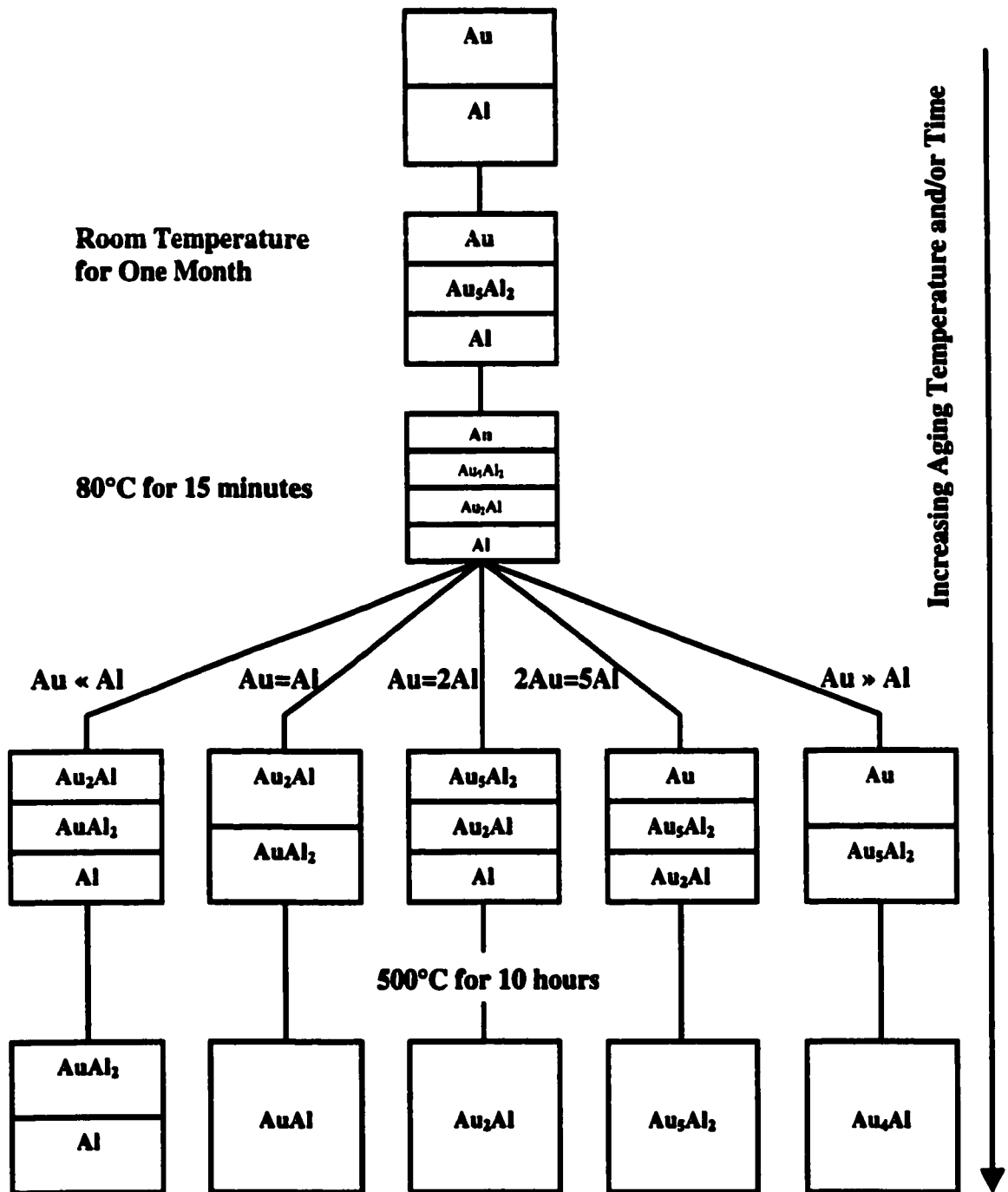
Figure 4. Sequence of Intermetallic Phase Formation in Au-Al Thin Film Reaction Systems with Increasing Aging Temperature and Time.[10]

which the supply of Au is plentiful, compared to the limited amount of Al. This observation was also made in the previous study performed by Galli et al. Though this result is applicable to the current study of Au-Al wirebonding, variations in samples, i.e., film diffusion couples as opposed to wirebonds, and thermal aging conditions should be taken into account in predicting the final intermetallic compound that is the most probable in the wirebonding system.

Overall, this study showed that depending on the relative quantity of each starting material available in the reacting systems at a given condition of thermal aging, specific Au-Al intermetallic phases can form. Even though the sequence of phase formation was well illustrated along with temperature and time, as shown in Figure 4, specific aging time and temperature for various intermediate phases were not specified. According to the results that the authors obtained, intermediate phases are assumed to form at temperatures between 80°C and 500°C at aging times between 15 minutes and 10 hours. In addition, unspecified film thickness values for thin and thick metallization made it hard for the reader to fully relate the results to wirebonding conditions.

Another study of intermetallic compound formation using Au-Al thin films was performed by Campisano et al.,[20] who investigated intermetallic compound formation and growth in the Au-Al system, by ion bombardment. The samples used for the study were thin layers of Au and Al, which were vapor deposited on glass substrates. The layer thickness was varied from 160 to 200 nm for Au and from 50 to 70 nm for Al. The substrate temperature during deposition was at -30°C. The aging time at room temperature was kept at a minimum, to decrease the amount of Au_5Al_2 formed. Instead

of thermal aging at higher temperatures, the amount of energy and dose of Kr ions was varied to induce the interdiffusion reaction for the formation and growth of the intermetallic compounds in the film couples. For the identification of the intermetallic phases and characterization of film thickness and uniformity in depth for Al, Au, and intermetallic phases, X-ray diffraction and backscattering spectra, respectively, were employed.

Campisano and his coworkers reported finding the Au_2Al and $AuAl_2$ phases formed right after Kr ions irradiation of the Au-Al thin films. The two phases were also found to form when Au-Al films, with Au_5Al phase previously formed at the interface between Au and Al, were irradiated by Kr ion bombardment.

Samples were also prepared by growing two different thicknesses of Au_5Al_2 layers at the Au-Al interface, to compare with the thermal behavior of the Au-Al film system, in which Au_5Al_2 layer formed after annealing at room temperature. The thicknesses of thin and thick Au_5Al_2 layers used for the study were 5 nm and 25 nm, respectively. It was found that the specific intermetallic compound formed in the samples was dependent on the amount of irradiation dose and the beam energy deposited in the Au-Al layers. When more energy was imparted to the Au side, more Au-rich intermetallic compounds formed. They noticed that one compound could be transferred to the other compound by changing the fraction of energy imparted to the layers. In addition, the thickness of the intermetallic layer was found to be linearly dependent on the square root of ion flow, i.e., the amount of ion dose. The overall results are summarized in Figure 5.
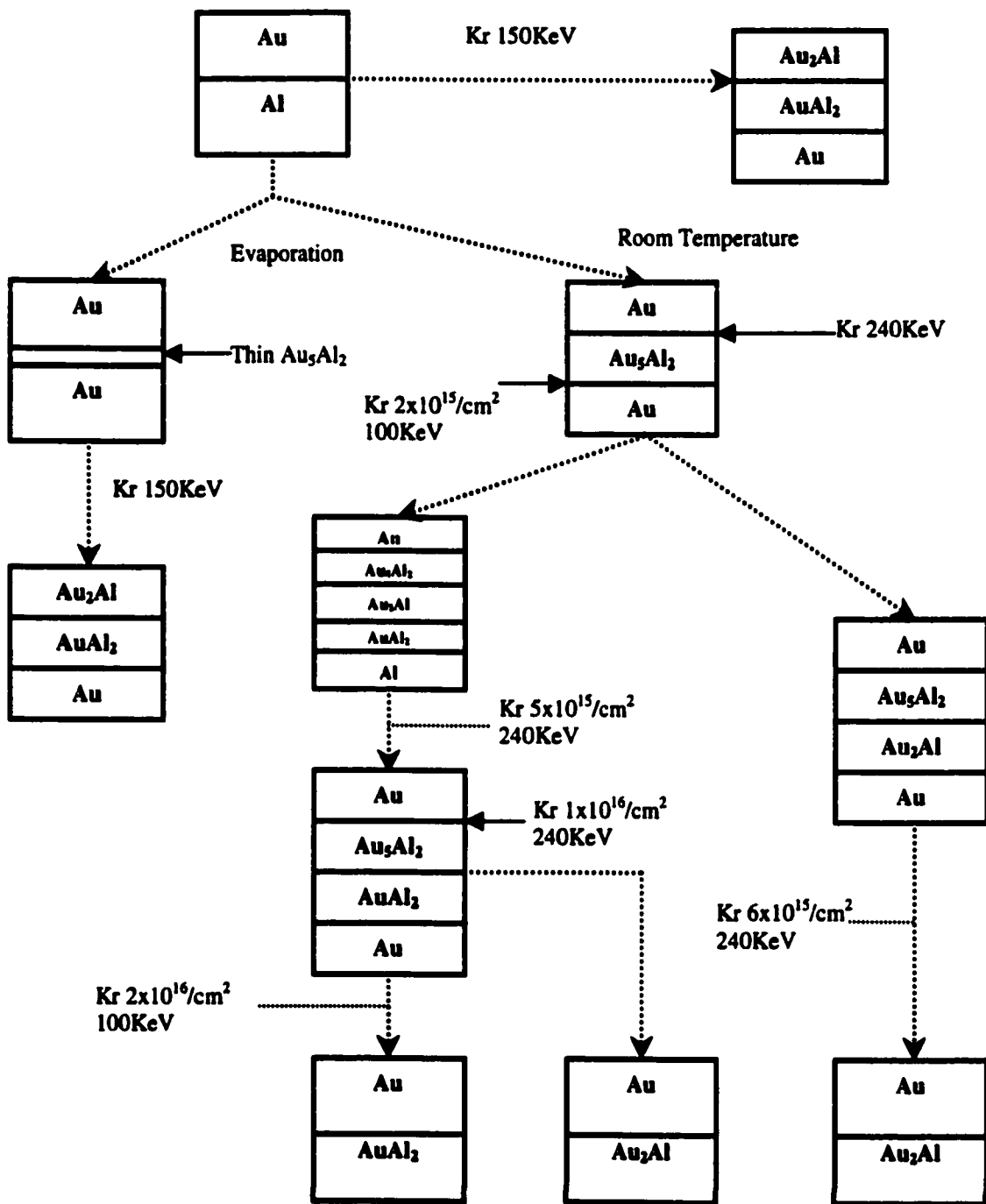
Figure 5. The sequence of phase formation in the Au-Al film couples after ion bombardment at -30°C.[20]

As demonstrated in Figure 5, the sequence and the amount of intermetallic compounds formed in the film layers were determined by beam energy and the density of ion flow. It was also well illustrated that the total energy imparted by the Kr ions determined the kind of intermetallic compound formed. For example, $AuAl_2$ layer was found to form in the sample with a thick Au_5Al_2 layer, when the ion bombardment at 100 KeV was projected to the interface between Au_5Al_2 and Al. When 240 KeV ion bombardment was positioned at the interface of Au and Au_5Al_2, Au_2Al formed as the primary intermetallic phase in the sample.

Overall, this study described the sequence of intermetallic compound formation and growth in Au-Al thin films, employing a new method of providing thermal activation, namely, Kr ion bombardment at different energy levels and densities. The correlation between the amount of Kr ions and energy levels to the standard thermal aging conditions, i.e., aging time and temperature, to which wire bonded devices are usually subjected, is not straightforward. The aging time required for the formation of the Au_5Al_2 phase, at room temperature, was not specified. Worth noticing in this study was that the Au_4Al and $AuAl$ phases were not formed by Kr ion induced reaction.

Kato analyzed Al film-Au bulk couples to investigate the intermetallic compound formation, measuring infrared radiance changes from the specimen surface as a function of the annealing time and temperature.[21] Surface emissivities of the intermetallic compounds were measured through the surface radiance changes and found to increase with increase in the Au stoichiometry on the Al-Au couple surface. The emissivity values obtained from the sample are shown in Table 5. The values were obtained using a

carbon black film, coated on oxidized silicon, as the emissivity standard. The intermetallic compounds appeared on the surface were identified using reflective electron diffraction (RED).

Table 5. Surface emissivities of starting metals and Au-Al intermetallic compounds at 250°C.[21]

Material	Al	AuAl$_2$	AuAl	Au$_2$Al	Au$_5$Al$_2$	Au$_4$Al	Au
Emissivity	0.050	0.067	0.073	0.083	0.088	0.120	0.058

The specimen used for the study, 1.0 ± 0.1 μm thick Al film vacuum deposited on a rolled Au plate, was thermally aged at temperatures ranging between 230°C and 350°C. Kato found a two-step radiance change in each specimen and measured the corresponding annealing times at which the radiance increased. The initial radiance value was found to increase with aging temperature. Changes in the radiance values corresponded to changes in the intermetallic phase at the surface. That is, a constant value at the first step of the radiance changed when another intermetallic phase formed at the specimen surface. RED analysis on the specimen, which was annealed for two aging times at 230°C, indicated the presence of AuAl$_2$ and Au$_4$Al as primary phases. Right after quenching of the specimen, Al and AuAl$_2$ were present on the surface. At the first annealing time, which can be approximated as less than 2 hours, AuAl$_2$ was shown as the primary phase, with a small amount of Au$_5$Al$_2$. At the second annealing time, which was approximately 3 hours, Au$_4$Al appeared, with a minor amount of Au$_5$Al$_2$.

Kato's study using the Al film-Au plate couple mainly focused on the formation of Au-Al intermetallic compounds at the surface of the specimen. However, a small

amount of AuAl, Au_2Al, and Au_5Al_2 phases was assumed to form inside the specimen. As aging time increased, most phases transformed into Au_4Al, the presence of which was reflected by RED analysis of the surface. The reaction was also found to be dependent on the amount of starting materials. That is, when the quantity of Al film was depleted, the intermetallic phases in the film transformed to the Au-rich phase after prolonged aging. This observation agrees with the results obtained by Manji et al.[10] Kato also noticed the formation of Au_4Al when there was a small amount of Al and a large supply of Au in the film-bulk couple.

Overall, this study introduced a new method of investigating the formation and growth of Au-Al intermetallic compounds. According to the results, the formation of $AuAl_2$ and Au_4Al after aging at 230°C for about 2 and 3 hours, respectively, can be expected. However, the lack of further information, such as specific aging times corresponding to the radiance changes at 230°C, make it hard to follow. Results for other aging temperatures between 230°C and 350°C, and details about sample preparation and analysis, were not fully discussed.

Various studies, based on Au-Al bulk couples, thin film couples, or thermocompression and ultrasonic wire bonded samples, have been discussed. Even though these studies provide valuable and extensive information about the formation and growth of Au-Al intermetallic compounds, as related to various sources of heat, these results are not directly applicable to the current study of Au-Al wirebonding due to the differences in sample and thermal aging condition. Additional studies for the formation

and growth of Au-Al intermetallic compounds, based on thermosonically wirebonded devices, are discussed in the following section.

Ramsey et al.[22] observed the formation of Au-rich intermetallic compounds in thermosonically wirebonded Au-Al systems. The intermetallic phases were identified using x-ray diffraction (XRD), and the presence of Au_5Al_2 and Au_4Al phases at the interface of wirebonds after heat treatment at 175°C for 5 hours was reported. The formation of an Al rich phase right after bonding was also reported, but the specific intermetallic phase was not identified.

Carrass et al.[23] also studied the formation of intermetallic compounds, as bonding temperature and time were varied. Specifically, intermetallic compound growth on the bond contact during ball bonding was observed. Bonding temperatures were varied from 30°C to 350°C, and bond times between 20 ms and 100 ms were employed. The maximum extent of intermetallic compounds formed when bond times between 8 and 10 ms were used. The bond temperature used for the investigation of optimal bond time was not specified. The maximum shear strength, which was proportional to the percentage of intermetallic compounds formed at the bond contact, was obtained when a bonding temperature of 250°C was used. For the study of bond temperature yielding maximum shear strength, the bond time was fixed at 6 seconds. Three phases of gold-aluminum intermetallic compounds, Au_5Al_2, Au_2Al and $AuAl_2$, at the ball bond interface right after thermosonic wirebonding, were identified, using energy dispersive x-ray (EDX).

During the study of electrical performance influenced by the intermetallic compounds, Trigwell and his coworkers[24] analyzed the intermetallic layers at the Au-Al interface. For the study thermosonically wirebonded MCM (multichip module) interconnects were examined.

Worth noticing in this study is the application of Field Emission Auger Electron Spectroscopy (FEAES) to analyze the bond interface. Though they presented the results obtained from Auger linescan along the interface layers, they did not specify the exact stoichiometry of the intermetallic compounds present at the Au wire and Al bond pad interface. This study assumed the presence of Au_5Al_2 or Au_4Al at the interface based on literature information, especially the study done by Philofsky.[12] It would strengthen the study if they could have experimentally confirmed the two specific intermetallic compounds at the interface. However, they were very descriptive in explaining how all the measurements, including the linescan method using SEM and Auger techniques, were performed to achieve the purpose of their study.

In summary, the above review of Au-Al intermetallic compound formation studies presents several important points as related to the formation of intermetallic compounds in various Au-Al alloy systems. There is general agreement that Au_5Al_2 is the dominant phase in any Au-Al system. This phase is found to form at room temperature. Heat treatment plays a major role in influencing the intermetallic compound formation and growth rates. The formation sequence and stoichiometry of the intermetallic compounds are determined by the heat or energy applied to the Au-Al diffusion couple. The amount of starting metals, Au and Al, also determines the kind of

intermetallic compound formed under specific thermal aging condition and new phases

nucleate from two existing phases in Au-Al specimens. Based on the earlier

investigations, Au_4Al is expected to be the final phase formed in thermosonically

wirebonded Au-Al interconnects. All of the Au-Al intermetallic compounds were also

found to be stable at temperatures ranging up to 500°C. Overall, the formation and

growth of intermetallic compounds vary with the kind of specimens, sample preparation

process, and thermal aging conditions. The Au-Al intermetallic compounds identified by

early researchers are summarized in Table 6, along with the descriptions of specimen

type and aging conditions.

Table 6. Au-Al intermetallic compound formation in early studies.

Researcher	Phase	Specimen	Temp (°C)	Time
Kashiwabara[11]	$AuAl_2$, AuAl, & Au_2Al	Al wire-Au film ultrasonic bonding	337 & 450	5 – 98 hours
Philofsky[12]	All five phases	Butt-welded diffusion couple	200-460	97 hours
Majni[10]	All five phases	Au film-Al film diffusion couple	25-500	15 min- 1 month
Campisano[20]	$AuAl_2$, Au_2Al, & Au_5Al_2	Au film-Al film diffusion couple	Kr ion bombardment	
Kato[21]	$AuAl_2$, Au_4Al	Al film-Au bulk couple	230-350	2-3 hours
Ramsey[22]	Au_5Al_2, Au_4Al	Au wire-Al film thermosonic bonding	175	5 hours
Carrass[23]	Au_5Al_2, Au_2Al & $AuAl_2$	Au wire-Al film thermosonic bonding	30-350	2~100 ms

2.3 Kinetics of Intermetallic Compounds

As seen in the earlier discussions of Au-Al intermetallic compounds, temperature and time are primary factors that influence the formation and growth of intermetallic compounds in the various binary alloy systems. Varying time and temperature in wirebonding or thermal aging processes can result in the formation of specific intermetallic compounds. The growth of intermetallic compounds follows a parabolic rate law:

$$x = K t^{\frac{1}{2}} \qquad (1)$$

where x is the intermetallic layer thickness, t is time, and K is the rate constant which depends on the interdiffusion coefficients between the neighboring phases.

$$K = C e^{(-E/kT)} \qquad (2)$$

where C is a constant, E is the activation energy for the intermetallic compound growth, k is Boltzmann's constant, and T is the absolute temperature in K.[3,12]

Philofsky[12] measured growth rates of each specific intermetallic compound at 400°C. His results are shown in Table 7, specifying neighboring phases present. Au_5Al_2 was found to have the highest rate constant regardless of the types of neighboring phases present. Au_2Al has the second highest rate. According to Equation (1), the phases with higher interdiffusion rates are expected to form thick intermetallic layers at a given temperature and time. The growth of the intermetallic layer with aging time, at an aging temperature of 400°C, is shown in Figure 6. Based on Table 7 and Figure 6, Au_5Al_2 is expected to be the first phase formed and also the major phase present in most samples that are thermally aged for time periods up to 40,000 seconds. Au_2Al is also expected to

Table 7. Rate constants of intermetallic phases formed at 400°C in the Au-Al system.[12]

Intermetallic Phase	Neighboring Phases Present	Rate Constant, K (cm^2/sec)
AuAl$_2$	Au$_5$Al$_2$, Al	7.50×10^{-11}
	Au$_2$Al, Al	7.75×10^{-12}
	AuAl, Al	-3.33×10^{-13}
AuAl	Au$_2$Al, AuAl$_2$	2.43×10^{-12}
Au$_2$Al	Au$_5$Al$_2$, AuAl$_2$	1.24×10^{-10}
	Au$_5$Al$_2$, AuAl	1.24×10^{-10}
Au$_5$Al$_2$	Au, AuAl$_2$	3.48×10^{-9}
	Au, Au$_2$Al	3.48×10^{-9}
Au$_4$Al	Au, Au$_5$Al$_2$	1.47×10^{-12}
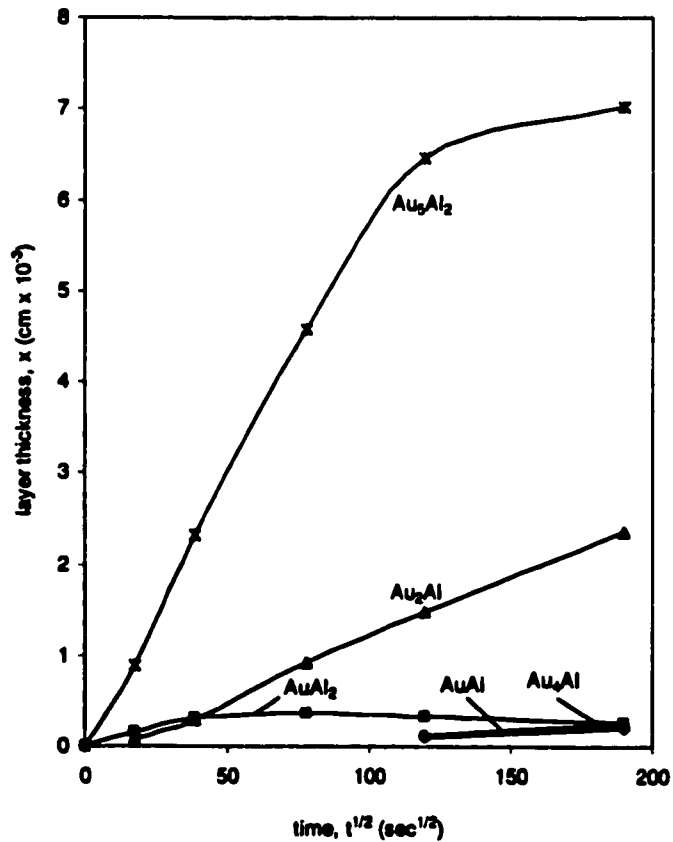
Figure 6. Intermetallic phase growth with aging time at 400°C.[12]

be present at the early stage of Au-Al wirebonding according to its higher growth rate. Worth noticing in Figure 6 is the initial presence of AuAl and Au_4Al phases, which are first observed after approximately 14,400 seconds. This implies that AuAl and Au_4Al are rarely seen immediately after wirebonding.

Philofsky showed that the growth of intermetallic compounds was temperature dependent by measuring the total intermetallic layer thickness at six different temperatures, which ranged between 200°C and 460°C. The results are shown in Figure 7. As illustrated in Figure 7, the growth rate of intermetallic layers is exponentially proportional to temperature. In addition, the results indicate that the growth rates within the range of aging temperatures followed the parabolic rate law as described in Equation (1).

Philofsky was thus able to determine the values of C and E in Equation (2) and a resulting Arrhenius equation was obtained as follows.

$$K = 5.2 \times 10^{-4} \exp(-15,900/RT) cm^2/sec \tag{3}$$

This equation is applicable for the total growth of intermetallic layers, aged at temperatures between 200°C and 460°C for time periods up to 97 hours. Sufficient supplies of gold and aluminum in the bonding area were assumed.

Using Equation (3), Philofsky approximated the time required for the Al metal in the bond area to be completely consumed and transformed into the intermetallic compounds, for a given aging condition. The penetration time was approximated for the four different thicknesses of Al metallization, i.e., 5,000 Å, 10,000 Å, 20,000 Å and 50,000 Å, for thermal aging temperatures between 150°C and 450°C. The results were

32
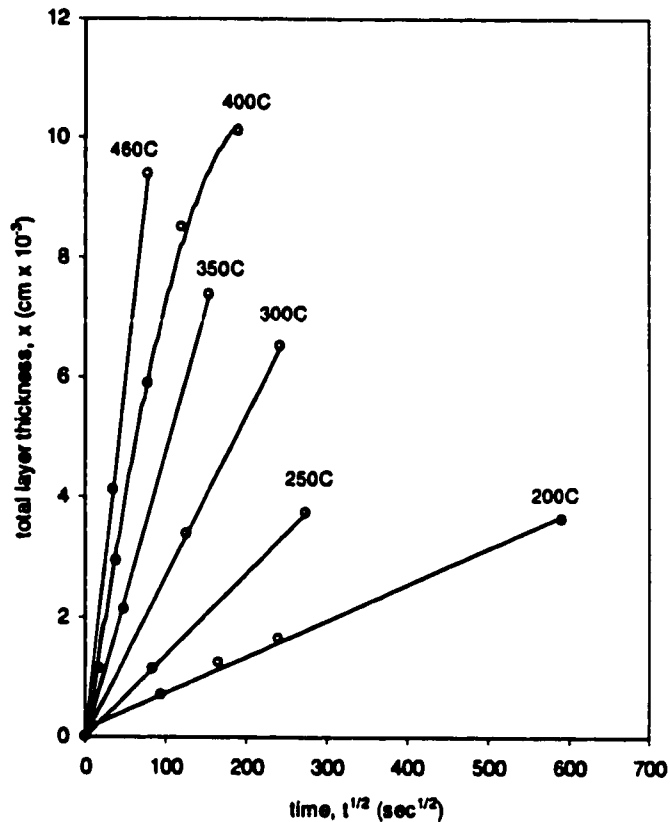
Figure 7. Temperature dependence of intermetallic layer growth.[12]

plotted as a function of aging temperature and are shown in Figure 8. The results in Figure 8 allow approximating the time required for the formation of intermetallic compounds in Au-Al wirebonding systems. However, there are limitations to the applicability of this figure on a broad basis. For example, when wirebonds with 10,000 Å thick Al are aged at 150°C, the only information obtainable from Figure 8 would be that the penetration time is longer than 75 minutes. In addition, variations in the penetration time can be expected since the differences in properties of specimen and bonding technique were not taken into account in the approximation.

33
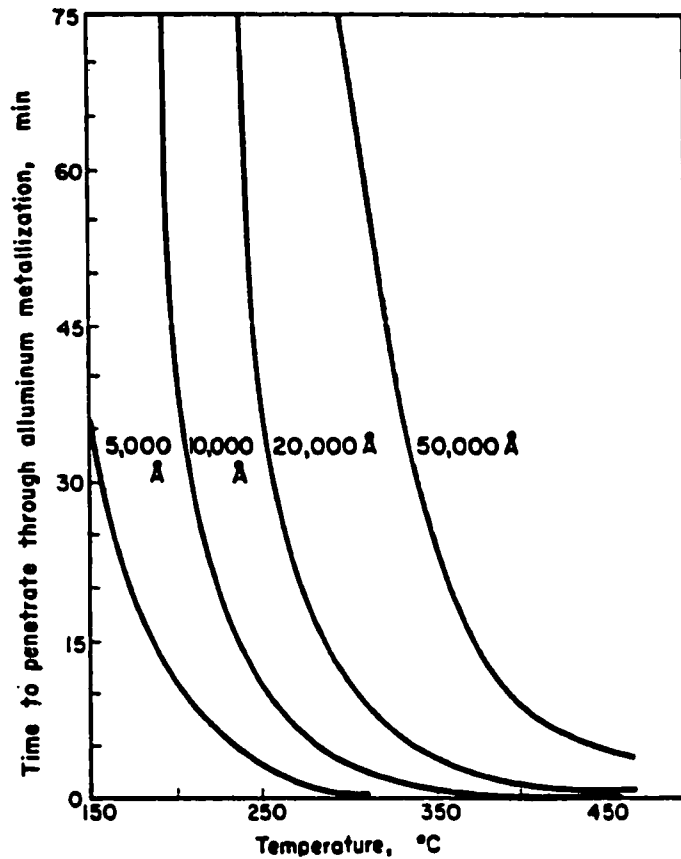
Figure 8. Time of penetration through aluminum metallization with various thickness, as a function of aging time.[12]

Worth noticing in his discussion related to Equation (3) is that the total intermetallic growth rate changed once all the aluminum in the bond pad was consumed. When Al was depleted for the formation of intermetallic compounds, the intermetallic growth continued but the growth rate decreased, resembling the rate of the slowest intermetallic phases in the specimens. In addition, it was found that intermetallic compounds grew into the gold wire and into other phases that had already formed at the interface.

Other researchers also studied the kinetics of Au-Al intermetallic compounds. Kashiwabara and Hattori[11] reported that the growth of the intermetallic compounds in the Al wire – Au plate ultrasonic bonding system followed the parabolic rate law. Their finding was based on samples which were thermally aged at temperatures from 250°C to 450°C and times of 30 minutes to 8 hours, in air.

Kato[21] also noticed that the relationship between the film thickness and annealing time satisfied the parabolic law when Al film-Au plate samples were exposed to an annealing temperature of 230°C. Overall, these studies show that the intermetallic compound growth follows the parabolic rate law regardless of the types of specimens used.

In addition to the effects of temperature and time on the intermetallic compound formation and growth during thermal aging, a study done by Carrass et al.[23] showed the possible effects of temperature and time used during the thermosonic wirebonding process. For the investigation of bonding temperature effect, the bonding time was fixed at 6 seconds. Carrass and his coworker confirmed that the growth of intermetallic compounds on the Au-Al bond contact followed the parabolic rate law when higher bonding temperatures, above 200°C, were used. In cases when the bonding temperatures ranged between 30°C and 150°C, the thickness of the intermetallic compounds did not correspond to the theoretical values obtained from the rate equation shown in Equation (1), based on the rate constant and activation energy values determined by Philofsky.[12]

They also reported the effect of bonding time on the intermetallic growth at the interface between the Au wire and the Al bond pad. They noticed that the amount of

intermetallic compounds formed at the interface increased logarithmically with bond time, which ranged from 2 ms up to 10 ms. As bond time exceeded 10 ms, no more intermetallic compounds were formed across the interfacial area. The intermetallic compounds covered approximately 78% of the bonding area and the amount stayed constant. They also noticed that there was no significant effect of bond time on the thickness of the intermetallic layers.

Overall, Carrass' study indicates that bond times and bond temperatures do not influence the intermetallic layer thickness when the temperature is below 150°C. Their results were also found to be contrary to the theoretical values, which was based on the parabolic rate law. Based on the results that Carrass and his coworker obtained, the rate law seems to work well in the thermal aging of Au-Al binary alloy systems rather than in wirebonding processes, which can be influenced by other parameters such as ultrasonic power, ultrasonic frequency, preheat temperature, etc.

Many researchers also obtained thermal activation energies for the growth of Au-Al intermetallic compounds. As shown in Table 8, there are variations in the activation energy determined. The variations seem to arise from various specimens used for the measurement and different initial conditions applied for the bonding process. In general, an activation energy of approximately 0.5-1.1 eV of energy is required to grow Au-Al intermetallic compounds, regardless of variations in sample preparation.

Table 8. Thermal activation energies for the growth of Au-Al compounds obtained by previous researchers.

Researcher	Specimen	Activation Energy (eV)
Onuki and Koizumi[3]	Au-wire, Al-film (electrode)	1
Kashiwabara and Hattori[11]	Au-Al wire couples	0.78
Weaver and Brown [12]	Au-Al films	1
Philofsky[12]	Au-Al wire couples	0.69
Galli and Majni[19]	Au-Al films	1.2±0.1
Charles et al.[25]	Thermosonic Au-Al bond	0.56
Chen[26]	Ultrasonic Al-Au bond	0.55
Onishi and Fukumoto[27]	Au-wire, Al-film	0.88

2.4 Kirkendall Voids

It is known that Kirkendall voids, induced by interdiffusion between Au and Al at the bond interface, increase the likelihood of bond failure.[3,27] Generally, Kirkendall voids form when the atomic flux across the interface of one species exceeds the flux in the opposite direction of the second species. As a result, vacancies build up and condense to form Kirkendall voids. Since the formation of Kirkendall voids is influenced by diffusion, differences in the diffusion samples and thermal aging conditions can cause variations in the formation rate of Kirkendall voids.[12]

In the case of Au-Al diffusion couples, Kirkendall voids form when either Au or Al diffuses out of one area faster than it can diffuse in from the other side of that area. In addition, Al is assumed to diffuse faster than Au.[12] This phenomenon is indicative of higher solubility and diffusivity of Al in the Au-Al diffusion system.

The formation of Kirkendall voids requires high temperature heat treatment.[7] Philofsky[12] found the formation of voids in primarily two phases, Au_5Al_2 and $AuAl_2$.

He reported the occurrence of voids in the Au_5Al_2 phase after thermal aging at temperatures higher than 300°C for more than one hour. When the aging temperature was above 400°C, voiding was found in $AuAl_2$. Azumawari et al.[28] also reported seeing Kirkendall voids in thermosonic Au-Al bonds. They reported that Kirkendall voids developed between the gold ball and the intermetallic layers. The specific intermetallic layers involved in the formation of Kirkendall voids were not identified. Trigwell et al.[24] also reported the presence of Kirkendall voids that developed below the interface, between the intermetallic compounds and the Au ball.

Kirkendall voids induce electrical failures in microelectronic devices by blocking the electrical path. Kirkendall voids also retard the formation of intermetallic compounds in microelectronic devices and induce mechanical failures by degrading the bond strength. During the investigation for the effect of Au-Al intermetallic compounds on electrical contact resistance and mechanical strength, Gerling[27] found that Kirkendall voids led to degradation in mechanical strength and raised the contact resistance. He reported that Kirkendall voids occurred in the intermetallic layers.

Gerling identified three general bond failure modes induced by Kirkendall voids.[3,27] First, Kirkendall voids form around the perimeter of the bond and restrict the electrical conduction path. As a result, the contact resistance is raised. This mode is usually seen in the Al metallization, the thickness of which ranges between 1.0 and 1.8 μm. Second, Kirkendall voids lead to electrical bond failure, causing an increase in the contact resistance. In this case, the intermetallic compounds form outside of the bond area and the formation of Kirkendall voids follow. Third, Kirkendall voids form

underneath the bond causing a decrease in the bond strength and finally lead to mechanical failure.

It was also reported that high temperature heat treatments induce microcracking in the intermetallic layers. Specifically, the microcracks are known to nucleate at the regions of high thermal stress in the intermetallic compounds.[12] These microcracks are often confused with Kirkendall voids, which occur due to the coalescence of vacancies produced by interdiffusion between elemental metals or alloys. Philofsky[12] noticed the formation of microcracks when the bulk couples were thermally aged at 400°C for 10 hours. The cracks were observed in the Au_5Al_2 phase.

Microcracking is considered to occur due to various volume changes between the intermetallic phases formed between Au and Al.[29] The volume change upon the formation of intermetallic compounds at the interface between Al wire and Au film was investigated by Kashiwabara and Hattori.[11] They observed a large increase in volume when AuAl was formed. The volume change was identified compared to the volume of Au and Al, which was calculated based on crystal structure and lattice parameter prior to the formation of intermetallic compounds. As for the interface between Au wire and Al film, Kato[29] calculated the volume change due to the intermetallic compound formation. The volume of intermetallic compounds was compared to the total volume of Au and Al. In addition, the thickness of Au-Al intermetallic compound was compared to that of Al film. The study showed that among $AuAl_2$, AuAl, and Au_4Al, Au_4Al had the largest variation in thickness. There was a five fold increase in the thickness of the intermetallic layer, compared to the thickness of Al. However, the molar volume of Au_4Al was found

to be smaller than the sum of those of Au and Al, but larger than that of Al. This observation was not specifically explained by Kato in his report. Variations in volume for two other intermetallic compounds, Au_2Al and Au_5Al_2, were not investigated in both studies performed by Kashiwabara et al. and Kato.

As related to the presence of microcracks in certain intermetallic phases, Philofsky[12] mentioned about the brittle nature of intermetallic compounds. He assumed that microcracks occurred at regions of high stress in the intermetallic compound layers since the intermetallic compounds were brittle. However, no data were presented to support his statement regarding the brittleness.

Overall, early studies agree that Kirkendall voids, which degrade the bond strength, are temperature and time dependent. The microcracks, induced by volume change in the formation of intermetallic compounds, are also influenced by temperature. In addition, earlier studies reported that Kirkendall voids and cracking occurred in the intermetallic layers. Thus, it is concluded that controlling temperature and time in bonding and aging processes can keep the wirebonds from degrading mechanically and electrically.

So far, various aspects of Au-Al intermetallic compounds have been discussed, from a thermosonic (Au-Al) wirebonding perspective. In Section 2.1, the formation of Au-Al intermetallic compounds and their properties were discussed in general. The formation of Au-Al intermetallic compounds is based on the interdiffusion between the pure components, Au and Al. This interdiffusion occurs because it decreases the Gibbs free energy in the binary alloy systems. According to the phase diagram[9], five Au-Al

40

intermetallic compounds, $AuAl_2$, $AuAl$, Au_2Al, Au_5Al_2, and Au_4Al, are possible. Each Au-Al intermetallic compound has its own characteristic physical properties, i.e., melting point, crystal structure, color, hardness, coefficient of thermal expansion, and resistivity.

The formation and growth of Au-Al intermetallic compounds, reported by early researchers, were reviewed in Section 2.2. Early studies showed that the dominant phase was Au_5Al_2 regardless of the types of diffusion couples and thermal aging conditions. It was found that time and temperature were primary factors influencing the types of Au-Al intermetallic compounds formed in a given Au-Al binary alloy system. Depending on the amount of starting materials, Au and Al, the kind of intermetallic compound formed under specific heat treatment can vary. Based on the review of early studies, Au_4Al was expected to be the final phase formed in the thermosonic Au-Al wirebonding system. The formation and growth of Au-Al intermetallic compounds were found to vary with the kind of specimens, sample preparation process, and conditions for heat treatment.

The kinetics of intermetallic compounds was discussed in Section 2.3. The growth rate of Au-Al intermetallic compounds follows a parabolic rate law, regardless of the kind of diffusion sample and thermal aging condition. However, it was found that the rate law worked better in the thermal aging of Au-Al binary alloy systems rather than in the wirebonding process.

Finally, the formation of Kirkendall voids and microcracks were discussed in Section 2.4. The formation of Kirkendall voids was found to be dependent on temperature and time. The formation of microcracks was induced by volume change in the formation of Au-Al intermetallic compounds and also dependent on temperature.

Both Kirkendall voids and microcracks, present in the intermetallic layers, were found to degrade the bond strength.

CHAPTER 3

Research Objective

Thermosonic wirebonding is the most widely used method for chip level interconnection. This technology is considered to be the most probable candidate for the fine pitch applications since wirebonding is more cost effective than other interconnect technologies, such as TAB and flip chip, at this time.

Thermosonic wirebonding involves a thin wire, which is attached to the metal film in the bond pad. Primary materials used for the current wirebonding are Au wire and Al metallization of the bond pad. When the two metals are bonded in the process of interconnection, Au-Al intermetallic compounds are formed due to the alloying reactions occurring at the bond interface.

Variations in the intermetallic compound formation and growth at the interface of Au wire and Al bond pad are expected as the environmental conditions surrounding the wirebonded devices are changed. The compositions of the intermetallic compounds will vary and the bond strengths are therefore expected to change.

The main objective of this study was to investigate the reliability of "encapsulated wirebonding", and compare it to standard wirebonding, for devices with Al metallurgy, under various thermal aging conditions.

CHAPTER 4

Experimental Methodology

4.1 Experimental Overview

The experimental work undertaken was divided into two major sections, sample preparation and sample evaluation. The sample preparation consisted of three parts: wire bonding, wire ball diameter measurement, and thermal aging of samples. The samples were evaluated by measuring the ball shear and bond pull strengths, investigating lifted balls, and examining the bond interface via metallographic cross-sections. The overall experimental procedures with the corresponding equipment have been summarized in a flow chart, as shown in Figure 9. The details for each of the above are contained in the following sections.

The investigation of Au-Al intermetallic compound formation, as it related to the reliability of the two types of fine pitch devices, was divided into five experiments. The first four experiments were considered as preliminary studies. The results obtained from the four experiments were incorporated into designing the extensive fifth experiment. The test matrix for each experiment is summarized in Table 9. As compared in Table 9, there are variations in the experimental conditions between the five experiments. Each preliminary experiment was carried out by varying one or more of the following bonding and/or thermal aging parameters: source of die, bonding temperature, aging temperature, aging time, oven for thermal aging, and wirebonding technique.
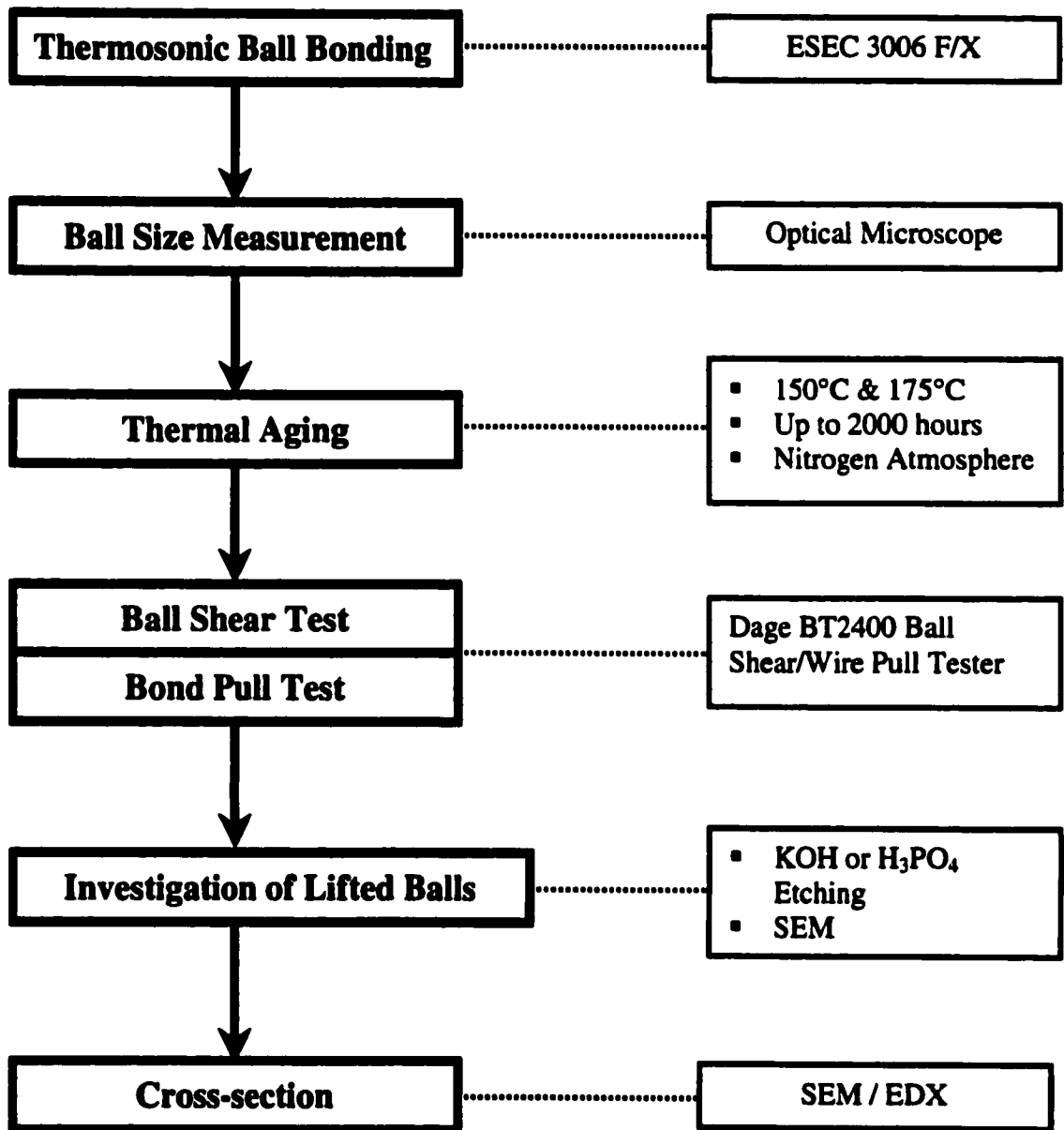
Figure 9. Flow Chart for Experimental Procedures.

Table 9. Description of each experiment with 296 CPGA, Cyrix MII.

Exp. No.	Source of Die	Source of Oven	Bond Temperature (°C)	Aging Temperature (°C)	Aging Time (hour)	WB Technique
1	SC	PTG	250	175	250	Std
						Encap
2	SC	RG	250	175	24 – 250	Std
						Encap
3	SC	RG	250	150	24 – 96	Std
						Encap
4	SG	RG	200	175	24 – 96	Std
			250			
5	SG	RG	200	150	24 – 2,000	Std
						Encap
				175	24 – 2,000	Std
						Encap

Experiments 1 to 3 were carried out to examine the effect of the different wirebonding techniques on the bond strength. Comparisons of the bond strengths were made between standard wirebonds and encapsulated wirebonds at a given thermal aging condition. In Experiment 4, two batches of standard wirebonds were compared, to study the effect of bond temperature on the bond strengths. Based on the results obtained from Experiments 1 to 4, Experiment 5 was performed to compare the bond reliability of standard and encapsulated wirebonding processes, employing prolonged thermal aging times up to 2,000 hours at the two aging temperatures, 150°C and 175°C.

4.2 Test Vehicle and Preparation

Two sets of identical packages were employed for the comparison study between standard wirebonding and encapsulated wirebonding processes. Ceramic packages, 296 I/O CPGA, with CMOS8 (0.25 µm) Cyrix MII processors produced by National

Semiconductor, as shown in Figure 10, were used as test devices. The dies were from either the Santa Clara (SC) or the Singapore (SG) facility of National Semiconductor. Every package was argon plasma cleaned for 15 minutes at 100°C before wirebonding. 99.99% pure gold wire with a diameter of 25.4 μm (1 mil) was thermosonically wirebonded to the 2 μm thick bond pad of aluminum/0.5% copper. A Model ESEC 3006 F/X wirebonder equipped with standard and encapsulated capillaries was used to bond 201 wires per sample package. The representative bonding process parameters applied for both types of wirebonding processes, i.e., standard and encapsulated wirebonding, are summarized in Table 10. The wirebonds produced by each technique are simply referred to as either standard or encapsulated wirebonds from this point forward. The bonding temperature used for the two types of wirebonding processes was either 200°C or 250°C, depending on the particular experiment.
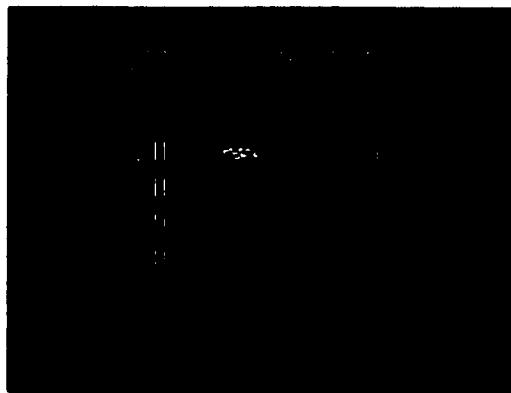
Figure 10. Top view of ceramic package, uncapped, 296 I/O CPGA with CMOS8 (0.25 μm) Cyrix MII (Package Dimension: 4.95 cm x 4.95 cm).

Table 10. Bonding parameters applied for standard and encapsulated wirebonding processes.

Bond Parameter	Standard	Encapsulated
Ultrasonic power (%)	13	13
Bond force (mN)	200	100
Bond time (ms)	14	14

After wirebonding, the ball diameters of 40 wires per sample were measured with an optical microscope. The average ball diameter and standard deviation for both types of wirebonds were determined. The samples were then thermally aged either at 150°C or 175°C for up to 2,000 hours in a nitrogen purged oven. The aging temperature and time were varied, depending on the particular experiment. Two ovens were used for thermal aging of the specimens. Both were Blue M Model POM7-336F-2X bake ovens. One was located in the premises of the Package Technology Group, and therefore designated as "PTG". The other was located in the premises of the Reliability Group, and designated as "RG". Samples were retrieved at the following test time points for inspection and bond strength measurement: 0, 24, 48, 96, 144, 250, 500, 750, 1,000, 1,250, 1,500, 1,750, and 2,000 hours.

4.3 Bond Strength Measurement

At each aging time, the bond pull and the ball shear tests were carried out on 40 wires around the four sides of the die in each package, in order to investigate the strength of the ball bond and characterize the interface between the Au wire ball and the Al bond pad. A Dage BT2400 Ball Shear/Wire Pull Tester, which enables the operator to record the failure mode of each wire during the pull and shear tests, was used. The failure

modes determined during the tests were visually confirmed by examining each bond pad under an optical microscope and the appropriate failure modes were assigned. The failure modes of the bond pull and the ball shear tests, based on JEDEC and military standards,[30,31] were employed. The failure modes are summarized in Table 11 and also shown in Figures 11 and 12.

Table 11. Failure modes for the bond pull and ball shear tests based on the JEDEC and military standards.[30,31]

Failure Mode	Bond Pull Test	Ball Shear Test
1	Ball lift	Ball shear
2	Wire neck break	Ball lift
3	Break in mid-span	Ball shear – leaving gold on pad
4	Wedge neck break	Cratering
5	Wedge lift	Ram contacts substrate

The bond pull test gives relative bond strength. The bond strength is assumed to be higher than that of Au wire if there are enough Au-Al intermetallic compounds formed at the interface and there is no bond degradation due to Kirkendall voids and/or microcracks. This test also shows the weakest point in the whole Au-Al wirebond system. Specifically, each failure mode corresponds to the weakest point and the relative pull strength is obtained at the breakage point.

The ball shear test provides insights into the bond structure quality. The ball shear strength is expected to increase with increase in the Au-Al intermetallic area. Based on the shear failure mode, the actual shear plane, i.e., Al, Au, or the intermetallic compounds, can be determined. In this study, each ball shear force was measured and then converted to the ball shear stress by dividing it by the ball size. This permits valid comparisons that take into account variations in the ball size.

a. Failure Mode 1 – Ball lift

b. Failure Mode 2 – Wire neck
breaks

c. Failure Mode 3 – Wire breaks
in mid-span

d. Failure Mode 4 – Wedge neck
breaks

e. Failure Mode 5 – Wedge lift
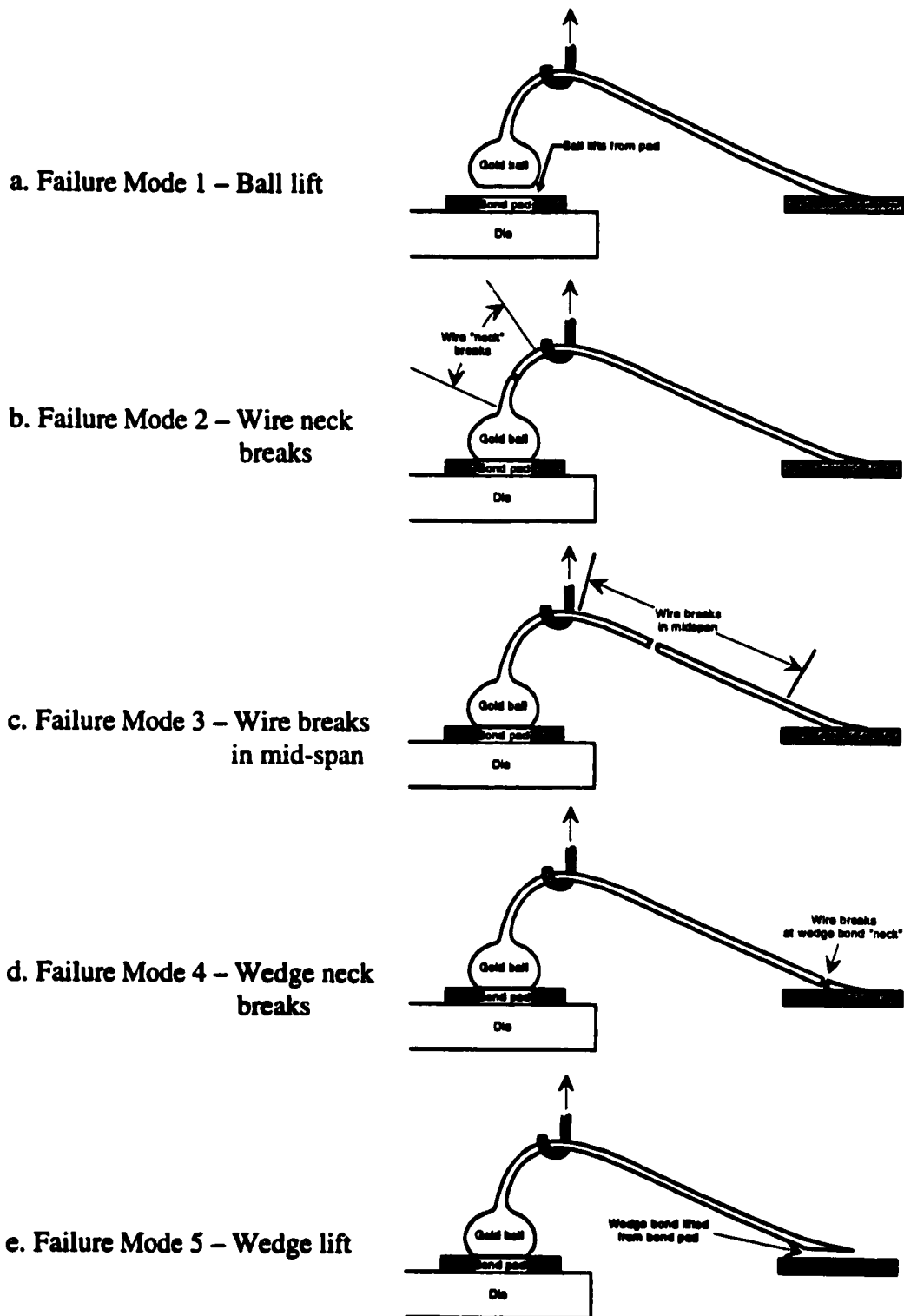
Figure 11. Failure Modes of the Bond Pull Test.
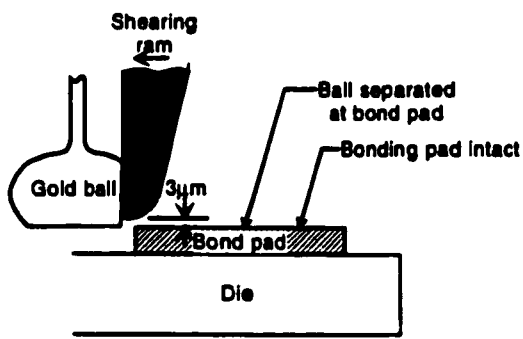
a. Failure Mode 1 – Ball lift
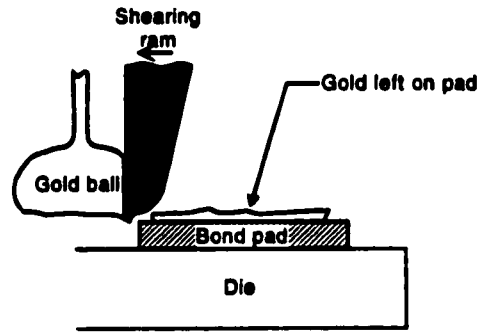
b. Failure Mode 2 – Ball shear
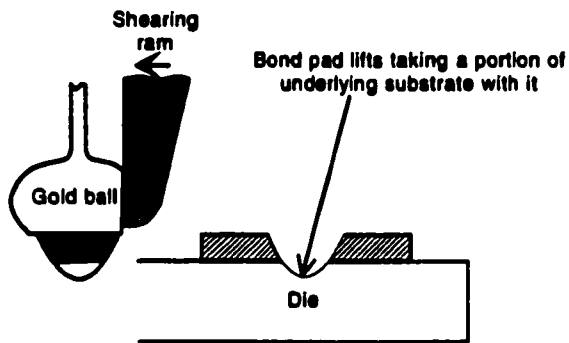
c. Failure Mode 3 – Cratering
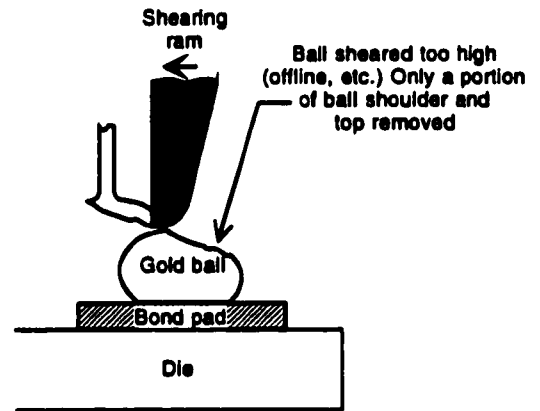
d. Failure Mode 4 – Wire shear
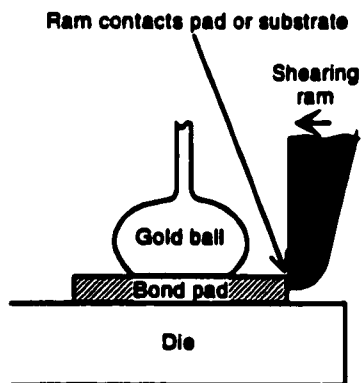
e. Failure Mode 5 – Ram contacts substrate

Figure 12. Failure Modes of the Ball Shear Test.

4.4 Investigation of Lifted Balls

For the characterization of the bond contacts with aging time, a ball lift method was employed, using either potassium hydroxide (KOH) solution or phosphoric acid (H_3PO_4) solution as follows.[22,23,32]

KOH Metal Etch

1) The sample packages were soaked in 10% potassium hydroxide (KOH) solution for 15 minutes under ultrasonic agitation to etch the Al on the wirebond interface.

2) The samples were rinsed in deionized water for 5 minutes under ultrasonic agitation.

3) A few drops of acetone solution were used on the cleaned samples for rapid drying in air.

H_3PO_4 Metal Etch

1) The sample packages were soaked in a beaker containing a 85% phosphoric acid (H_3PO_4) solution, which was placed on a heater block so that the temperature of the solution was stabilized at 80°C.

2) The samples were left in the solution for approximately 2 hours.

3) The samples were then rinsed in deionized water, in acetone, and then dried in air.

After the chemical treatment the balls were loosened and then easily lifted using a very fine needle. The bottom surfaces of 5-10 lifted balls per sample were examined using scanning electron microscopy (SEM). The etch-resistant intermetallic compounds formed at the interface of the gold ball and the aluminum bond pad were observed. Based on the SEM photos of the lifted balls, the percentage of Au-Al intermetallic compounds to the ball size was evaluated using a square grid sheet.

This method allowed determination of the relationship between the bond strength and the ball area covered by the intermetallic compounds during bonding and thermal aging. Since temperature and time influence the formation and growth of the intermetallic compounds, the ratio is expected to vary with thermal aging temperature and time.

4.5 Cross-sectioning

For the investigation of the formation of the intermetallic compounds during the two bonding processes, the wirebonds were cross-sectioned right after bonding. Additional metallographic examinations of the intermetallic layer growth were performed on the cross-sectioned wirebonds aged at two different temperatures, 150°C and 175°C, for 500, 1,500, and 2,000 hours. The bond interfaces of the cross-sectioned samples were examined under an optical microscope and a scanning electron microscope (SEM). Examinations of the samples with energy dispersive x-ray (EDX) allowed evaluation of the intermetallic phases formed, as a function of aging time and temperature. It also provided information about the intermetallic layer thickness uniformity and the thickness of Al layer consumed during the alloying reaction. For the intermetallic growth rate evaluation, four Au ball bonds on each package were cross-sectioned. The intermetallic layer thickness was measured at five different locations across the bond. The average and standard deviation values were obtained based on a total of 20 thickness values measured for each package. A SEM micrograph from a cross-sectioned ball bond, as shown in Figure 13, illustrates the procedure used for the thickness measurements. As shown in Figure 13, the thicknesses for the intermetallic layers were measured, using a

53

ruler, on the two areas around the ball periphery, two areas located at 1/3 distance from each side of the ball perimeter and one area in the middle of the ball bond. The values obtained were converted using the scale shown at the bottom of the SEM micrograph. In addition, metallographic examinations of the cross-sectioned samples enable investigation of the primary reasons causing bond strength degradation, if there is any. For example, microcracks and/or Kirkendall voids present in the intermetallic layers can be visually detected.
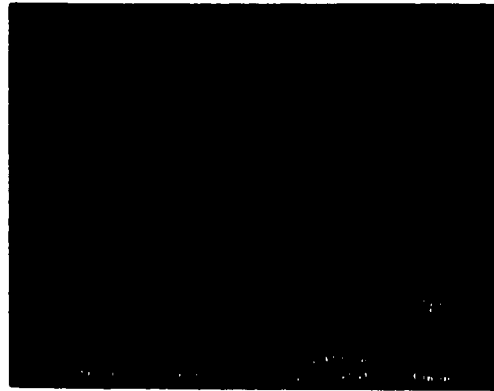
Figure 13. Cross-section of the ball bond showing the interface. Intermetallic thickness was measured on five different regions across the bond (Magnification: 1500x).

The bond interfaces of cross-sectioned samples were quantitatively analyzed employing energy dispersive x-ray (EDX) spectroscopy. The purpose of this analysis was to determine the composition of the intermetallic layers at the interface. For the identification of stoichiometry of the intermetallic compounds, a linescan was performed at a region which was 27 μm distant from the left edge of the ball bond, as shown in Figure 14. The linescan started from the Au rich region, which was 10 μm distant from the Al bond pad, continued across the interface, and stopped at the region near the bottom of Al bond pad. The spot size for the linescan was approximately 1 μm. EDX analysis

across the bond interface provided information on compositional changes in the intermetallic compounds as related to specific aging times and temperatures. In addition, the specific intermetallic compound could be identified and correlated with any degradation in the bond strength.
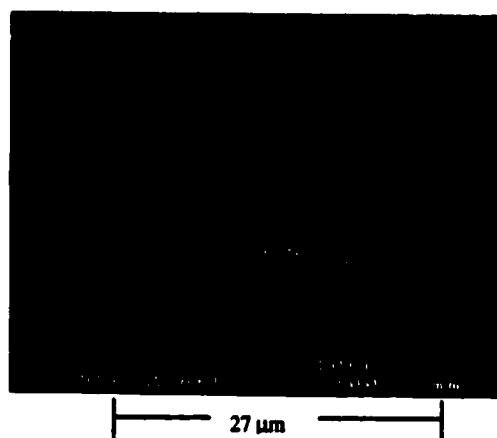
Figure 14. A SEM micrograph showing the points for EDX linescan across the intermetallic interface. The numbers, 1 and 2, indicate the starting and end points (Magnification: 2300x).

4.6 Student Two-tail *t*-test

All test results obtained for the standard and "encapsulated" wirebonding processes were compared statistically, employing a two-tail *t*-test at the 95% confidence level. This permitted valid comparisons between the two wirebonding technologies.

CHAPTER 5

Results and Discussion

The investigation of Au-Al intermetallic compound formation, as it related to the reliability of two types of fine pitch devices, was divided into five experiments. The first four experiments, Experiments 1 through 4, were considered as preliminary studies. The results obtained from the four experiments were incorporated into planning an extensive fifth experiment, Experiment 5. The results obtained from each preliminary experiment are discussed in Section 5.1. Results of preliminary experiments are compared to each other and discussed in Section 5.2, followed by the results and discussion of Experiment 5 in Section 5.3.

5.1 Results of Preliminary Experiments: Experiments 1 through 4

Experiments 1 through 3 were carried out to examine the effect of different wirebonding techniques on the bond strength. Comparisons of the bond strengths were made between standard wirebonds and encapsulated wirebonds after thermal aging, as described in Table 9. In Experiment 4, two batches of standard wirebonds were compared to study the effect of bond temperature on the bond strengths. The results of each experiment are presented and discussed in Sections 5.1.1 through 5.1.4, for Experiments 1 through 4, respectively.

5.1.1 Experiment 1

Experiment 1 was performed to investigate the effect of different wirebonding techniques, standard wirebonding as opposed to encapsulated wirebonding, on the bond strength. Standard and encapsulated wirebonds were thermally aged at 175°C for 250

hours. Sample parts were tested right after bonding and after 250 hours of thermal aging. The bond pull and ball shear strengths for both types of wirebonds were measured and compared to each other.

5.1.1.1 Bond Pull Strength

Standard and encapsulated wirebonds, thermally aged at 175°C for 250 hours, were evaluated using bond pull and ball shear tests. The results are plotted in Figures 15 through 20. As shown in Figure 15, both standard and encapsulated wirebonds showed a decrease in the average pull force. After 250 hours of aging, large variations in the pull force were observed. A Student t-test performed at the 95% confidence level indicated that the pull forces for standard wirebonds were statistically different from those for encapsulated wirebonds. However, the force values for both types of wirebonds were not statistically different from each other at 0 hour, before thermal aging. This indicated that thermal aging at 175°C influenced the bond strength for both types of wirebonds.

Failure modes of the pull test obtained from standard and encapsulated wirebonds were recorded and plotted in Figures 16 and 18, respectively. The corresponding average pull forces for each failure mode were plotted as a function of aging time in Figures 17 and 19 for standard and encapsulated wirebonds, respectively. In the case of standard wirebonds, the frequency of Mode 1 Failure, ball lifting, increased as aging time increased, as can be seen in Figure 16. However, none of the wirebonds had Mode 1 Failure before thermal aging began. In contrast, the frequency of Mode 2 Failure, wire neck breaking, decreased with aging time; before thermal aging at 175°C, all wirebonds showed Mode 2 Failure. The corresponding average pull forces for both failure modes

are shown in Figure 17. Large variations were found in the force for Mode 1 Failure. The average pull force for Mode 2 Failure did not change, as shown in Figure 17.
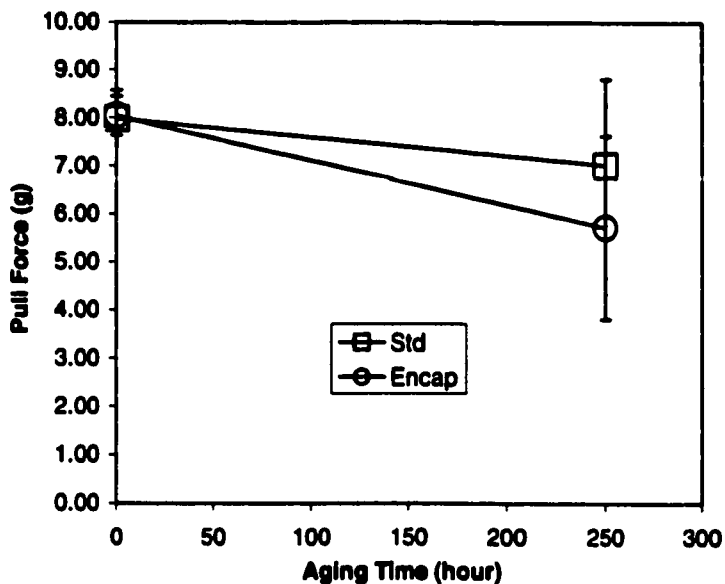
Figure 15. Pull force as a function of aging time for both types of wirebonds at 175°C.

Similar results in the failure modes were obtained for encapsulated wirebonds as well. As shown in Figure 18, the frequency in Mode 1 Failure increased with aging time. However, there were no Mode 1 Failures at 0 hour, before thermal aging was begun. The frequency in Mode 2 Failure decreased with aging time. The frequency of this failure mode was 100% before thermal aging. The corresponding pull forces for the two failure modes are shown in Figure 19. Again, wide variations were found in the force for Mode 1 Failure, as was observed in the case of standard wirebonds. The average pull force for Mode 2 Failure did not vary with aging time.
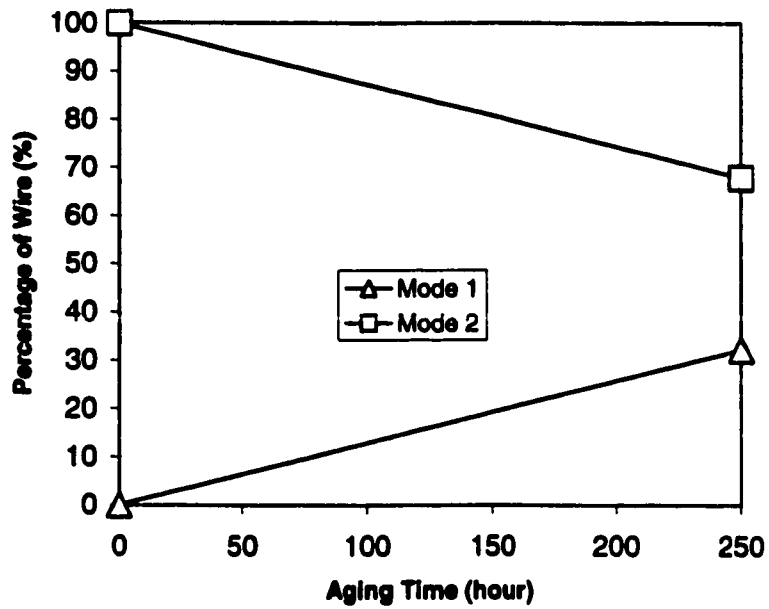
Figure 16. Pull force failure mode as a funtion of aging time for standard wirebonds aged at 175°C.
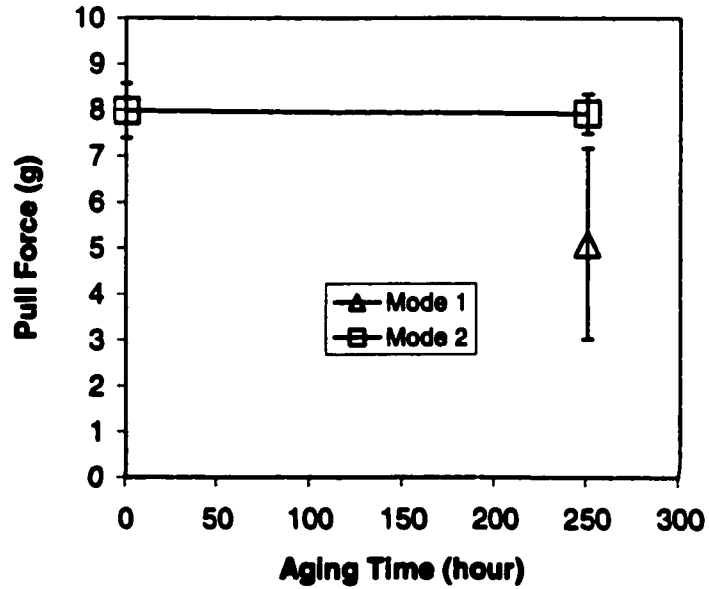
Figure 17. Pull force of each failure mode as a function of aging time for standard wirebonds at 175°C.
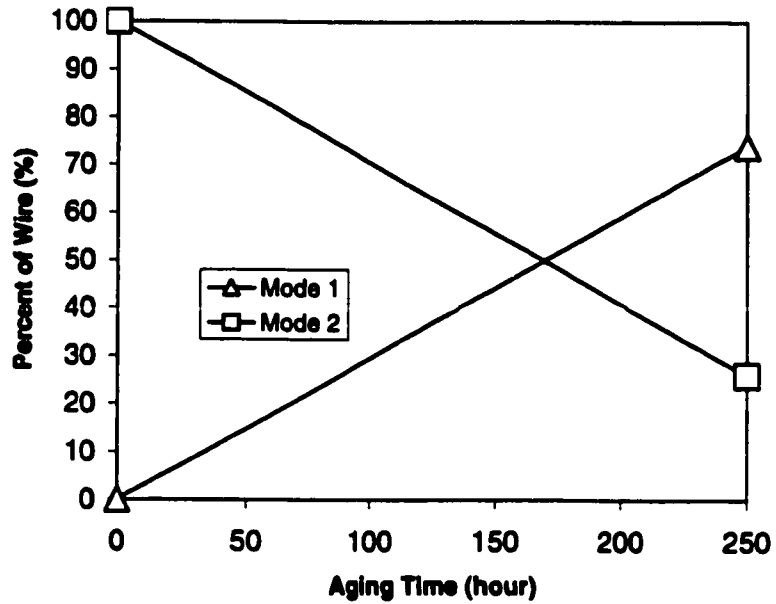
Figure 18. Pull force failure mode as a function of aging time for encapsulated wirebonds at 175°C.
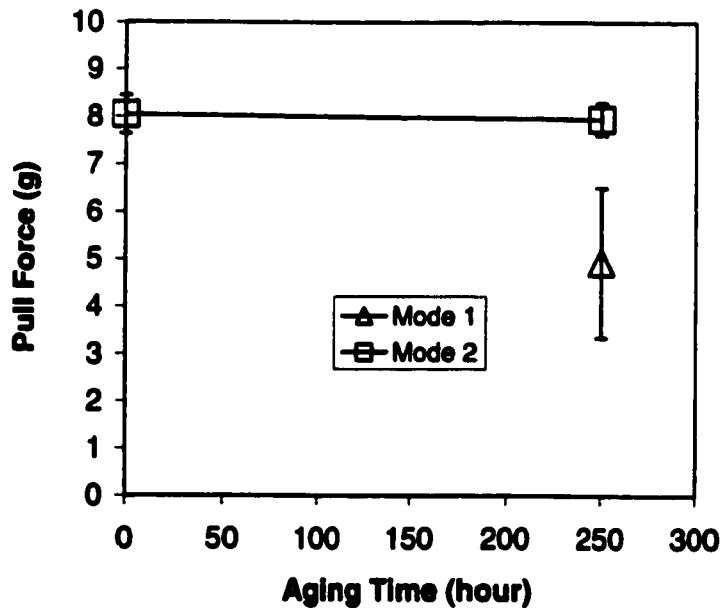
Figure 19. Pull force of each failure mode as a function of aging time for encapsulated wirebonds at 175°C.

5.1.1.2 Ball Shear Strength

The average shear strengths for standard and encapsulated wirebonds were determined and plotted as a function of the aging time, as shown in Figure 20. In the case of standard wirebonds, the average shear strength increased at the aging time of 250 hours. In contrast, the average shear strength for encapsulated wirebonds decreased from 109.58 MPa before thermal aging to 108.72 MPa after 250 hours of thermal aging. However, a t-test confirmed that they were not significantly different at the 95% confidence level. Results of t-tests, performed on the shear strengths for both types of wirebonds at 0 and 250 hours, indicated that the shear strengths for standard wirebonds were statistically different from the strengths for encapsulated wirebonds. Once thermal aging began, standard wirebonds yielded greater shear strengths.
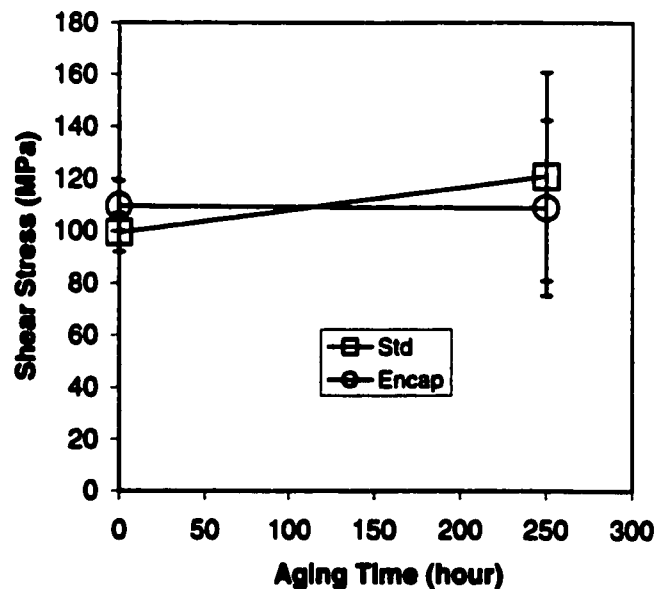
Figure 20. Shear stress as a function of aging time for standard and encapsulated wirebonds aged at 175°C bake temperature.

Overall, the pull forces for both standard and encapsulated wirebonds decreased with aging time. After 250 hours of aging at 175°C, wide variations were found in the force. Both types of wirebonds did not show Mode 1 Failure, i.e., ball lifting, before thermal aging. However, this failure mode became frequent after 250 hours of aging. Wide variations were found in the pull force for Mode 1 Failure. In contrast, the frequency of Mode 2 Failure, i.e., wire neck breaking, decreased from 100%, before thermal aging, to less than 40%, after 250 hours of aging for both types of wirebonds. However, the pull forces for Mode 2 Failure did not vary with aging time.

The shear strengths for standard wirebonds increased once thermal aging began. The strengths for encapsulated wirebonds decreased slightly after 250 hours of aging. Wide variations were found in the shear strengths for both types of wirebonds after 250 hours. Based on the pull and shear test results for both types of wirebonds, it was concluded that encapsulated wirebonding was comparable to standard wirebonding.

5.1.2 Experiment 2

Standard and encapsulated wirebonds were thermally aged at 175°C. Sample parts were removed and tested at different times, 24, 48, 96, and 250 hours. The bond pull and ball shear strengths for both types of wirebonds were measured and compared to each other at each aging time. A ball lift technique was used to investigate the intermetallic compound formation after the wirebonding processes.

5.1.2.1 Bond Pull Strength

The overall variation in wirebond pull force, as a function of aging time, was similar for the two processes, as shown in Figure 21. The average pull force for both

wirebonding processes gradually declined with aging time. The maximum pull forces, 8.1 and 8.2 g, were obtained at 0 hour for the standard and encapsulated wirebonds, respectively. One standard deviation (±1σ) scatter bands in Figure 21 indicate that the pull force of the wires from both wirebonding processes decreased as aging time increased.
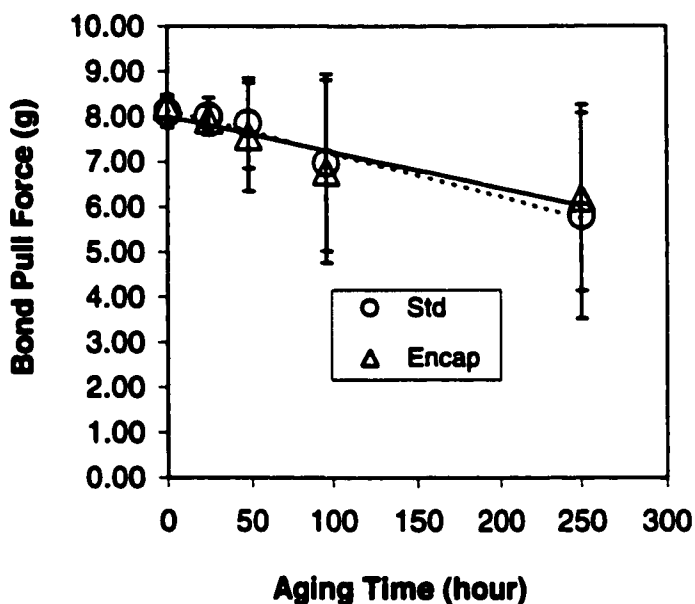
Figure 21. Bond pull force as a function of aging time for standard and encapsulated wirebonds at 175°C.

The data presented in Figure 21 were then sorted according to the failure mode. These are plotted, as a function of aging time, in Figures 22 through 25. In Figure 22 the data for the standard wirebonds are shown. At the smaller aging times, Mode 2 Failure dominated. Mode 1 Failure, ball lifting, did not occur until 48 hours of aging. After that, the frequency of Mode 2 Failure, wire neck breaking, decreased as aging time increased. By the 250 hour aging time, Mode 1 Failure was more frequent than Mode 2 Failure.
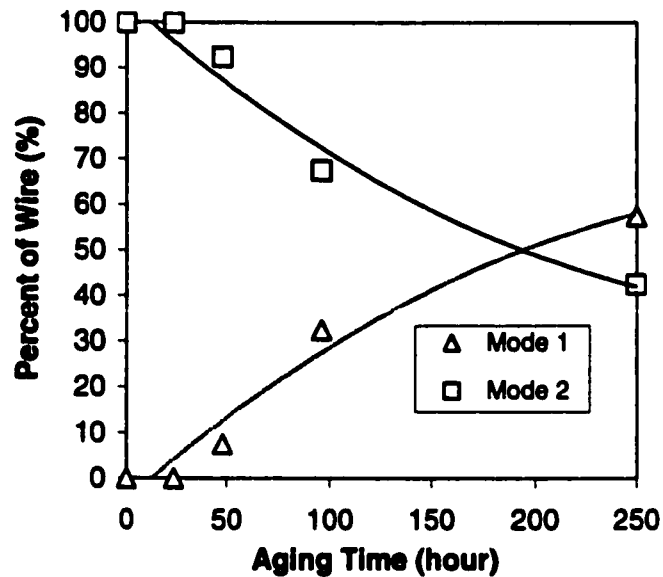
Figure 22. Bond pull failure mode as a function of aging time for standard wirebonds at 175°C.

The actual pull forces measured are plotted in Figure 23. The average pull force for Mode 2 Failure was found not to vary with aging time. Further, there was very little variation in the pull forces. This is indicative that the neck region does not undergo microstructural or metallurgical changes during the aging process. The average pull force for Mode 1 Failure decreased with increasing aging time in an asymptotic manner. Wide variations in the pull force were also found. This could be indicative of variations in the extent of intermetallic compound formation at the interface or simply the result of complex fracture patterns at this interface.

Failure modes of the bond pull test for the encapsulated wirebonds are plotted in Figure 24. The frequency of Mode 2 Failure, which consisted of 100% before aging was begun, decreased with increase in aging time. Mode 1 Failure was first observed in the 24-hour sample. As aging time increased, the frequency of Mode 1 Failure increased.
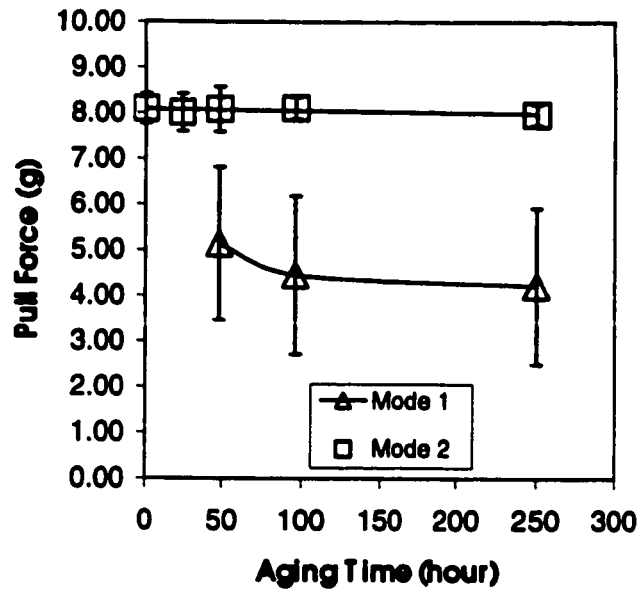
Figure 23. Bond pull force of failure mode for standard wirebonds aged at 175°C.
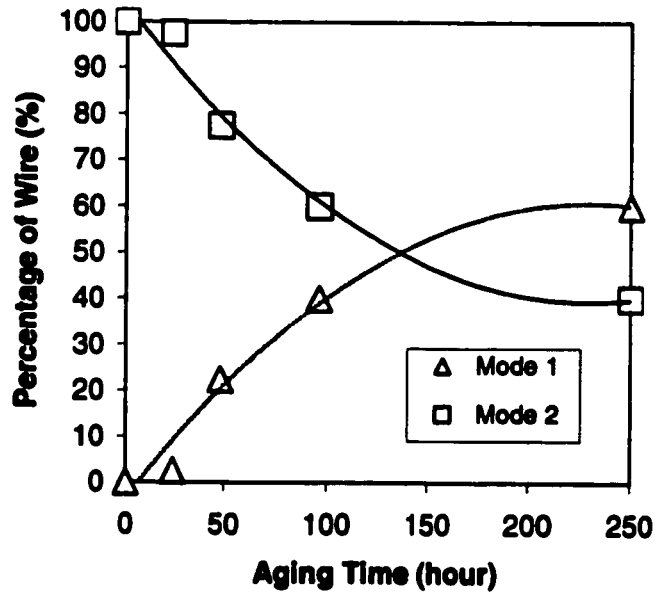
Figure 24. Bond pull failure mode as a function of aging time for encapsulated wirebonds at 175°C.

The average pull forces as a function of aging time are plotted, for both Mode 1 and 2 Failures, in Figure 25. The average pull forces for Mode 1 and 2 Failures followed the same trends observed in the standard wirebonds, when aged for up to 96 hours. The average pull force for Mode 2 Failure did not vary with aging time and there was little variation in the pull force. The average pull force of Mode 1 Failure declined, with wide variations, as aging time increased. The data from the 250-hour sample show a significant drop in the values for Mode 2 Failure and a significant rise for Mode 1 Failure. However, as can be seen from Figure 25, there were large variations in the data for this temperature, resulting in a large standard deviation. The data for 250 hours were not statistically different from the data for 96 hours for either mode failure. The wide variations in the pull force for encapsulated wirebonds are probably due to variations in the extent of intermetallic compounds formed at the interface. The bond pull forces for encapsulated wirebonds yielded the same results as for standard wirebonds, i.e., the pull force for Mode 2 Failure does not vary with aging time and the pull force for Mode 1 Failure decreases in an asymptotic manner.

The pull forces obtained from the 0-hour samples, for the standard and encapsulated processes, were found to be statistically different from each other. However, t-test comparison for other aging times showed that the bond forces obtained from the standard wirebonds are not statistically different from the values obtained from encapsulated wirebonds.
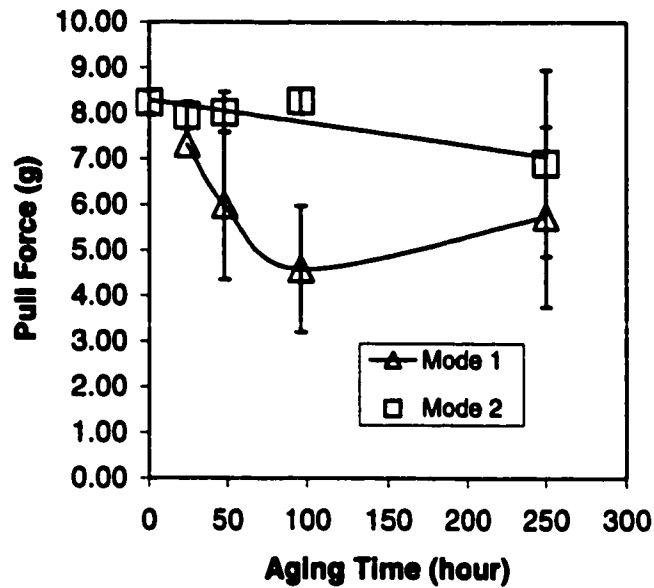
Figure 25. Bond pull force of failure mode as a function of aging time for encapsulated wirebonds at 175°C.

5.1.2.2 Ball Shear Strength

Both standard and encapsulated wirebonds showed a similar trend in the degradation of shear strength with aging time. In addition, the overall variation was found to be similar in both types of wirebonds. The average shear strength increased up to the 24-hour aging time and then gradually declined with increasing aging times, as illustrated in Figure 26. Maximum shear strengths were obtained for both types of wirebonds when aged for 24 hours. As aging time increased, so did the scatter ($\pm 1\sigma$) in the data. The data, shown in Figure 26, for the standard wirebonds reveal that the shear strength started decreasing when the wirebonds were aged longer than approximately 75 hours, i.e., the shear strength drops below the initial value of 106 MPa.
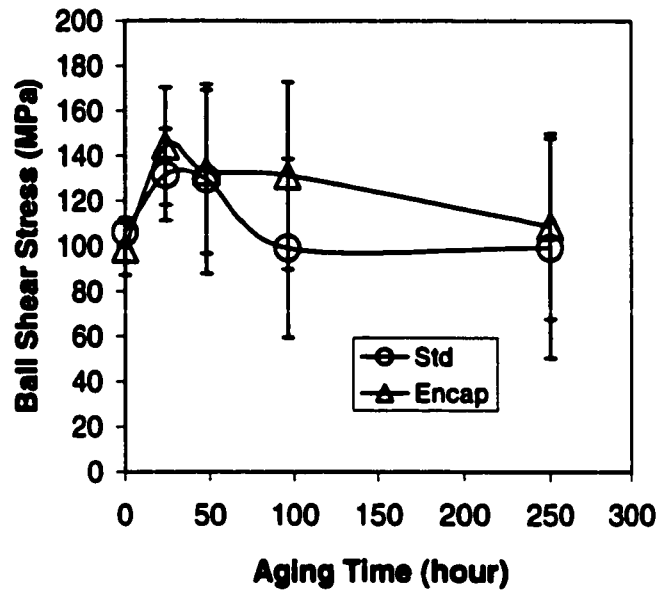
Figure 26. Ball shear strength as a function of aging time.

When comparing the shear strength data for the standard and encapsulated wirebonding processes, it can be seen that for the standard wirebonding process, samples aged for 96 hours and 250 hours had shear strengths lower than the initial value at 0 hour. In contrast, the ball shear strengths for the encapsulated wirebonding process, while still showing a decline after 24 hours of aging, do not fall to values below the initial shear strength even when aged for 250 hours. The degradation in shear strength, with aging time, appears to be slower for the encapsulated wirebonding process, as compared to the standard wirebonding process.

According to the *t*-test results for the shear strength, the shear strengths of the standard wirebonds were statistically different from the strengths of the encapsulated wirebonds at the 0, 24, and 96 hours aging times, but yielded statistically similar shear strength values at the 48 and 250 hours aging times.

5.1.2.3 Investigation of Lifted Balls

A ball lift method was employed for the investigation of area uniformity for both types of wirebonds. In this experiment, KOH etching was used to detach the Au ball from the bond pad. The overall trend in the formation of intermetallic compounds during ball bonding was similar for both standard and encapsulated wirebonding processes. The ball lift results from both types of wirebonds immediately after ball bonding are shown in Figure 27 and Table 12. The bond contacts examined under SEM revealed that a significant amount of the intermetallic compounds had formed at the interface between the gold ball and the aluminum bond pad during ball bonding.

As shown in Figure 27(a), in the standard wirebonding process, the intermetallic compounds formed and grew at the bond interface before thermal aging had begun. Some non-reacted spots, i.e., areas without the intermetallic compounds, were also observed across the bond area. Most were concentrated around the bond periphery. The average percentage of the intermetallic compounds for the standard wirebonding process, as listed in Table 12, indicates that approximately 60% of the bond area was immediately covered by the intermetallic compounds once ball bonded.

SEM micrographs of the lifted balls for the encapsulated process, as shown in Figure 27(b), showed the intermetallic compounds formed at the Au-Al bond interface during ball bonding. The intermetallic compounds were evenly spread across the bond area and non-reacted sections were found around the bond perimeter. The trend observed in the distribution of the intermetallic compounds on the bond area could be indicative of variations in the interdiffusion reaction zone at the interface.[23] Similarly, the

intermetallic compounds covered approximately 60% of the bond area when the encapsulated wirebonding process was used, as shown in Table 12.
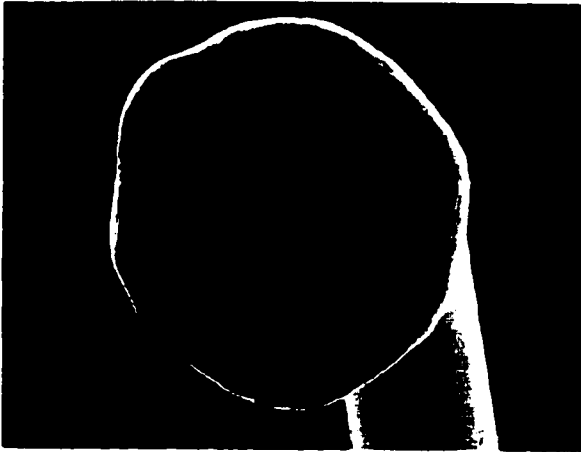
(a)
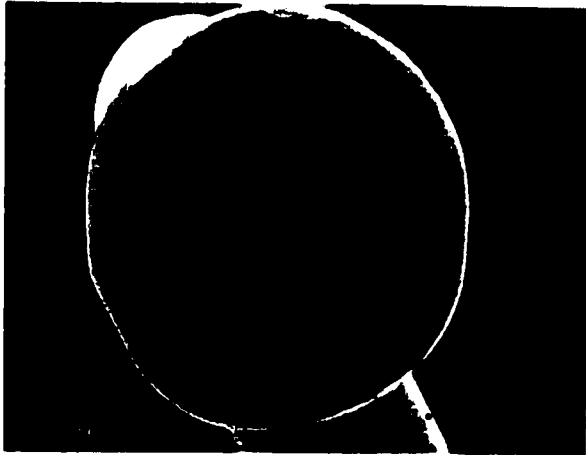
(b)

Figure 27. SEM micrographs of the lifted balls for the standard (a) and encapsulated (b) processes.

Table 12. Percentage of intermetallic compounds formed during ball bonding.

Wirebonding Process	Percentage of Intermetallic Compounds	
	Average (%)	Standard Deviation
Standard	58.90	4.88
Encapsulated	56.04	5.95

The results from the bond pull and the ball shear tests for standard and encapsulated wirebonding processes yielded insights about the bond quality when subjected to thermal exposure. The overall variations in the pull and shear strengths with aging time are probably due to the bond degradation at the interface. This could be related to various intermetallic compounds formed at the Au-Al interface and Kirkendall voiding developed in the intermetallic layers during the aging process.[12,22] Overall trends observed in the pull and shear test results, for both standard and encapsulated wirebonding processes, are in good agreement with the literature,[3] but further study with extended aging periods at 175°C is required for better comparison. Investigation of the lifted balls also revealed that both wirebonding processes produced about the same amount of intermetallic compounds during ball bonding.

The test results indicate that the reliability of encapsulated wirebonding process is comparable to the standard process. Although the encapsulated wirebonding process yielded higher values in the shear strength, additional studies employing extended aging times are required to determine whether the encapsulated wirebonding process is superior to the standard process in terms of wirebonding reliability merits.

5.1.3 Experiment 3

This experiment was performed to investigate the effect of different wirebonding techniques on the bond strength. Instead of thermal aging at 175°C, standard and encapsulated wirebonds were aged at 150°C. Sample parts were removed and tested at 24, 48, and 96 hours. The bond pull and ball shear strengths for both types of wirebonds were measured and compared to each other for each aging time.

71

5.1.3.1 Bond Pull Strength

In both types of wirebonds, the average pull strength and the corresponding standard deviation did not vary greatly with aging time, as shown in Figure 28. However, once thermal aging started, slightly higher pull strengths were obtained from standard wirebonds than from encapsulated wirebonds. Student *t*-test results indicated that the pull strengths obtained from standard wirebonds, aged for 24, 48, and 96 hours, were statistically different from the strengths of the encapsulated wirebonds.
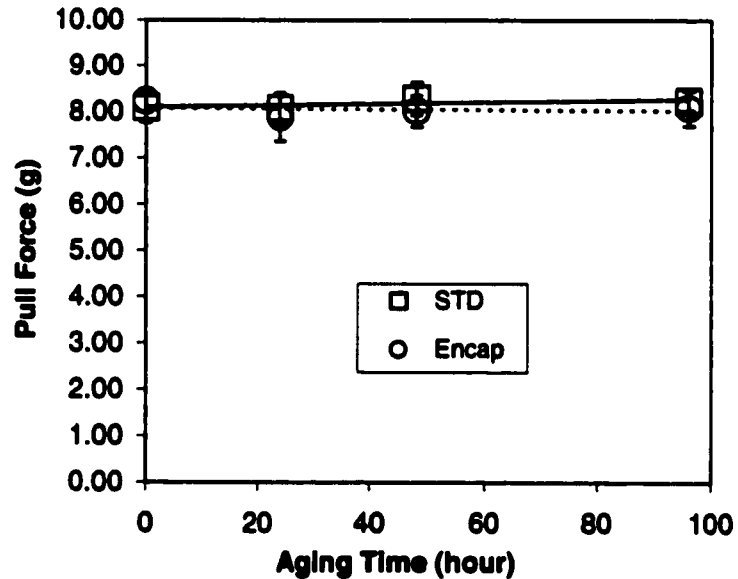
Figure 28. Pull force as a function of aging time for standard and encapsulated wirebonds at 150°C.

During the bond pull test of standard wirebonds, only Mode 2 Failure, which indicates the breaking of wire at the neck region, was observed. Variation in the average pull strength for the failure mode was small. This indicates that the neck region did not undergo any metallurgical changes during the aging process. Compared to the standard wirebonds, Mode 1 Failure, i.e., wire ball lifts, was observed in the 24 and 96 hour aged

encapsulated samples. As can be seen in Figure 29, a very small proportion of the wirebonds, i.e., one out of 40 wirebonds, failed in Mode 1 during the bond pull test for the two aging times.
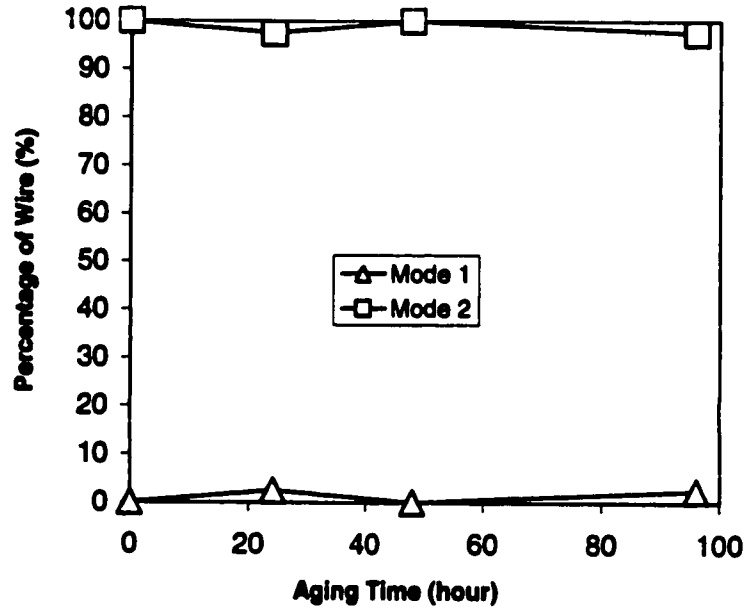
Figure 29. Pull force failure mode as a function of aging time for encapsulated wirebonds aged at 150°C.

The corresponding average pull forces for each failure mode were plotted as a function of aging time, and is shown in Figure 30. There was little variation in the average pull forces for Mode 2 Failure for the encapsulated wirebonds. The pull force did not vary with aging time. As mentioned in the case of standard wirebonds, this indicates that there were no microstructural changes in the neck region during the aging process at 150°C for 96 hours.
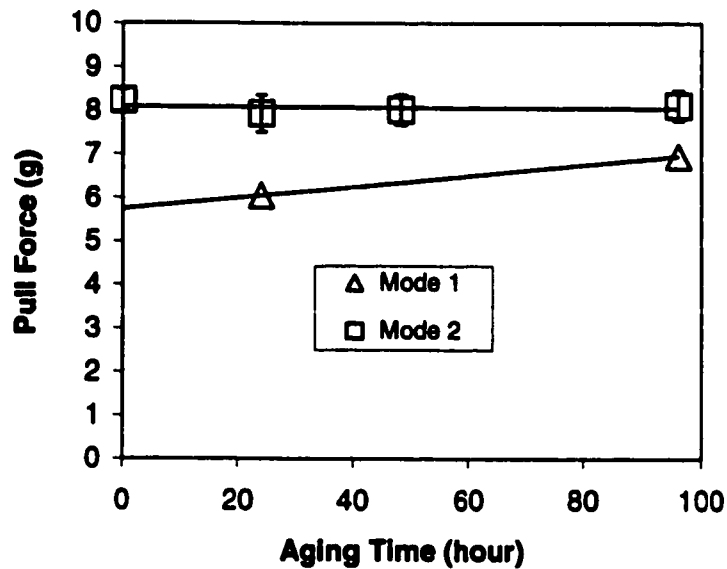
Figure 30. Pull force of failure mode as a function of aging time for encapsulated wirebonds aged at 150°C.

5.1.3.2 Ball Shear Strength

Variations in the shear strength for both standard and encapsulated wirebonds are shown in Figure 31. Both types of wirebonds followed a similar trend, in which the shear strength increased with aging time. Variation in the shear strength also increased with aging time. Overall, greater average shear strengths were obtained from encapsulated wirebonds once thermal aging started. However, *t*-test comparisons showed that for thermal aging times of 48 and 96 hours both standard and encapsulated wirebonds yielded statistically similar shear strengths. At two other aging times, 0 and 24 hours, the strengths for both types of wirebonds were found to be statistically different from each other. After 24 hours of thermal aging, greater shear strength was obtained from encapsulated wirebonds. However, the shear strength of standard wirebonds was greater than that of encapsulated wirebonds before thermal aging was begun.
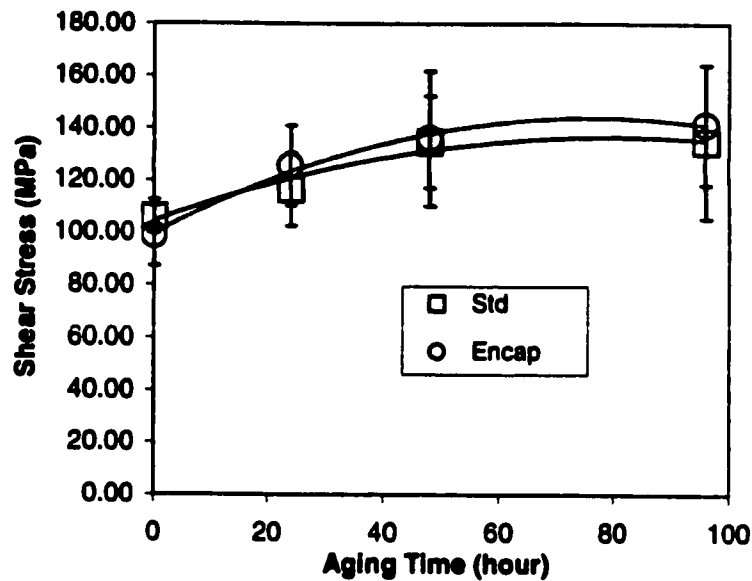
Figure 31. Shear strengths as a function of aging time for standard and encapsulated wirebonds at 150°C.

Based on the pull and shear test results obtained from standard and encapsulated wirebonds, it was found that the two wirebonding processes were comparable to each other, as related to the bond reliability merits. However, it was thought that better bond contacts were made during the standard wirebonding process than encapsulated wirebonding process, based on the bond pull failure modes obtained from both types of wirebonds.

5.1.4 Experiment 4

As shown in Table 9, only the standard wirebonding technique was employed for this experiment. The main objective of this experiment was to compare the bond strengths of two types of standard wirebonds, prepared at two different bonding temperatures: 200°C and 250°C. The wirebonds were aged at 175°C. Bond pull force and ball shear force were measured at aging times of 0, 24, 48, and 96 hours. For the

shear strength comparison, the shear force rather than the shear stress was used since there was very little variation in the ball size for both sets of standard wirebonds.

5.1.4.1 Bond Pull Strength

As shown in Figure 32, the average pull forces for the 250°C bonding temperature, were higher than those for 200°C bonding temperature. This was found to be the case for all thermal aging time periods up to 96 hours, at 175°C. The t-test results performed at each aging time revealed that the average pull forces obtained from two types of standard wirebonds were statistically different from each other at the 95% confidence level. In both types of standard wirebonds, only Mode 2 Failure, i.e., wire breaks at the neck, was found. This indicates that relatively good bonds were made at the bond interface between the Au wire ball and the Al bond pad at both bonding temperatures, 200°C and 250°C.
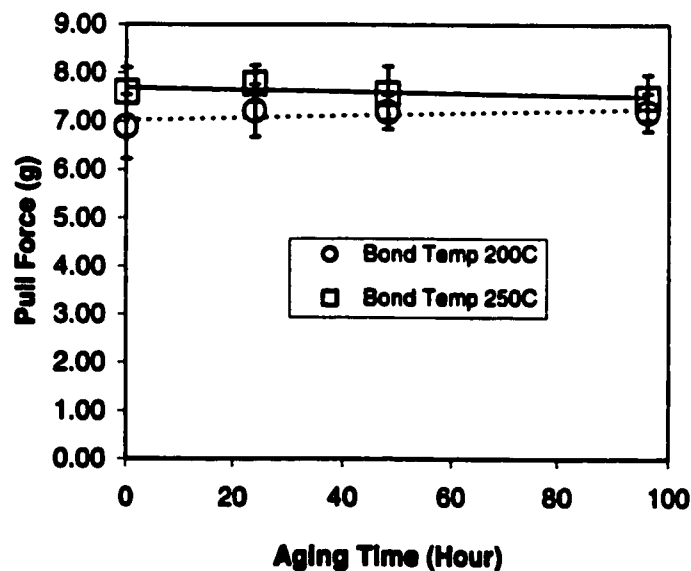

Figure 32. Pull force as a function of aging time at 175°C aging temperature.

5.1.4.2 Ball Shear Strength

The ball shear test results obtained from both types of standard wirebonds showed that the bonding temperature did not influence the shear force once the aging time exceeded 48 hours. As shown in Figure 33, variations in the shear force increased with aging time in both types of standard wirebonds. The average shear forces of the standard wirebonds formed at the 250°C bonding temperature were greater than those of the wirebonds formed at 200°C when aged for up to 24 hours. However, the difference between the shear force values for the two types of standard wirebonds decreased as aging time increased, until 96 hours. The t-test results obtained for 48 and 96 hour aging times confirmed that the shear forces of standard wirebonds bonded at 250°C were not statistically different from those of the standard wirebonds bonded at 200°C. At 0 and 24 hour aging times, the higher bonding temperature of 250°C was found to have greater effect on the ball shear force than the bonding temperature of 200°C, yielding higher force values.

Overall, the effect of bonding temperature on the bond pull force was more obvious than on the ball shear force. The standard wirebonds prepared at the higher bonding temperature, 250°C, yielded greater pull forces during the bond pull test. In the case of the shear test results, the influence of the high bonding temperature was not so obvious at aging times greater than 24 hours. The higher bonding temperature was observed to have a greater effect on the shear forces in both types of wirebonds which had been unaged and aged for 24 hours. At these two aging times, greater shear forces were obtained from the wirebonds prepared at 250°C bond temperature. In general, it

was noted that high bonding temperature enhanced the bond strength. This can be related to the interdiffusion of Au and Al, which is temperature dependent.[3]
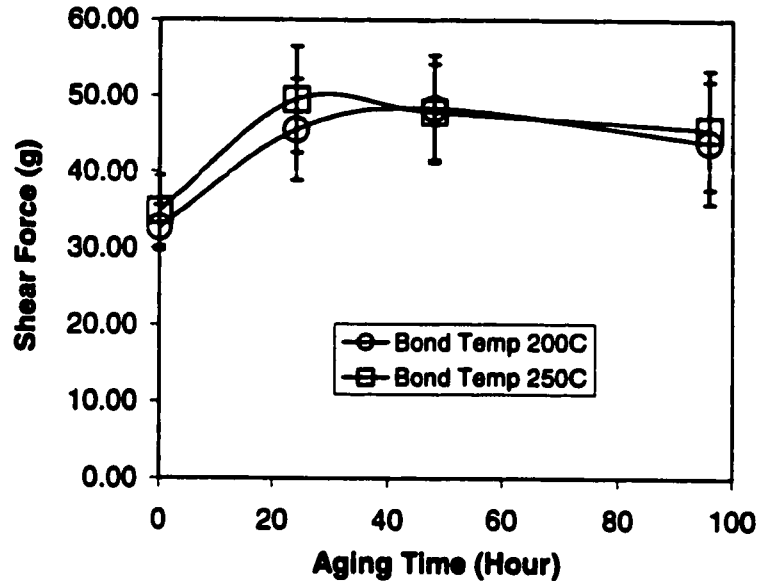
Figure 33. Shear force as a function of aging time at 175°C aging temperature for both bond temperatures, 200°C and 250°C.

5.2 Comparison between Preliminary Experiments

The results obtained from the four preliminary experiments, i.e., Experiments 1 through 4, were compared with each other and are discussed based on the bond pull force and ball shear strength performance. Comparison of the results between Experiments 1 and 2 are presented in Section 5.2.1. Results of Experiment 2 are compared with those of Experiment 3 in Section 5.2.2, followed by the comparison between Experiments 2 and 4 in Section 5.2.3.

5.2.1 Comparison of Experiment 1 and Experiment 2

The bond strength results from Experiment 1 were compared with those from Experiment 2 to determine the effect(s) of mixing ovens employed for thermal aging on the bond strength. The PTG oven was used for thermal aging in Experiment 1. In the case of Experiment 2, the RG oven was employed. In both experiments, identical specimens were thermally aged at 175°C. For this comparison, the bond pull and ball shear strengths were measured for both standard and encapsulated wirebonds. Four sets of strength data from the two bake ovens, i.e., PTG and RG ovens, were plotted as a function of aging time.

5.2.1.1 Bond Pull Strength

As shown in Figure 34, a large variation was observed between the two sets of pull force data when standard wirebonds were thermally aged for 250 hours. The *t*-test comparisons, at the 95% confidence level, indicated that the pull forces of the two sets of standard wirebonds, which were thermally aged at 175°C in two different bake ovens, were statistically different from each other, regardless of aging time. Since the two sets of standard wirebonds yielded different initial pull forces before thermal aging was begun, this comparison was inconclusive for determining the effect of mixing ovens on the bond strength.

In the case of the pull forces obtained from the two sets of encapsulated wirebonds, as shown in Figure 35, the average pull force of encapsulated wirebonds aged in RG oven was greater than that of encapsulated wirebonds aged in PTG oven before and after thermal aging. However, the *t*-test results revealed that the pull forces for
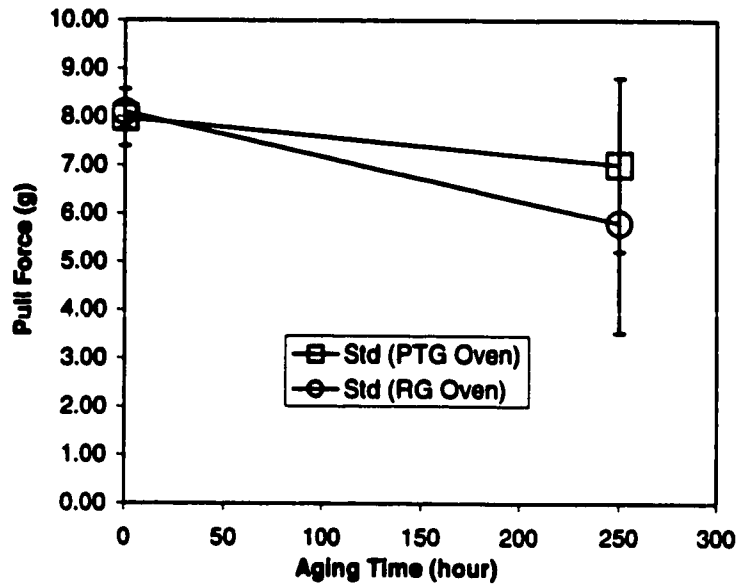
Figure 34. Pull force of standard wirebonds at 175°C as a function aging time for two different bake ovens.
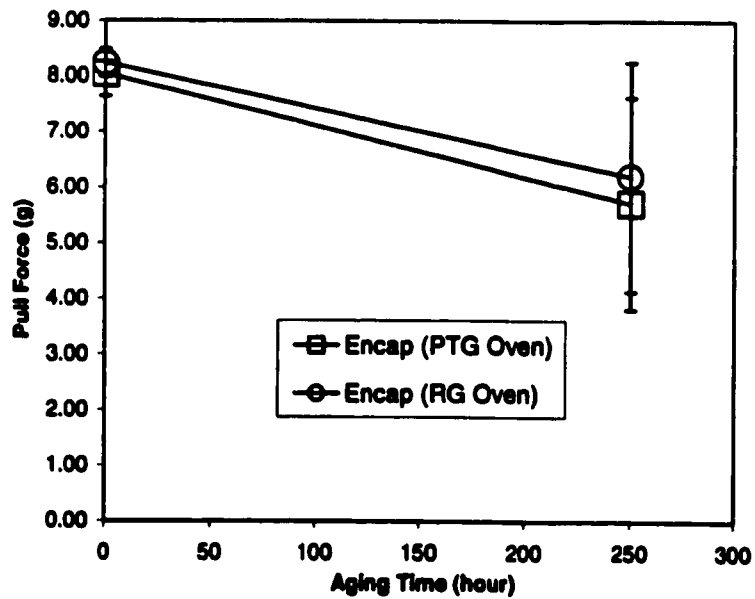

Figure 35. Pull force of encapsulated wirebonds at 175°C as a function of aging time for two different ovens.

encapsulated wirebonds from two different ovens were not statistically different. According to the observation made on the pull force data for the two sets of encapsulated wirebonds, it was concluded that mixing ovens had no significant effect on the bond strength degradation.

5.2.1.2 Ball Shear Strength

The shear strengths of standard wirebonds from the two types of bake ovens were plotted as a function of thermal aging time, as shown in Figure 36. The t-test results showed that two sets of shear strength data were statistically different regardless of aging time. Since there was a significant variation in the initial shear strengths between the two sets of standard wirebonds before thermal aging, it was improper to make a comparison between two sets of the shear strength data after 250 hours of thermal aging. Therefore, this comparison was inconclusive.
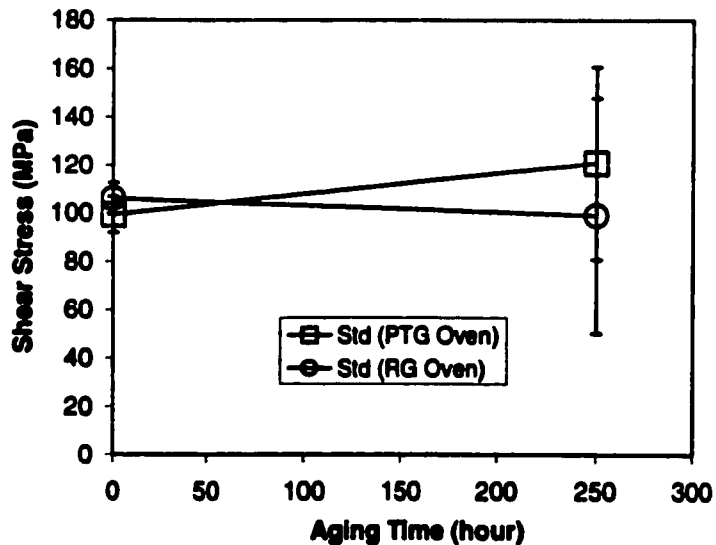

Figure 36. Shear strength of standard wirebonds at 175°C as a function of aging time for two different ovens.

Two sets of the shear strengths for encapsulated wirebonds are shown in Figure 37. The *t*-test results revealed that the average shear strengths from two types of encapsulated wirebonds were not statistically different from each other after 250 hours of thermal aging. However, the initial strength values, prior to thermal aging, were found to be statistically different from each other.
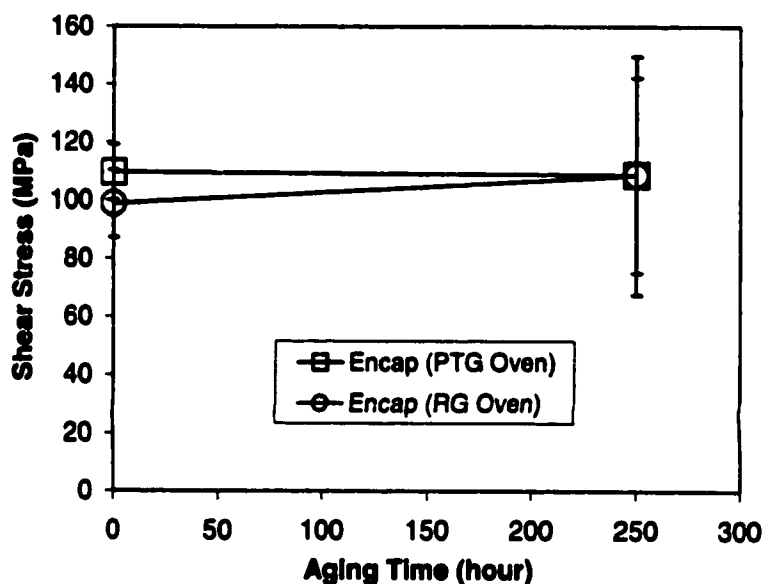
Figure 37. Shear stress of encapsulated wirebonds at 175°C as a function of aging time for two different ovens.

Overall, the comparison of the results from Experiments 1 and 2 was inconclusive, even though a minor effect of mixing ovens on the bond strength was observed in the pull force data for encapsulated wirebonds. However, the mixing of ovens should be done carefully and should be avoided if it is possible in order to reduce probable experimental errors. Therefore, all the subsequent experiments, Experiments 3, 4, and 5, were performed using the same oven used in Experiment 2, i.e., the RG oven.

5.2.2 Comparison of Experiment 2 and Experiment 3

The results from Experiment 2 were compared to those from Experiment 3, to investigate the effect of thermal aging temperature (150°C and 175°C) on the bond strength. Standard and encapsulated wirebonds were tested after aging for 24, 48 and 96 hours. The bond pull and ball shear strengths for both types of wirebonds, aged at two different temperatures, were measured and compared to each other at each aging time.

5.2.2.1 Bond Pull Strength

Variations in the pull forces obtained from standard and encapsulated wirebonds were examined based on the plots of pull force as a function of thermal aging time, as shown in Figures 38 and 39. As can be seen in Figure 38, the average pull force for standard wirebonds, aged at 175°C, started decreasing after thermal aging for 24 hours. However, no significant change was observed in the case of standard wirebonds aged at 150°C, for time periods up to 96 hours. The t-test results showed that there were significant variations in the two sets of pull force data, after 24 hours of aging.

The same observations were made for encapsulated wirebonds, aged at 150°C and 175°C, for time periods up to 96 hours. As shown in Figure 39, variations in the pull force increased with thermal aging time. Significant differences in the average pull forces first occurred at 48 hours of aging. Both standard and encapsulated wirebonds aged at 150°C showed greater pull force values than those wirebonds aged at 175°C, for all aging times. This might be due to the grain growth occurring in the Au wire above the ball. This area of the wire is known as the heat affected zone (HAZ) and contains larger grains than those in the original wire before wirebonding.[3] Since the
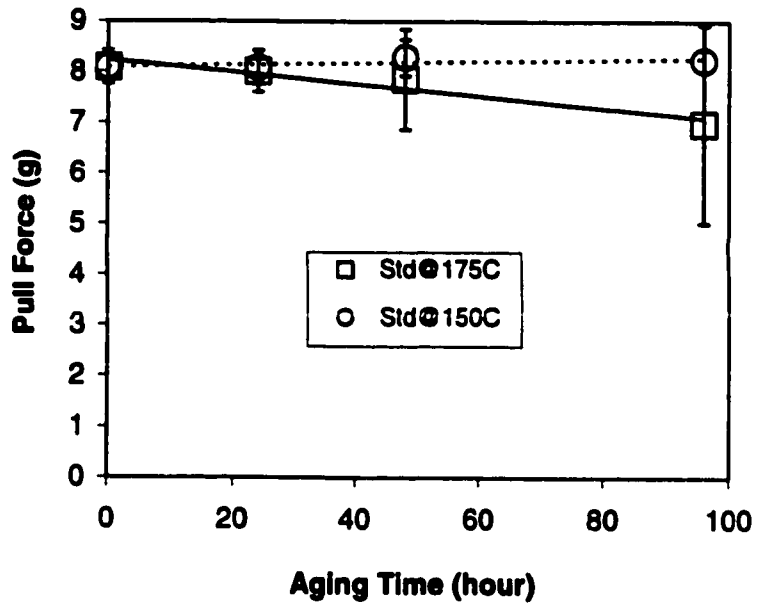
83

Figure 38. Pull force as a function of aging time for standard wirebonds aged at 175°C and 150°C.
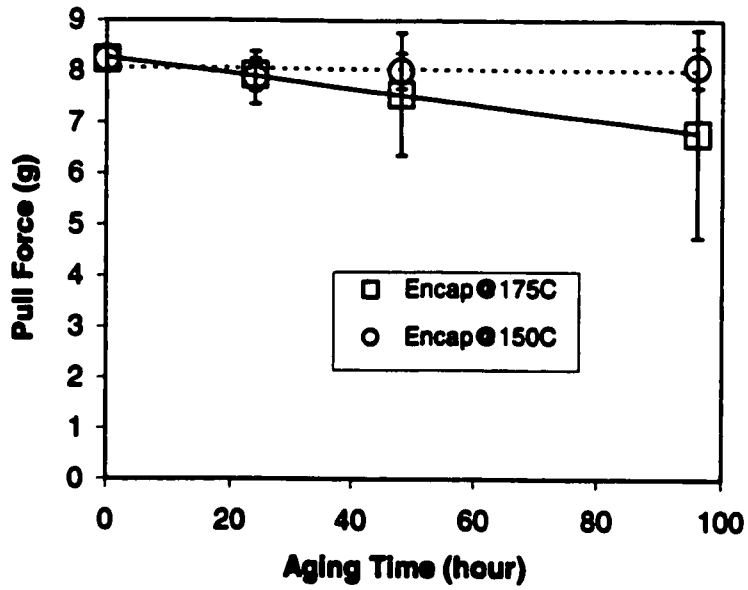

Figure 39. Pull force as a function of aging time for encapsulated wirebonds aged at 150°C and 175°C.

grain growth is temperature and time dependent, larger grains are expected at higher temperatures,[5,7] and larger grain size yields lower strength. The bond pull test results obtained from both standard and encapsulated wirebonds at the two aging temperatures are consistent with information available in the literature.[3,5,7]

5.2.2.2 Ball Shear Strength

Changes in the shear strength for the standard and encapsulated wirebonds at the two aging temperatures, 150°C and 175°C, are shown in Figures 40 and 41, respectively. When standard wirebonds were aged at 175°C, the shear strength increased to reach the maximum strength at 24 hours and started decreasing as thermal aging proceeded, as can be seen in Figure 40. When the wirebonds were aged at 150°C, the average shear strength increased with aging time. Variations in the shear strengths for two sets of standard wirebonds at 150°C and 175°C were not significant at 48 hours. However, the shear strengths for two sets of wirebonds at aging times of 24 and 96 hours were statistically different from each other. Once thermal aging exceeded 48 hours, the wirebonds aged at 150°C had higher shear strengths than those aged at 175°C.

Similar observations were made for the two sets of encapsulated wirebonds aged at 150°C and 175°C, as well. When they were aged at 175°C, the average shear strength increased and yielded the maximum strength at 24 hours. As thermal aging exceeded 24 hours, the strength started decreasing with aging time, as shown in Figure 41. When the wirebonds were aged at 150°C, the shear strength increased with aging time. Variations in the shear strengths obtained from two sets of encapsulated wirebonds at 150°C and
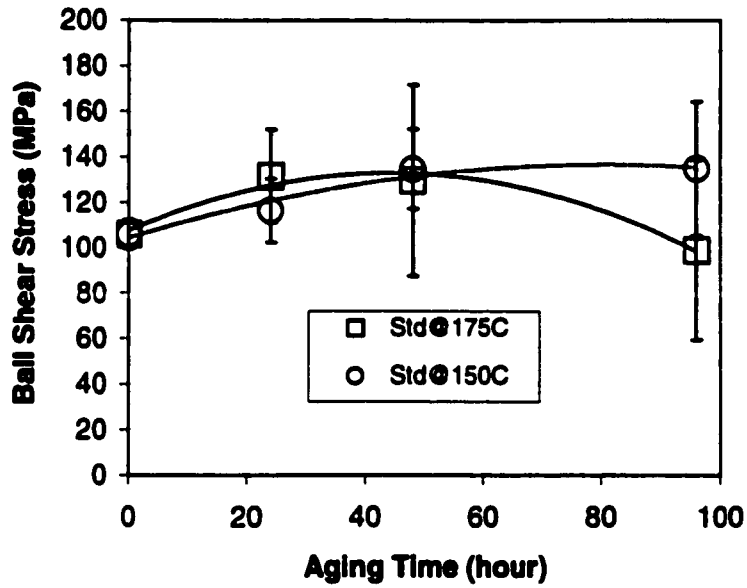
Figure 40. Shear stress as a function of aging time for standard wirebonds aged at 150°C and 175°C.
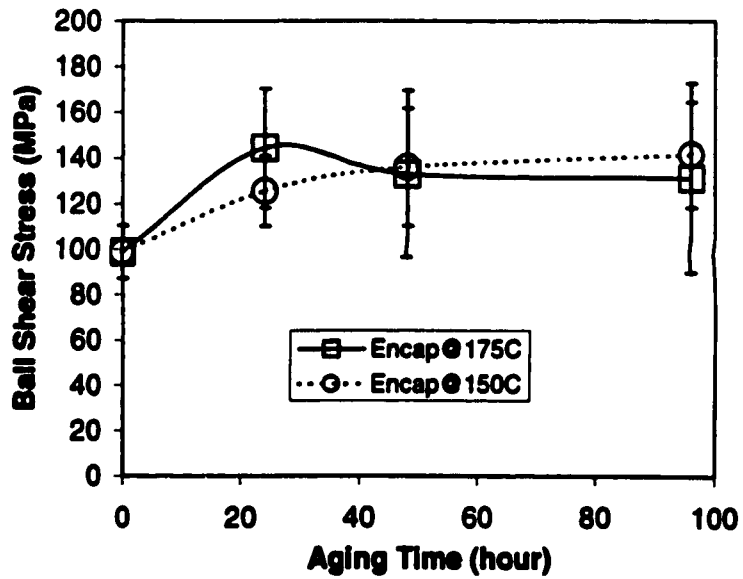

Figure 41. Shear stress as a function of aging time for encapsulated wirebonds aged at 150°C and 175°C.

175°C were not significant at aging times of 48 and 96 hours, as illustrated in Figure 41.

Overall, the comparison between Experiments 2 and 3 showed that the higher aging temperature, 175°C, induced the degradation of bond strength more rapidly than the lower temperature, 150°C. In both standard and encapsulated wirebonds under 175°C aging condition, the pull and shear strengths decreased after thermal aging of 24 hours. These comparison results confirmed that high aging temperature played a major role in influencing the bond qualities related to the bond strength changes.

5.2.3 Comparison of Experiment 2 and Experiment 4

As noted in the comparison of Experiments 1 and 3, wide variations in the pull and shear strengths were observed in both standard and encapsulated wirebonds that were aged for time periods up to 250 hours. These fluctuations indicated early bond failures, based on National Semiconductor's internal specifications for the bond pull and ball shear tests. During the investigation for the main reason causing the early bond failure, surface contamination of the dies was suspected, since impurities on the bond area were known to accelerate the bond degradation.[3] Therefore, in order to determine if surface contamination affects the pull and shear strengths of the bonds, the results for standard wirebonds between Experiments 2 and 4 were compared.

5.2.3.1 Bond Pull Strength

The overall changes in the pull force for standard wirebonds with two different dies, i.e., SC and SG dies, can be observed in Figure 42. The average pull forces of the wirebonds with SC dies decreased with aging time. In the case of wirebonds with SG dies, there was no significant change observed in the average pull force as a function of

aging time. However, comparisons made between the two sets of pull force data at 48 and 96 hours indicated that they were not statistically different from each other.
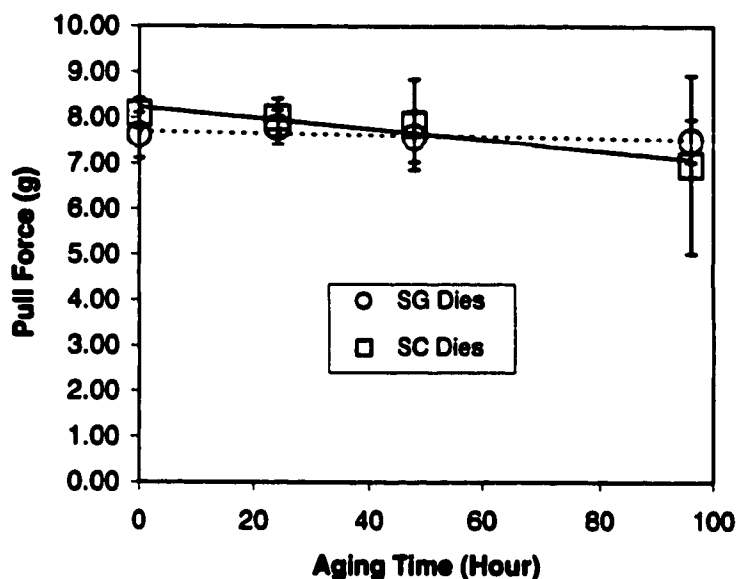

Figure 42. Pull force as a function of aging time at 175°C aging temperature.

The modes of the failures during the bond pull test were examined for the two sets of standard wirebonds. The wirebonds with SG dies displayed only Mode 2 Failures, i.e., wire breaks at the neck. In contrast, both Mode 1 and 2 Failures were found in the wirebonds with SC dies. The results are shown in Figure 43. As shown in Figure 43, Mode 1 Failure, i.e., ball lifts, was more frequent as aging time passed 24 hours. This indicates a rapid degradation in the pull strength for the wirebonds with SC dies. Since the two different mode failures were assigned to the wirebonds with SC dies, the average pull forces for Mode 2 Failure in Figure 42 were sorted out and plotted in Figure 44, for better comparison.
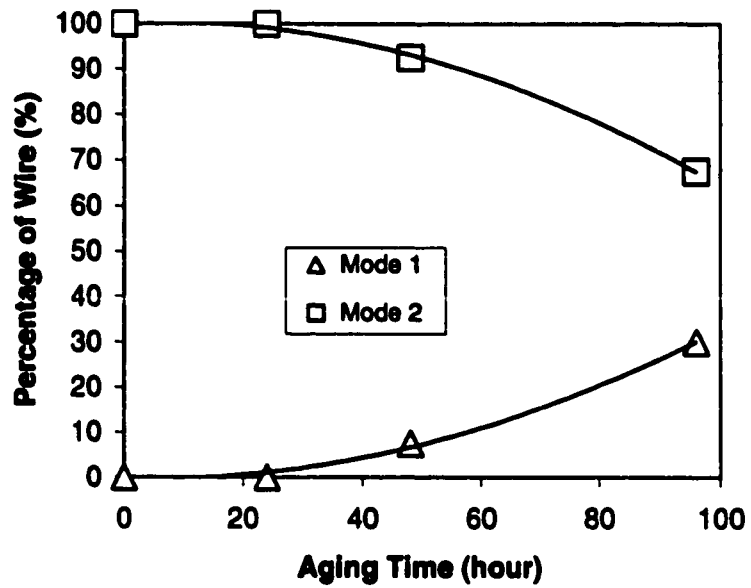
Figure 43. Failure mode of the bond pull test for standard wirebonds with SC dies as a function of aging time.
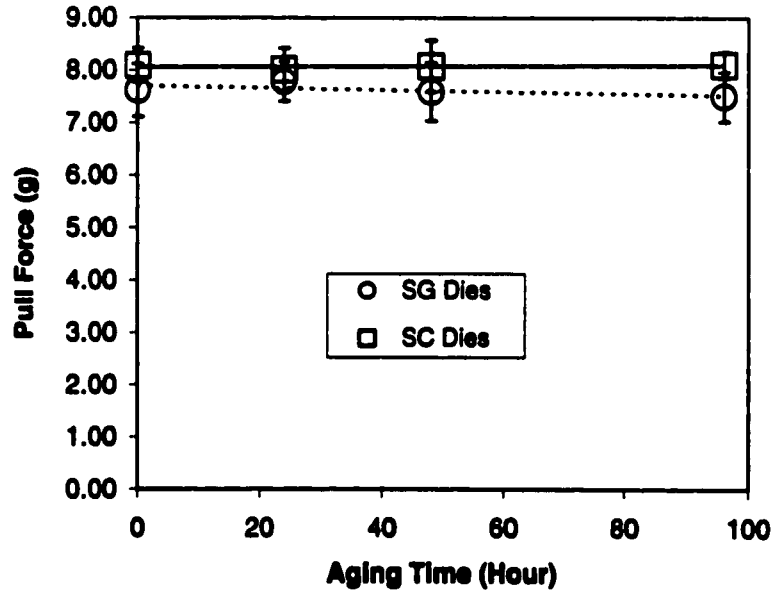

Figure 44. Pull force of Failure Mode 2 for standard wirebonds with two different dies as a function of aging time.

Greater average pull forces were obtained from standard wirebonds with SC dies than from standard wirebonds with SG dies, for all aging times, as depicted in Figure 44. Student t-test results also confirmed that they were statistically different from each other. The average pull forces for both sets of wirebonds were constant during the 96 hours of aging at 175°C. The bond pull forces based on Mode 2 Failure indicated that the Au wire above the ball bond did not undergo any metallurgical change during the aging process. This also revealed that the pull strength degradation, observed in Figure 42, was primarily due to the bond degradation occurring at the bond interface. It is thought that this bond degradation is related to the alloying reaction at the interface.

5.2.3.2 Ball Shear Strength

The shear test results showed distinct differences between two sets of standard wirebonds, as can be seen in Figure 45. The wirebonds with SG dies showed a rapid rise in shear strength after thermal aging of 24 hours. The strength gradually decreased as the thermal aging proceeded. A similar trend was observed in the case of standard wirebonds with SC dies. The maximum average shear strength was obtained from the wirebonds aged for 24 hours. At aging times longer than 24 hours, the shear strength started decreasing. Overall, standard wirebonds with SG dies yielded greater shear strengths than those with SC dies, for all aging times. The two sets of shear strength data were found to be significantly different from each other at all aging times, by a t-test at the 95% confidence level.
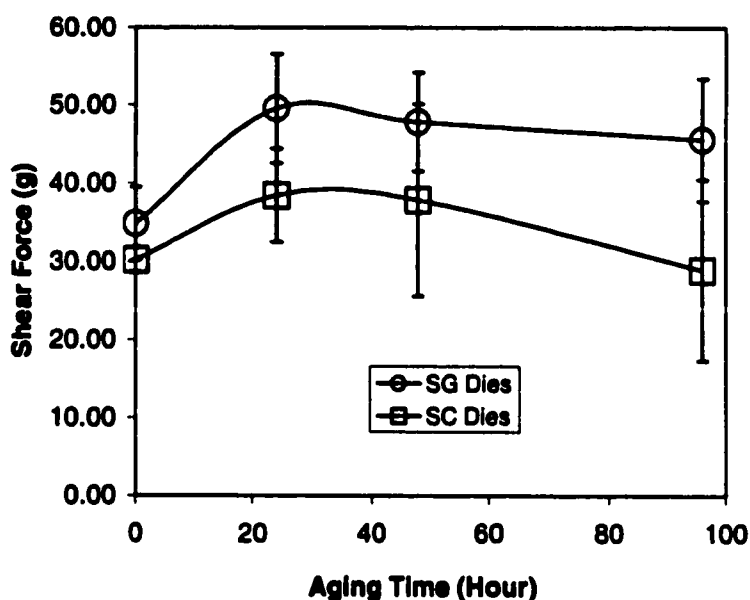
Figure 45. Shear force as a function of aging time for standard wirebonds with two different dies.

In summary, this comparison showed the effect of dies, from different sources, on the bond quality. While the difference in the source of dies did not greatly influence the degradation in the pull strength, the effect was found to be greater on the shear strength. Overall, better bond qualities were obtained from the wirebonds with SG dies. However, no further investigation was pursued to verify the possible cause since it was beyond the scope of this project.

5.3 Extensive Experiment: Experiment 5

An extensive comparison study between the two types of wirebonds, standard and encapsulated wirebonds, was performed employing two aging temperatures, 150°C and 175°C, and extended aging times of up to 2,000 hours. The test matrix for this experiment is shown in Table 13.

Table 13. Test Matrix for Experiment 5.

Source of Die	Source of Oven	Bond Temperature (°C)	Aging Time	Aging Temperature (°C)	Wirebonding Technique
SG	RG	200	Up to 2000 hours	150	Standard
					Encapsulated
				175	Standard
					Encapsulated

SG dies were thermosonically wirebonded at the bond temperature, 200°C, using the two types of wirebonding processes, for the specimens used in this experiment. The wirebonds were then thermally aged at either 150°C or 175°C, for time periods up to 2,000 hours in the RG bake oven. The bond qualities obtained were investigated based on the bond pull and ball shear test results and SEM metallographic examinations. These are discussed in Sections 5.3.1 through 5.3.4.

5.3.1. Investigation of Lifted Balls

The relationship between bond area uniformity and lateral diffusion of Au and Al, as was pointed out by Carrass et al.,[23] was observed in both types of wirebonds aged at 150°C and 175°C. The bottom surfaces of the Au balls were examined under SEM and the percentage of bond area covered by the intermetallic compounds was approximated. SEM micrographs of the lifted balls for standard and encapsulated wirebonds are shown in Figures 46 through 49. SEM micrographs of the lifted balls for standard wirebonds are shown in Figures 46 and 47. As shown in Figure 46(a), approximately 65% of the bond area was covered by the intermetallic compounds during the bonding process. The intermetallic compounds were spread across the bond area, and there were also some

non-reacted regions. These non-reacted regions without the intermetallic compounds were scattered across the bond area, but more concentrated around the bond periphery.

SEM micrographs for standard wirebonds aged for 24 hours at 150°C are shown in Figures 46(b) through 46(f). More than 85% of the bond area was found to be covered by the intermetallic compounds. The non-reacted regions, which had been present in the middle of the bond area right after bonding, disappeared. However, non-reacted regions were still found around the bond perimeter. As thermal aging continued, the percentage of the intermetallic bond area slowly increased, as shown in Figures 46(c) through 46(f). It was observed that the concentration was highest in the center of the bond and decreased as the distance from the center increased. According to this observation, it was assumed that the intermetallic compounds grew laterally from the bond center towards the bond periphery. It appeared that this growth continued until the bond area was completely covered by the intermetallic compounds, as shown in Figure 46(f).

When the higher aging temperature, 175°C, was used, the lateral growth of Au-Al intermetallic proceeded more rapidly than at 150°C. After thermal aging for 24 hours, approximately 90% of the bond area was covered by the intermetallic compounds, as can be seen in Figure 47(a). An additional 24 hours of thermal aging did not significantly increase the amount of lateral growth across the bond area, as shown in Figure 47(b). After 96 hours, the intermetallic compounds covered most of the bond area and complete coverage was found at 144 hour aging time, as shown in Figures 47(c) and 47(d).
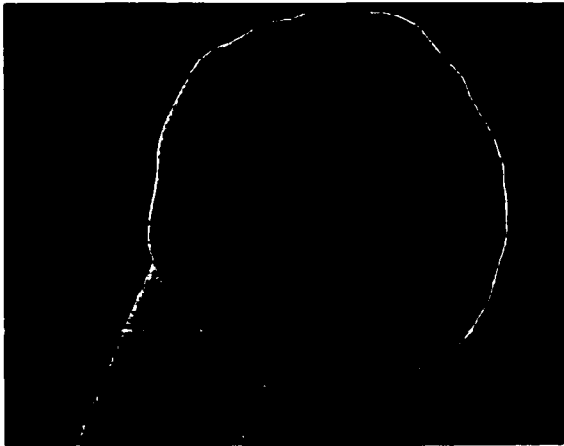
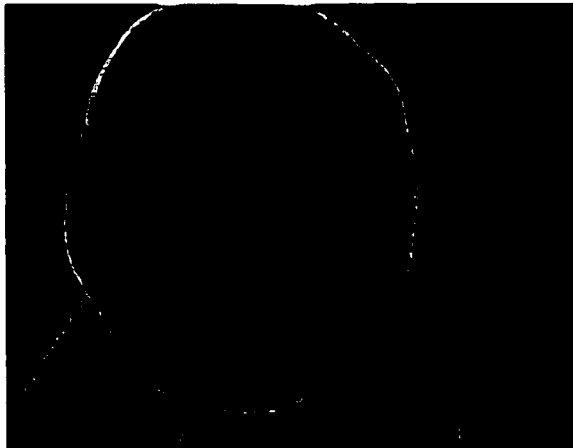**Figure 46(a).**
Standard wirebond
right after bonding.

Figure 46(b).
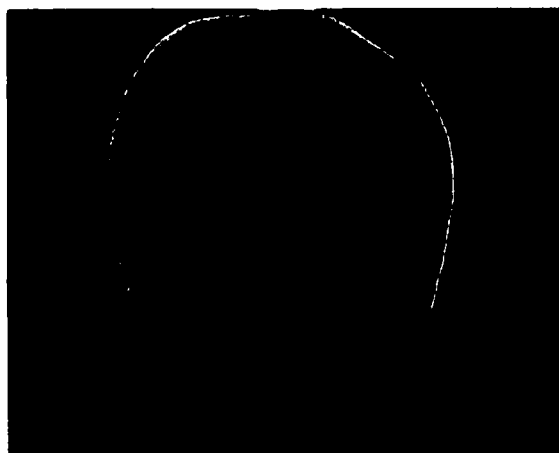Standard wirebond
aged at 150°C for 24
hours.
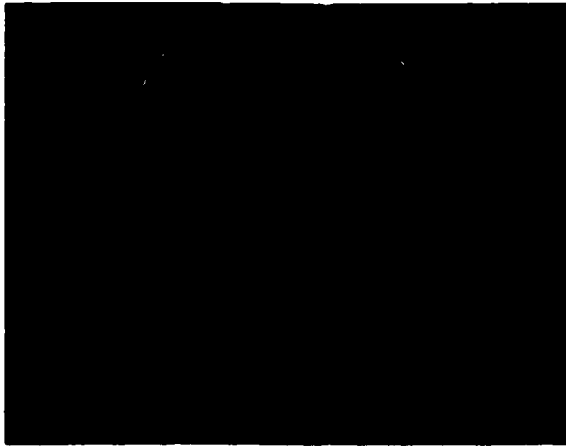

Figure 46(c).
Standard wirebond
aged at 150°C for 48
hours.

Figure 46(d).
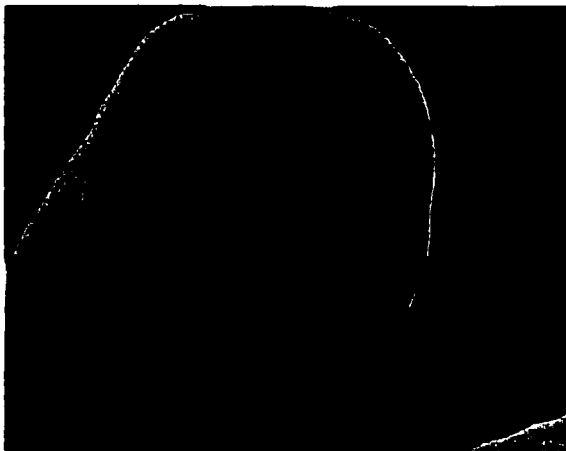Standard wirebond
aged at 150°C for 96
hours.

Figure 46(e).
Standard wirebond
aged at 150°C for 144
hours.

Figure 46(f).
Standard wirebond
aged at 150°C for 250
hours.

Figure 46. SEM micrographs of lifted balls obtained from standard wirebonds right after bonding (a) and thermal aging at 150°C for 24 hours (b), 48 hours (c), 96 hours (d), 144 hours (e), and 250 hours (f).
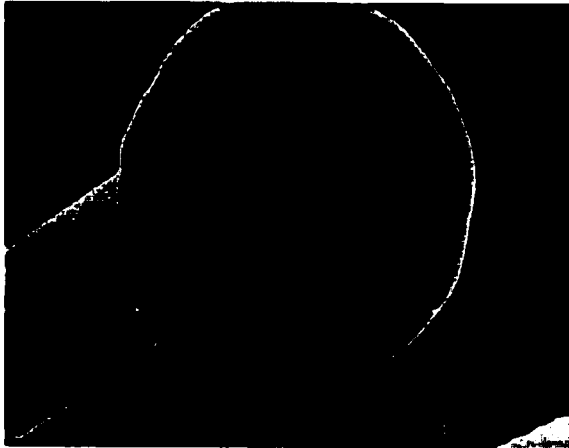
Figure 47(a).
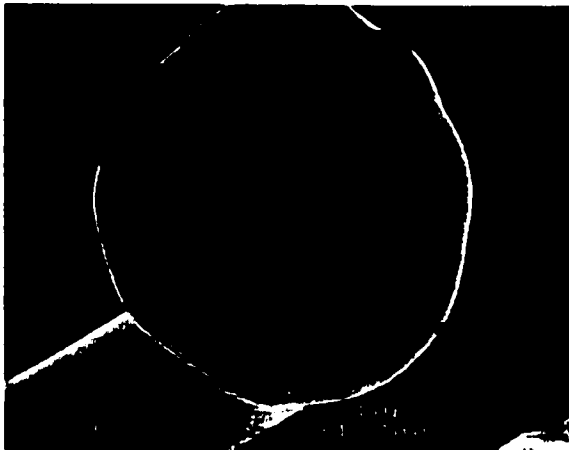Standard wirebond
aged at 175°C for 24
hours.

Figure 47(b).
Standard wirebond
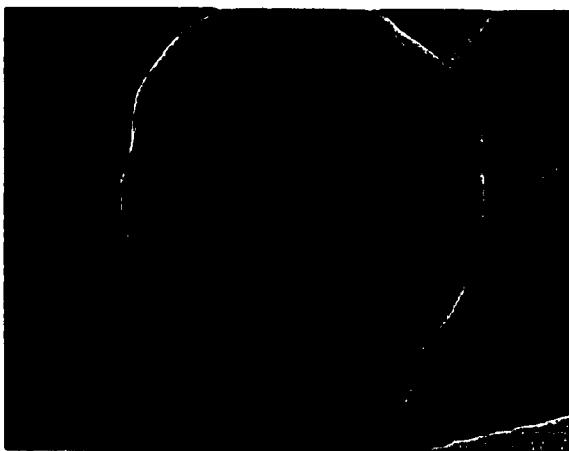aged at 175°C for 48
hours.

Figure 47(c).
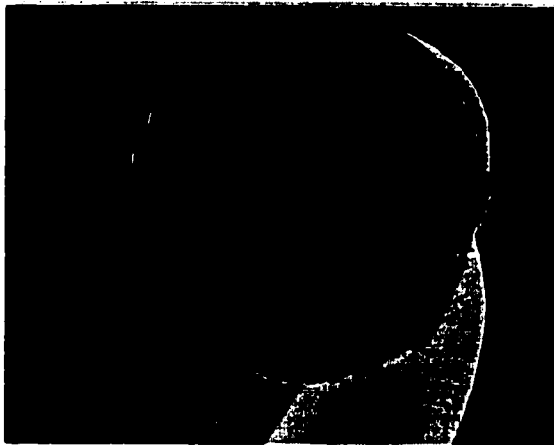Standard wirebond
aged at 175°C for 96
hours.

Figure 47(d).
Standard wirebond
aged at 175°C for 144
hours.

Figure 47. SEM micrographs of lifted balls obtained from standard wirebonds after aging for (a) 24 hours, (b) 48 hours, (c) 96 hours, and (d) 144 hours at 175°C.

The overall trend in the lateral growth of the intermetallic compounds observed for encapsulated wirebonds was similar to the trend observed for standard wirebonds. SEM micrographs of the lifted balls for encapsulated wirebonds aged at 150°C and 175°C are shown in Figures 48 and 49. As observed in the case of standard wirebonds, it was also noticed that approximately 65% of the bond area was covered by the intermetallic compounds during the encapsulated bonding process, as shown in Figure 48(a). The change in the intermetallic bond area along with thermal aging at 150°C can be seen in Figures 48(b) through 48(h). It was noticed that the percentage of area covered by intermetallic compounds did not vary greatly between the 24 and 48 hour time points, as shown in Figures 48(b) and 48(c).

Figure 48(a).
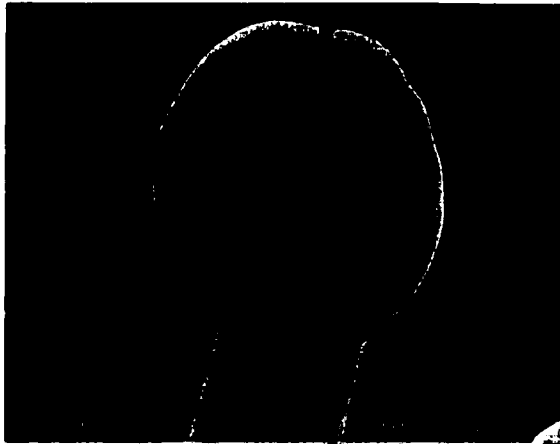Encapsulated wirebond
right after bonding.

Figure 48(b).
Encapsulated wirebond
aged at 150°C for 24
hours.

Figure 48(c).
Encapsulated wirebond
aged at 150°C for 48
hours.

Figure 48(d).
Encapsulated wirebond aged at 150°C for 96 hours.

Figure 48(e).
Encapsulated wirebond aged at 150°C for 144 hours.

Figure 48(f).
Encapsulated wirebond aged at 150°C for 250 hours.

Figure 48(g).
Encapsulated wirebond
aged at 150°C for 500
hours.

Figure 48(h).
Encapsulated wirebond
aged at 150°C for 750
hours.

Figure 48. SEM micrographs of lifted balls obtained from encapsulated wirebonds right after bonding (a), thermal aging at 150°C for (b) 24 hours, (c) 48 hours, (d) 96 hours, (e) 144 hours, (f) 250 hours, (g) 500 hours, and (h) 750 hours.

Figure 49(a).
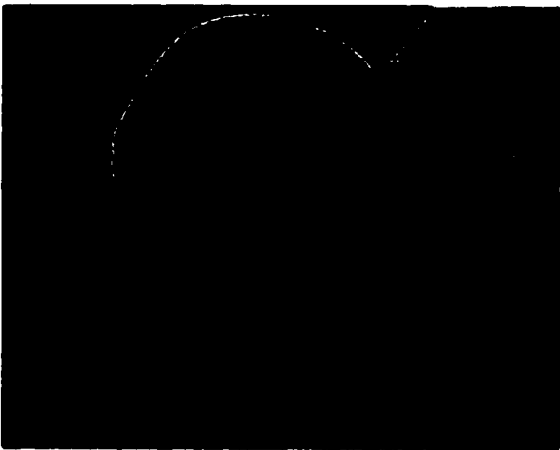Encapsulated wirebond
aged at 175°C for 24
hours.

Figure 49(b).
Encapsulated wirebond
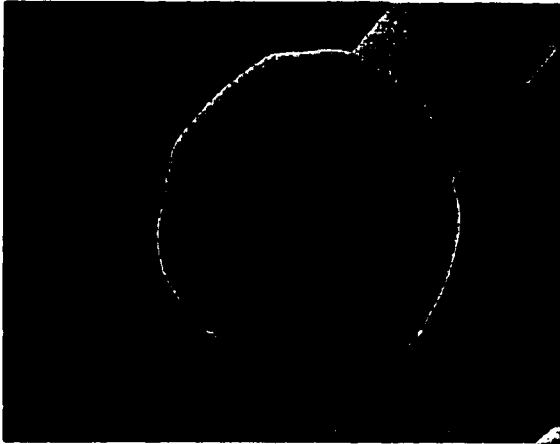aged at 175°C for 48
hours.

Figure 49(c).
Encapsulated wirebond
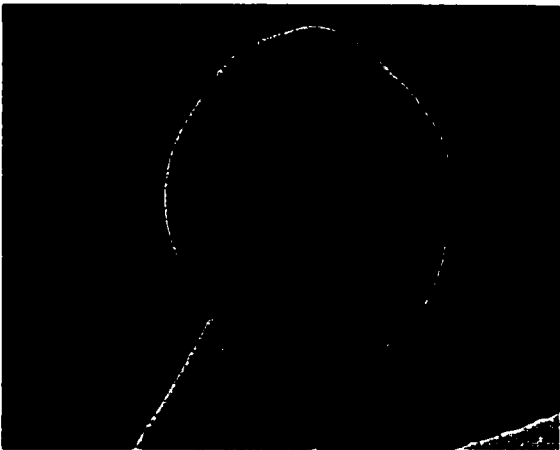aged at 175°C for 96
hours.

Figure 49(d).
Encapsulated wirebond
aged at 175°C for 144
hours.

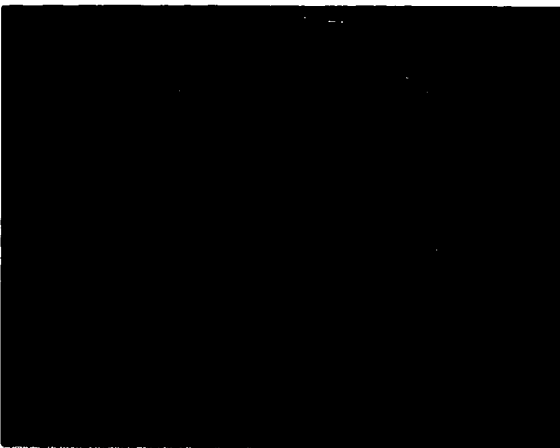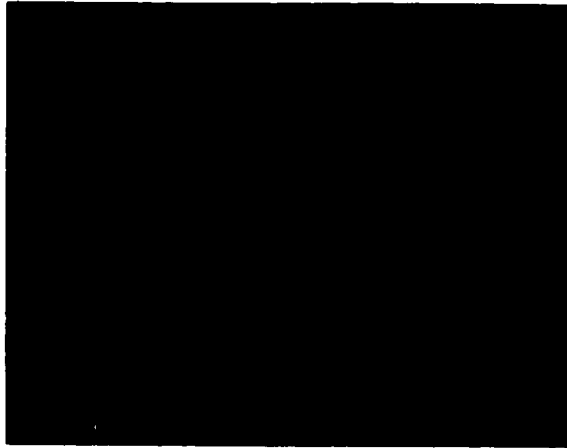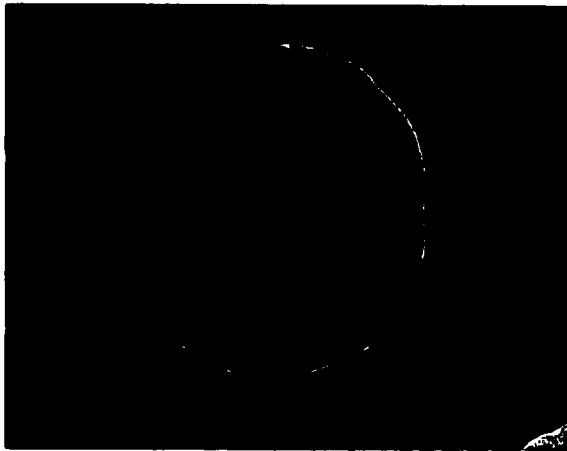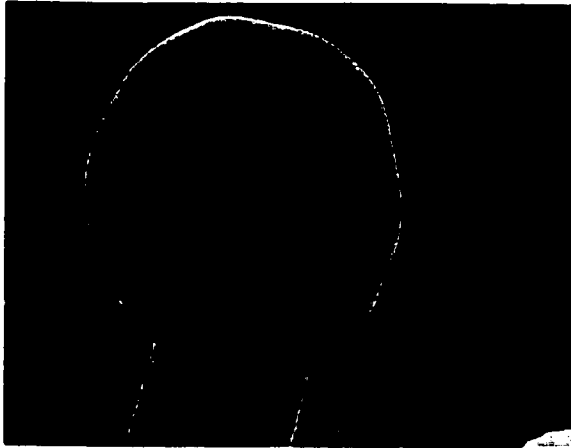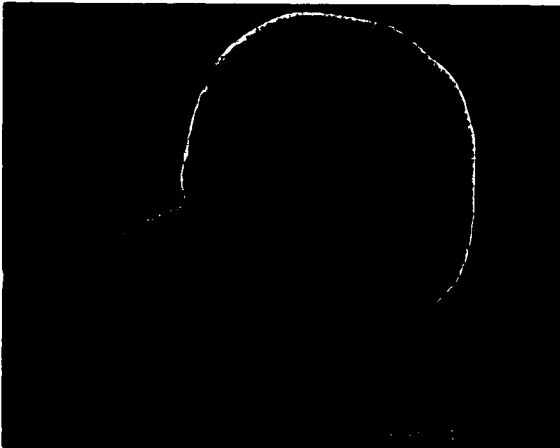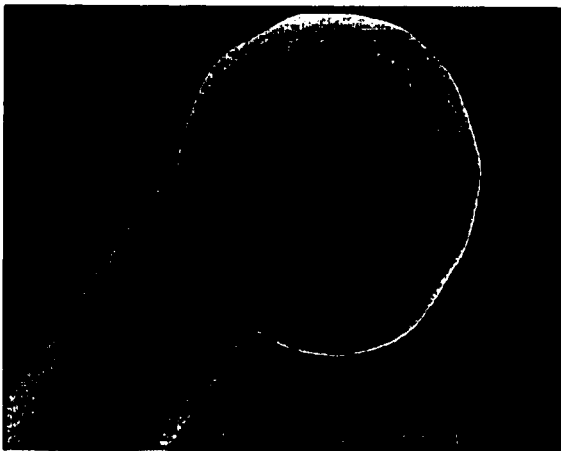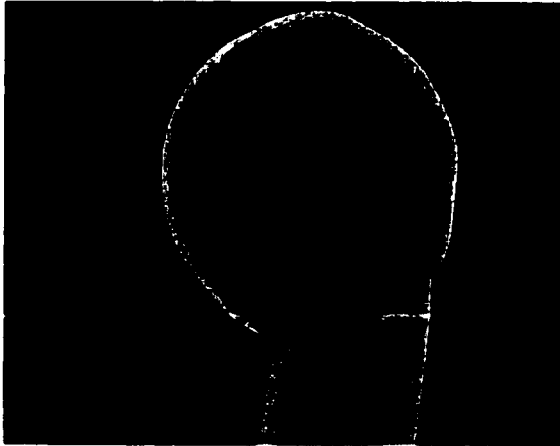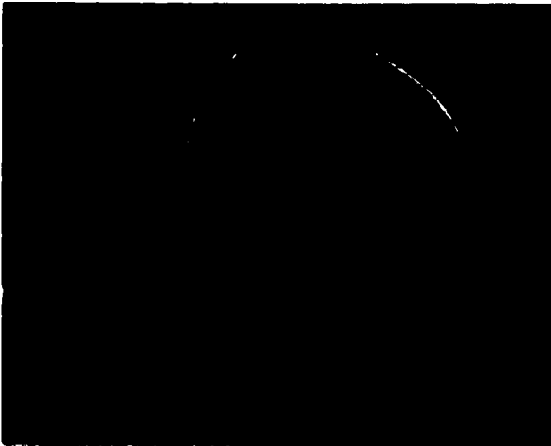**Figure 49(e).**
Encapsulated wirebond
aged at 175°C for 250
hours.

Figure 49. SEM micrographs of lifted balls obtained from encapsulated wirebonds after aging at 175°C for (a) 24 hours, (b) 48 hours, (c) 96 hours, (d) 144 hours, and (e) 250 hours.

In the aging time interval between 96 and 144 hours, the percentage of bond area covered by intermetallic compounds did not change significantly, as shown in Figures 48(d) and 48(e). After thermal aging for 750 hours, it was found that the bond area was completely covered by intermetallic compounds, as shown in Figure 48(h). As was found in the case of the standard wirebonds aged at 150°C, the intermetallic compounds were found to grow from the bond center towards the bond periphery as thermal aging continued.

When encapsulated wirebonds were thermally aged at 175°C, the lateral growth of the intermetallic compounds occurred rapidly, compared to the case of encapsulated wirebonds at 150°C. SEM micrographs of the lifted balls for encapsulated wirebonds at 175°C are shown in Figures 49(a) through 49(e) and support this finding. As aging time increased, more Au-Al intermetallic compounds were formed and spread across the bond interface. The intermetallic reaction zones in the bond center seemed to progress towards the bond perimeter as thermal aging continued. After 250 hours of thermal aging, the intermetallic compounds completely covered the bond area.

The percentages of the intermetallic bond area, which were approximated based on SEM micrographs for both standard and encapsulated wirebonds at 150°C and 175°C, were plotted as a function of aging time, in Figure 50. It was found that the lateral growth of the intermetallic compounds at the bond interface occurred most rapidly in standard wirebonds which were aged at 175°C. After 250 hours of thermal aging, 100% of the bond area were covered by the intermetallic compounds in both standard wirebonds aged at 150°C and encapsulated wirebonds at 175°C. The longest aging time

to obtain 100% of the intermetallic bond area was required for encapsulated wirebonds aged at 150°C. Overall, it was noticed that the growth of intermetallic compounds across the bond interface proceeded faster when the standard wirebonding technique was employed. However, statistically similar amounts of the intermetallic compounds were observed in both types of wirebonds during the bonding process.
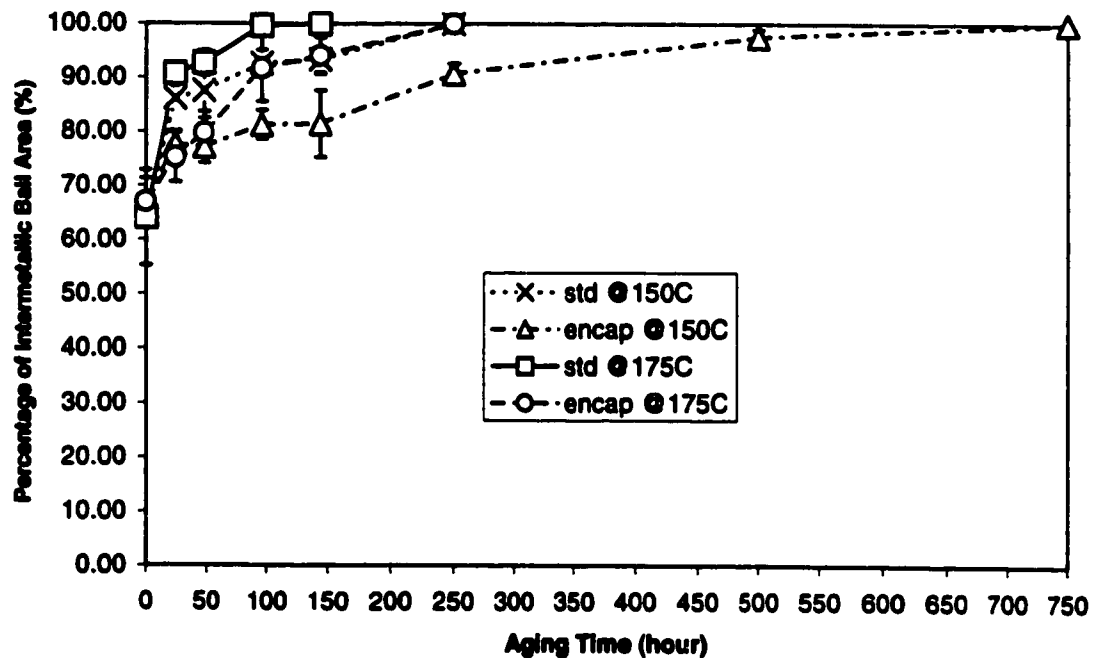
Figure 50. Intermetallic bond area as a function of aging time at 150°C and 175°C.

5.3.2. Cross-sections

In this section, cross-sections of standard and encapsulated wirebonds are examined and discussed in Section 5.3.2.1, based on micrographs. In Section 5.3.2.2, the results obtained from the measurement of intermetallic layer thickness are discussed. Results of EDX analyses on the bond interface are presented and discussed in Section

5.3.2.3, followed by the discussion of Kirkendall voids and microcracks in Section 5.3.2.4.

5.3.2.1 Examination of Cross-sectioned Samples

Cross-sectioned wirebonds were examined under an optical microscope and SEM. Cross-section micrographs for both standard and encapsulated wirebonds are shown in Figures 51 through 68. Cross-sections for both types of wirebonds, stored at room temperature for 2,000 hours, are presented in Figures 51 and 60, respectively. For the study of the formation and growth of the intermetallic compounds along with thermal aging at 150°C and 175°C, cross-sectioning was done on both types of wirebonds at every 500-hour aging time interval, up to 2,000 hours. Cross-section micrographs for standard wirebonds aged at 150°C and 175°C are shown in Figures 52 through 55 and Figures 56 through 59, respectively. Cross-section micrographs for encapsulated wirebonds aged at 150°C and 175°C are presented in Figures 61 through 64 and Figures 65 through 68, respectively.

Three distinct areas were found, based on color differences. The gold wire ball, the aluminum bond pad, and the region between the Au wire ball and Al bond pad were yellow, silvery white and tan, respectively. It was thought that the tan area, at the interface between the Au ball and the Al metal of the bond pad, corresponded to Au-Al diffusion layers.[3] The Au-Al diffusion layers were in light gray in the SEM micrographs, as shown in Figures 51(b) through 68(b). These regions were identified as Au-Al intermetallic layers by EDX.
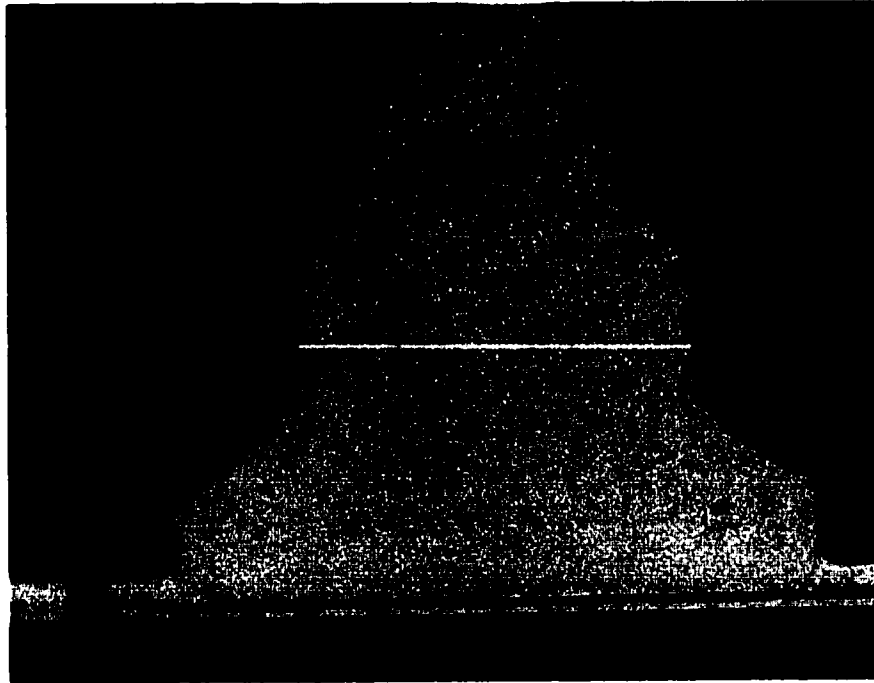
(a)

(b)
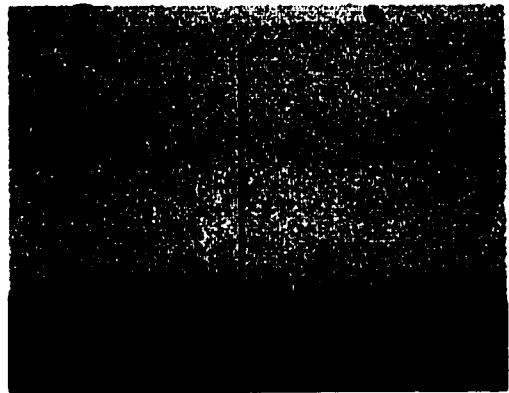
(c)

Figure 51. Standard wirebond aged at room temperature for 2,000 hours: micrographs taken from (a) an optical microscope, (b) SEM, and (c) SEM at high magnification showing a linescan used for EDX analysis.

(a)

(b)

(c)

Figure 52. Standard wirebond aged at 150°C for 500 hours: micrographs taken from (a) an optical microscope, (b) SEM and (c) SEM at high magnification showing a linescan used for EDX analysis.

(a)

(b)

(c)

Figure 53. Standard wirebond aged at 150°C for 1,000 hours: micrographs taken from (a) an optical microscope, (b) SEM and (c) SEM at high magnification showing a linescan used for EDX analysis.

(a)

(b)

(c)

Figure 54. Standard wirebond aged at 150°C for 1,500 hours: micrographs taken from (a) an optical microscope, (b) SEM and (c) SEM at high magnification showing a linescan used for EDX analysis.

(a)

(b)

(c)

Figure 55. Standard wirebond aged at 150°C for 2,000 hours: micrographs taken from (a) an optical microscope, (b) SEM and (c) SEM at high magnification showing a linescan used for EDX analysis.

(a)

(b)

(c)

Figure 56. Standard wirebond aged at 175°C for 500 hours: micrographs taken from (a) an optical microscope, (b) SEM, and (c) SEM at high magnification showing a linescan used for EDX analysis.

111
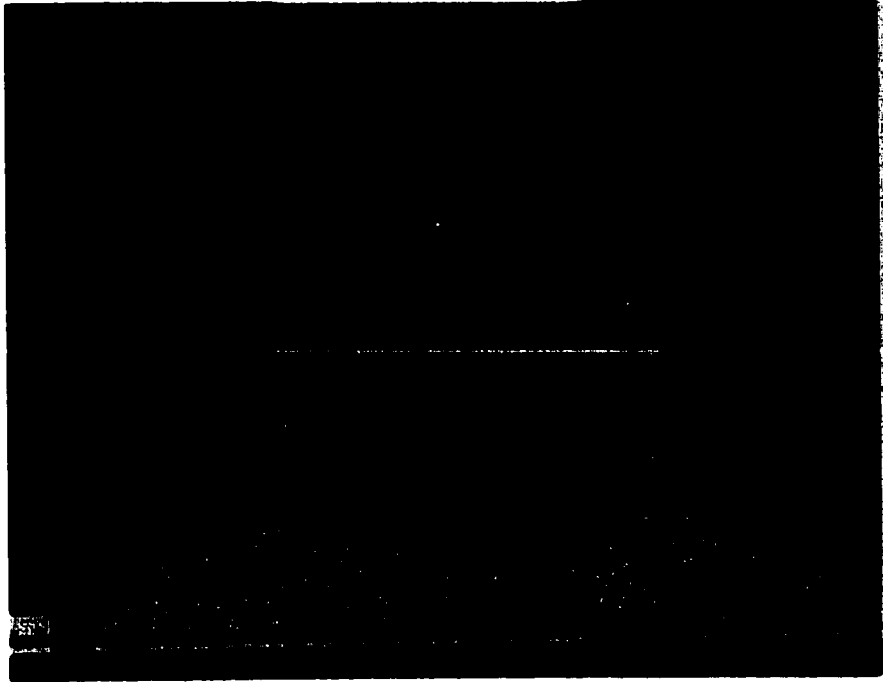
(a)
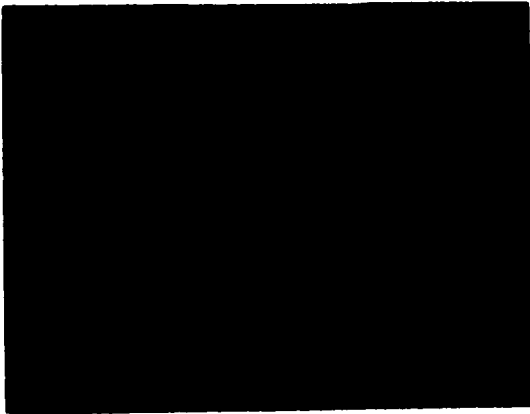
(b)
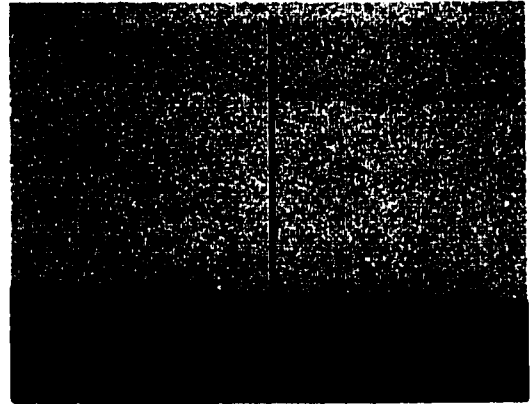
(c)

Figure 57. Standard wirebond aged at 175°C for 1,000 hours: micrographs taken from (a) an optical microscope, (b) SEM, and (c) SEM at high magnification showing a linescan used for EDX analysis.
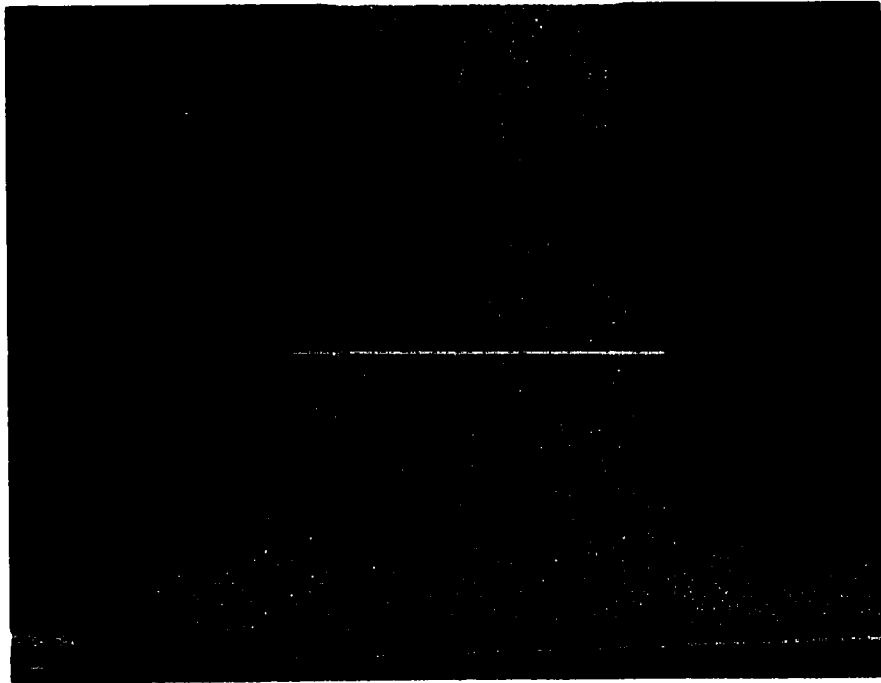
(a)

(b)

(c)

Figure 58. Standard wirebond aged at 175°C for 1,500 hours: micrographs taken from (a) an optical microscope, (b) SEM, and (c) SEM at high magnification showing a linescan used for EDX analysis.

(a)

(b)
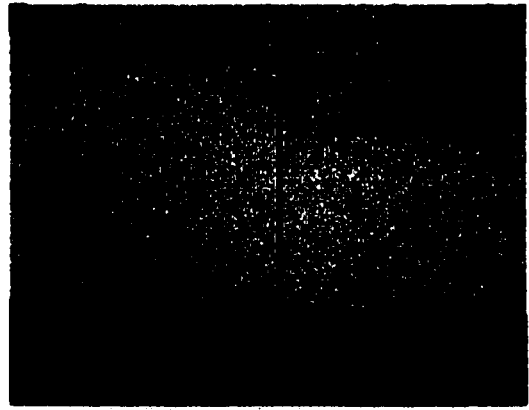
(c)

Figure 59. Standard wirebond aged at 175°C for 2,000 hours: micrographs taken from (a) an optical microscope, (b) SEM, and (c) SEM at high magnification showing a linescan used for EDX analysis.
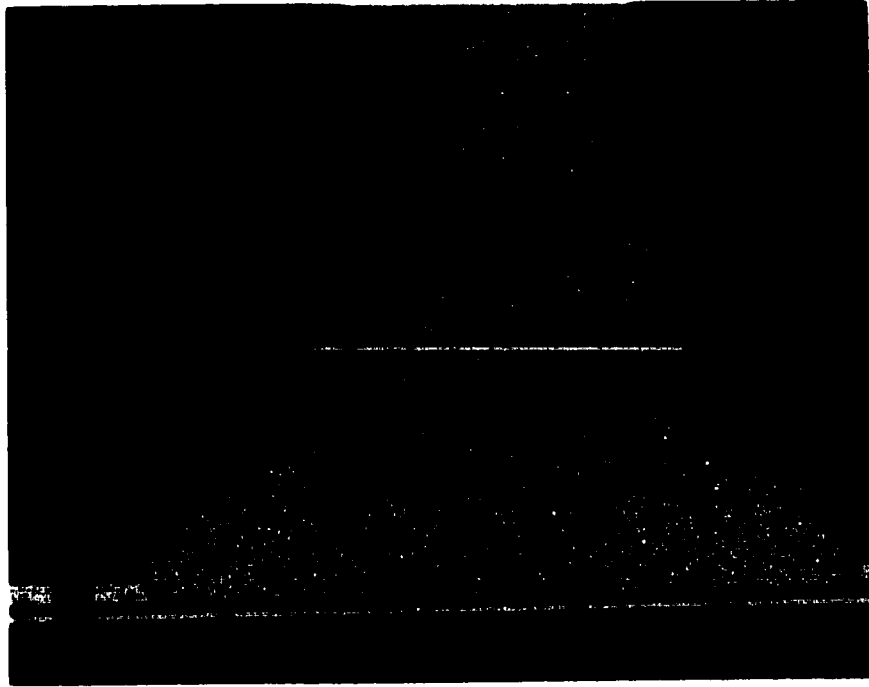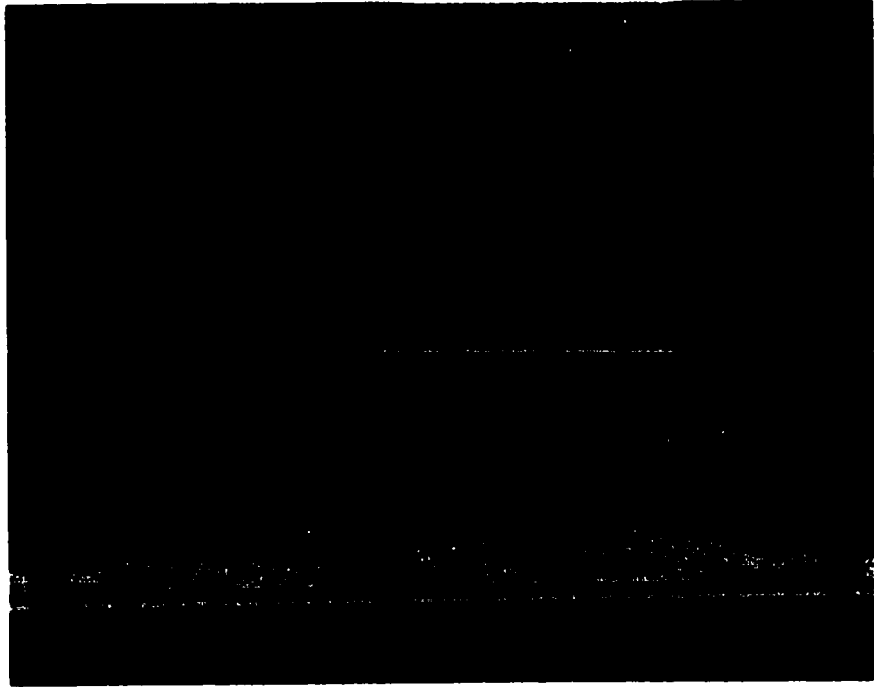
(a)
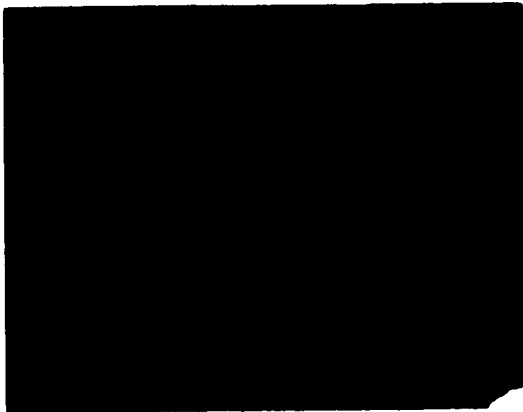
(b)
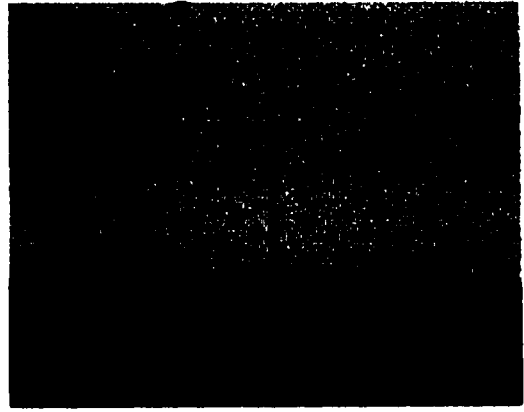
(c)

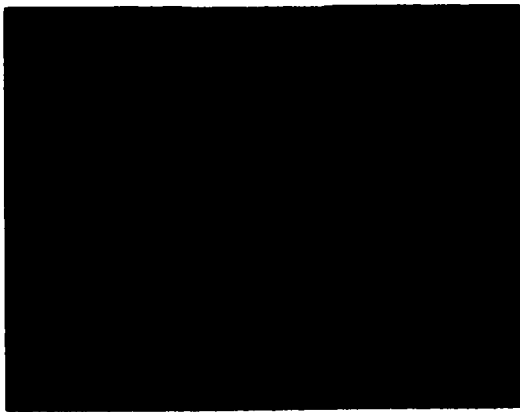**Figure 60.** Encapsulated wirebond aged at room temperature for 2,000 hours: micrographs taken from (a) an optical microscope, (b) SEM, and (c) SEM at high magnification showing a linescan used for EDX analysis.
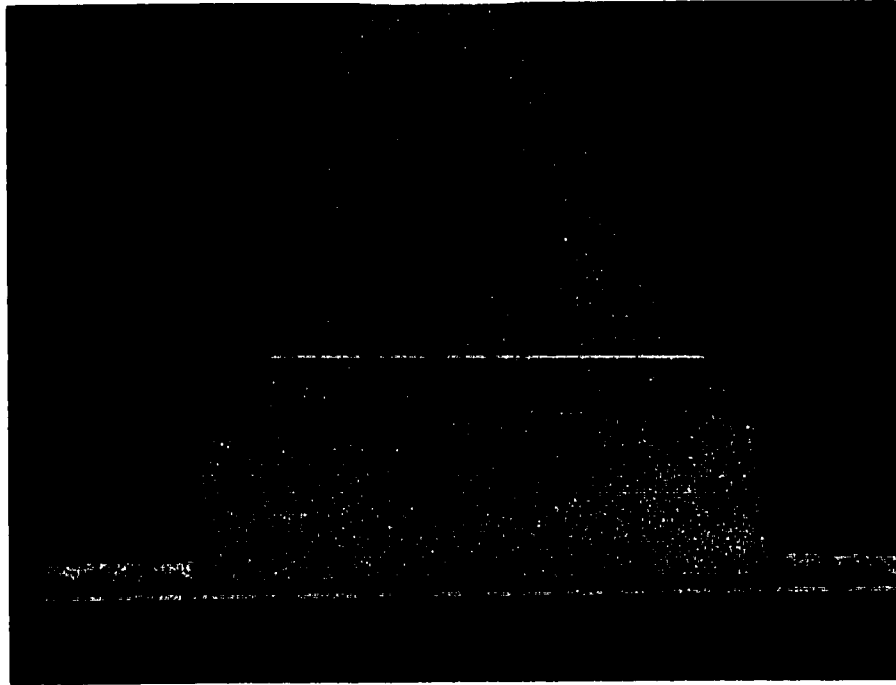
(a)
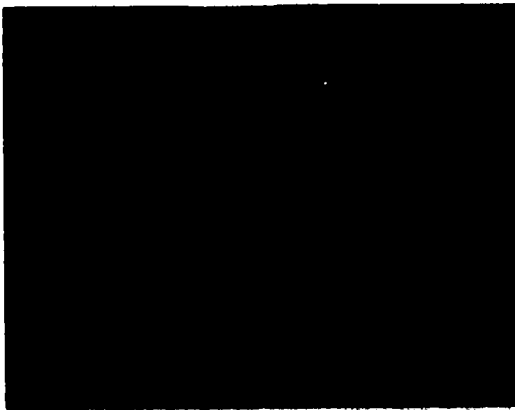
(b)
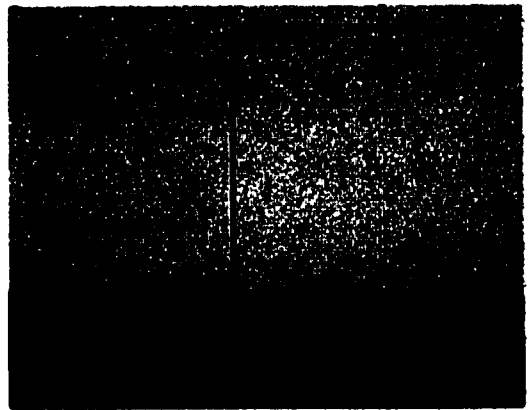
(c)

Figure 61. Encapsulated wirebond aged at 150°C for 500 hours: micrographs taken from (a) an optical microscope, (b) SEM, and (c) SEM at high magnification showing a linescan used for EDX analysis.
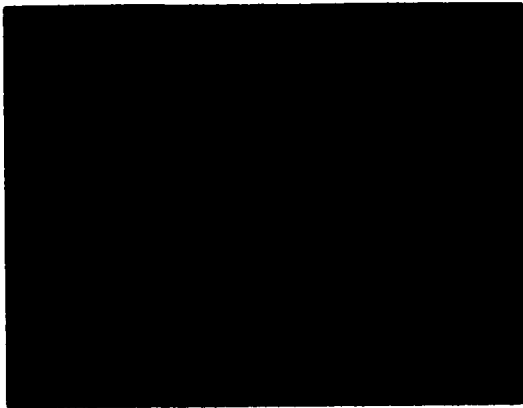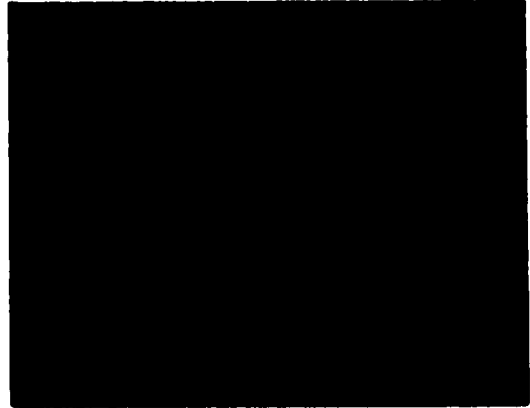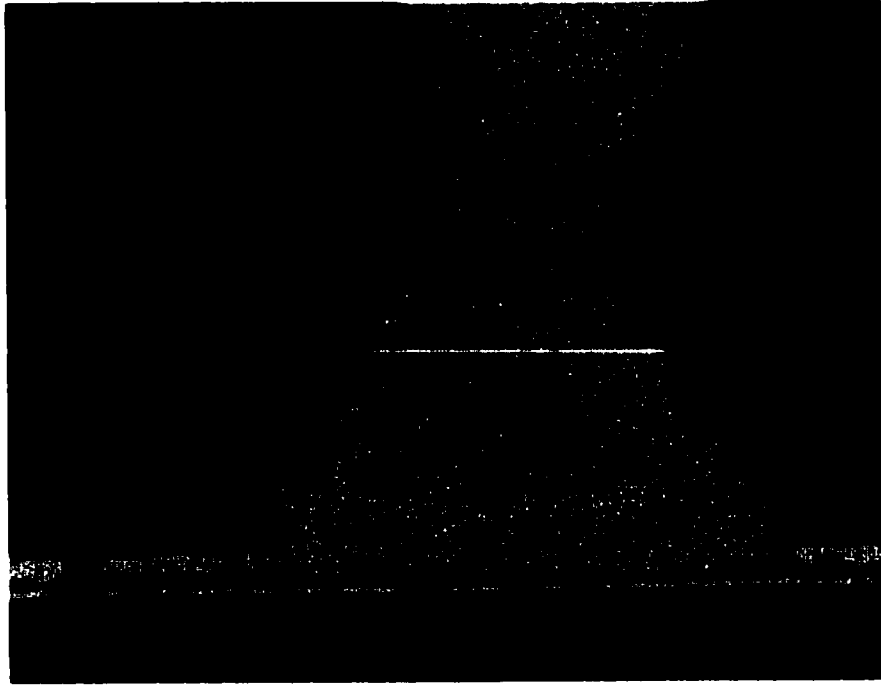
(a)

(b)

(c)

Figure 62. Encapsulated wirebond aged at 150°C for 1,000 hours: micrographs taken from (a) an optical microscope, (b) SEM, and (c) SEM at high magnification showing a linescan used for EDX analysis.
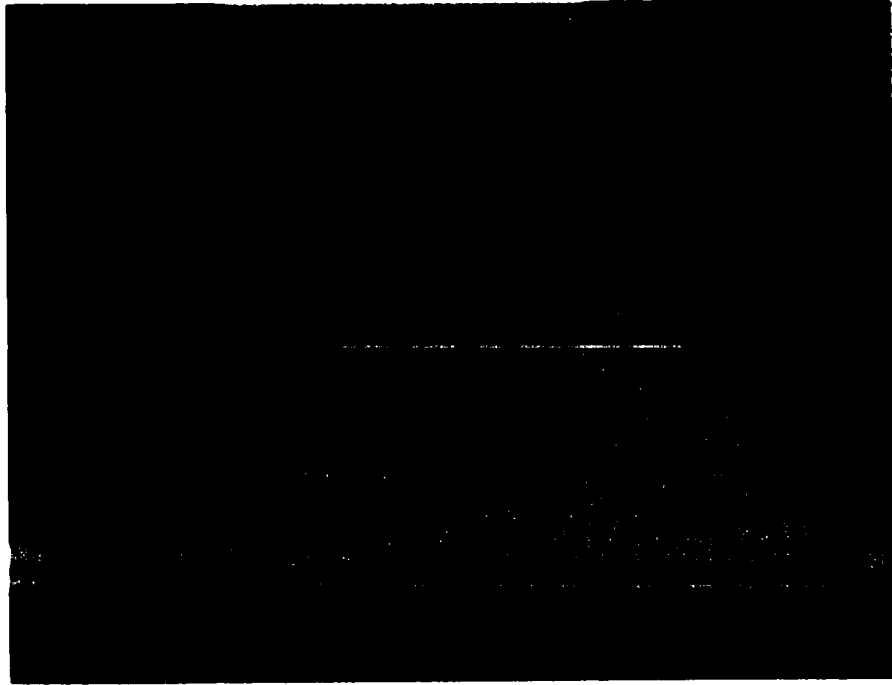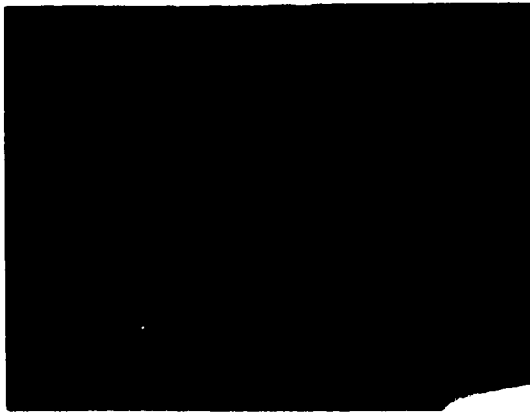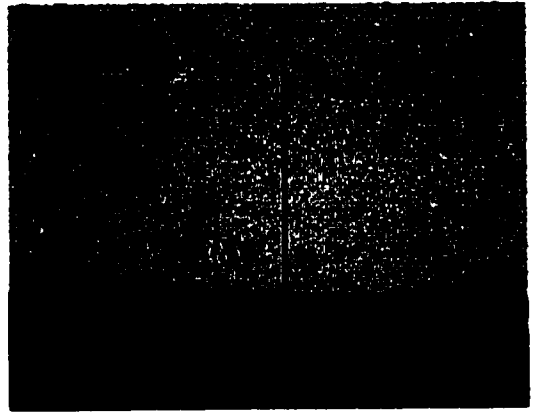
Figure 63. Encapsulated wirebond aged at 150°C for 1,500 hours: micrographs taken from (a) an optical microscope, (b) SEM, and (c) SEM at high magnification showing a linescan used for EDX analysis.
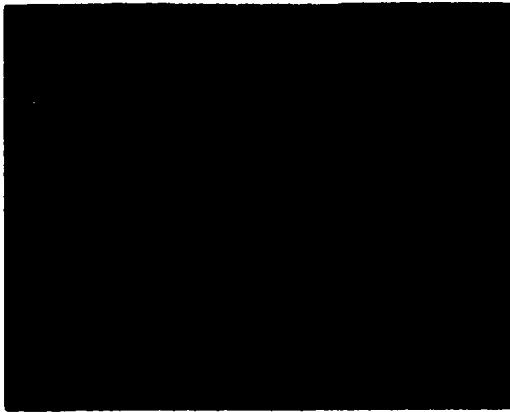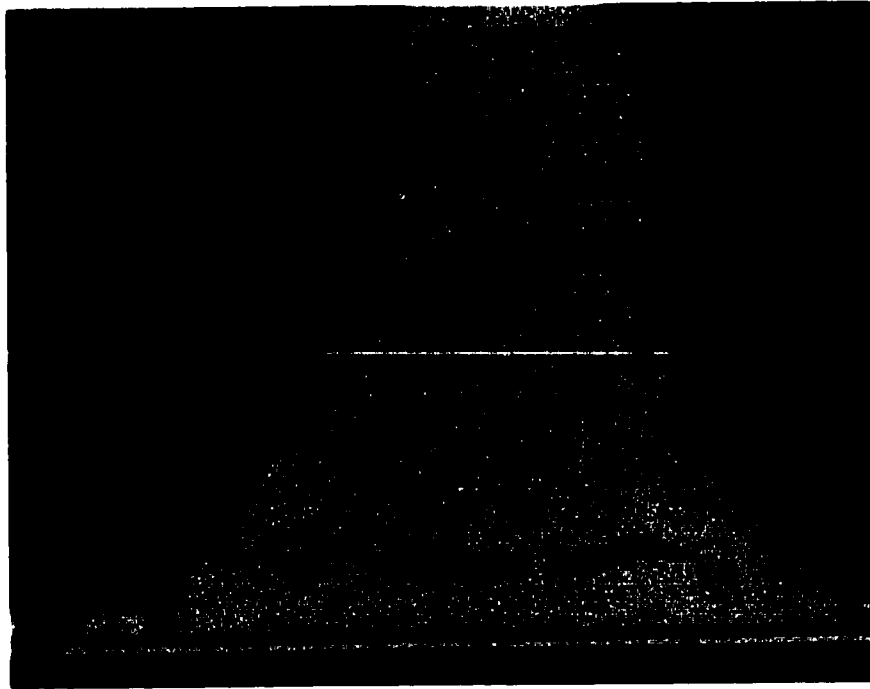
(a)
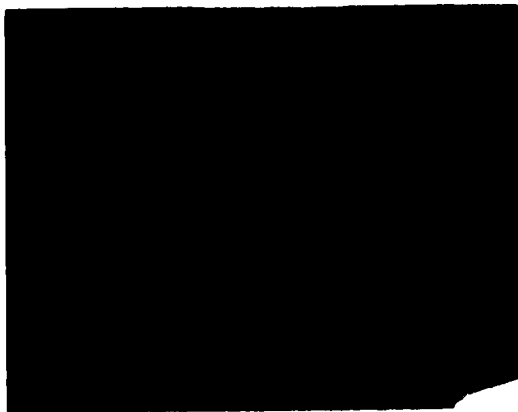
(b)
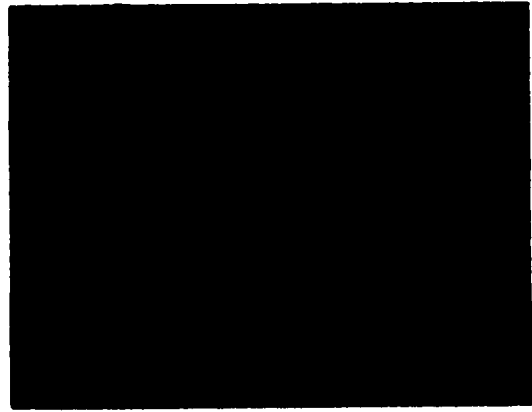
(c)

Figure 64. Encapsulated wirebond aged at 150°C for 2,000 hours: micrographs taken from (a) an optical microscope, (b) SEM, and (c) SEM at high magnification showing a linescan used for EDX analysis.
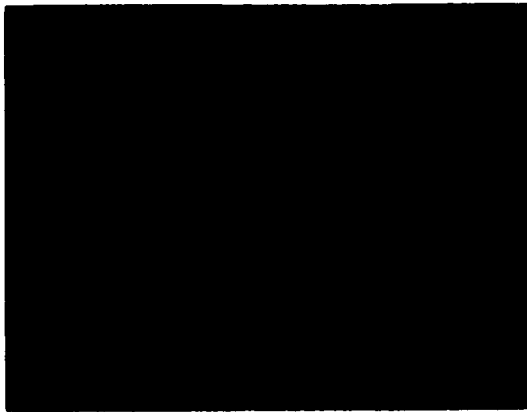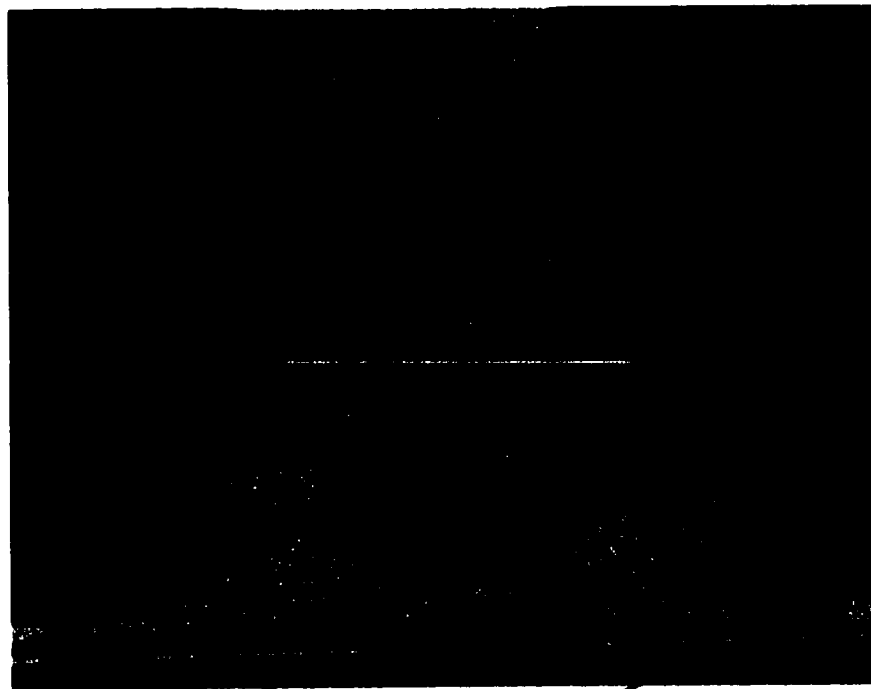
(a)   Purple regions
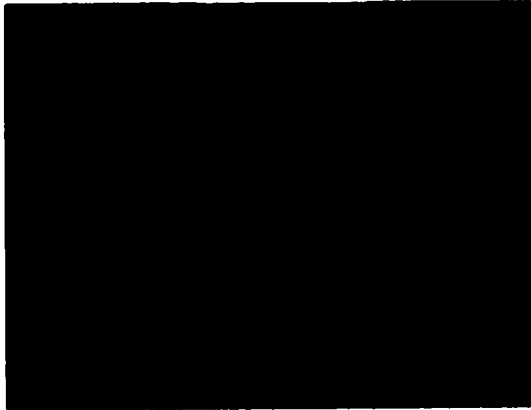
(b)   (c)

Figure 65. Encapsulated wirebond aged at 175°C for 500 hours: micrographs taken from (a) an optical microscope, (b) SEM, and (c) SEM at high magnification showing a linescan used for EDX analysis.
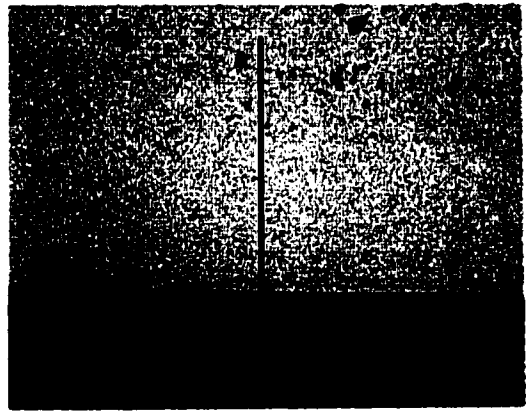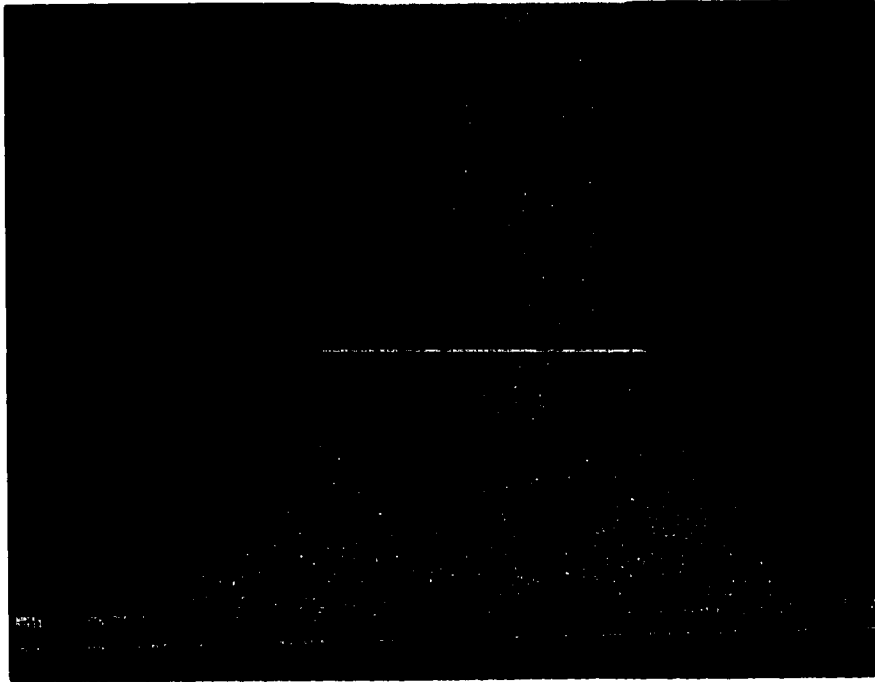
(a)
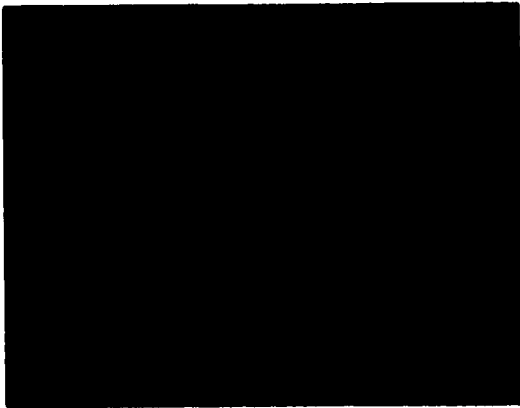
(b)
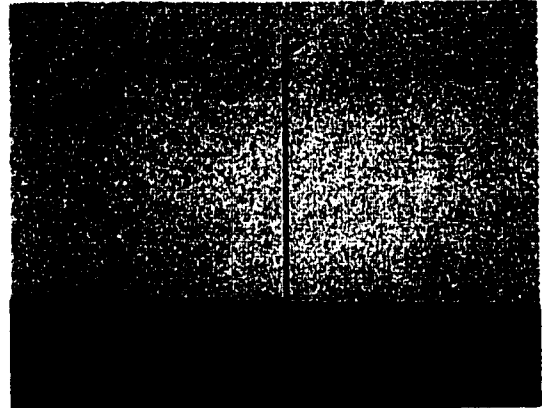
(c)

Figure 66. Encapsulated wirebond aged at 175°C for 1,000 hours: micrographs taken from (a) an optical microscope, (b) SEM, and (c) SEM at high magnification showing a linescan used for EDX analysis.
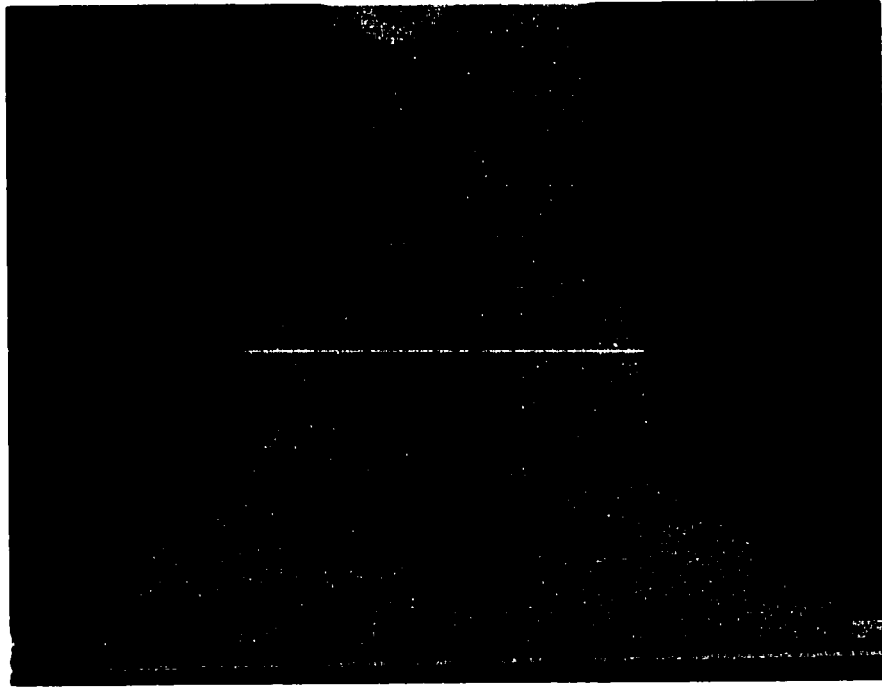
(a)

(b)
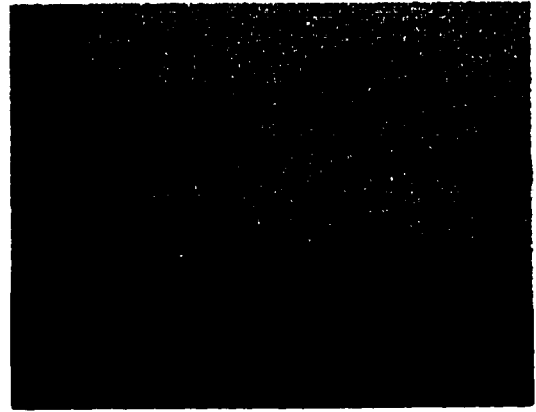
(c)

Figure 67. Encapsulated wirebond aged at 175°C for 1,500 hours: micrographs taken from (a) an optical microscope, (b) SEM, and (c) SEM at high magnification showing a linescan used for EDX analysis.
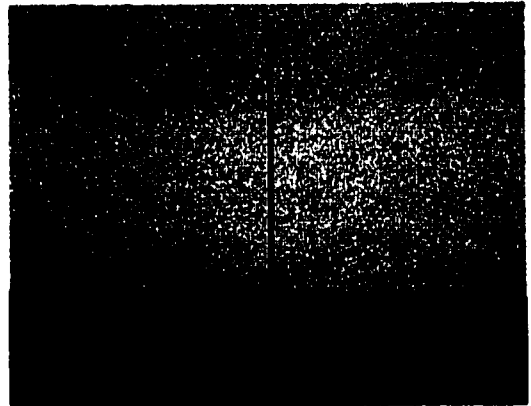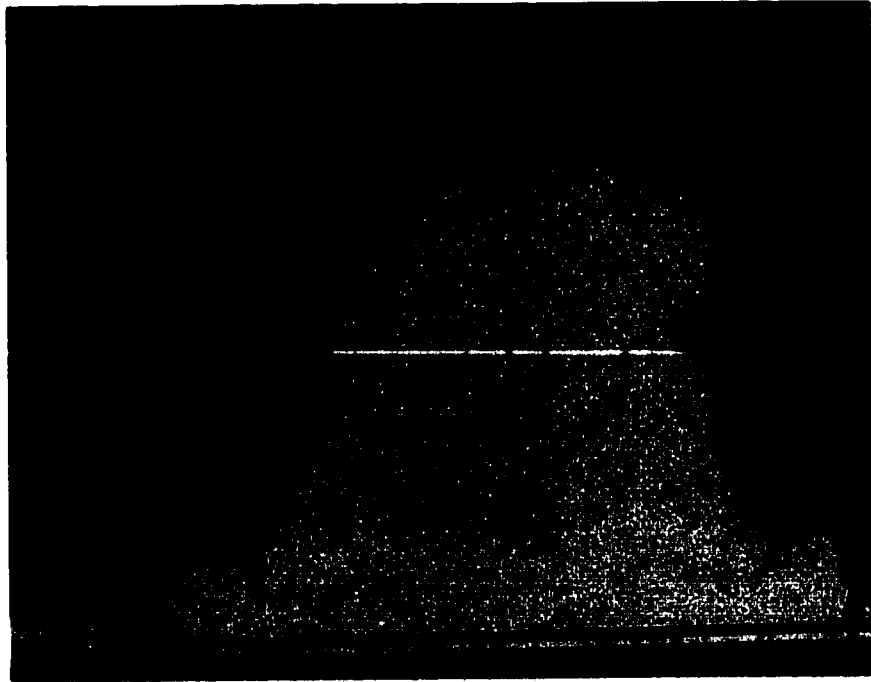
(a)

(b)
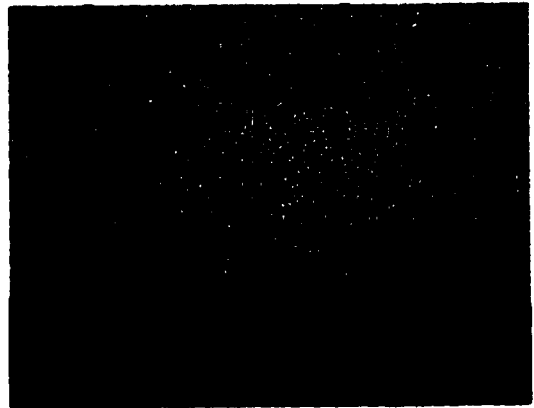
(c)

Figure 68. Encapsulated wirebond aged at 175°C for 2,000 hours: micrographs taken from (a) an optical microscope, (b) SEM, and (c) SEM at high magnification showing a linescan used for EDX analysis.

The cross-section micrographs for the standard wirebonds, aged at room temperature and 150°C, are shown in Figures 51 through 55. As can be seen in Figure 51, a significant amount of Au-Al intermetallic compounds was formed when the standard wirebonds were aged at room temperature for 2,000 hours. Compared to the case of standard wirebonds aged at room temperature, more intermetallic compounds were formed in the standard wirebonds once thermal aging at 150°C began, as shown in Figures 52 through 55. It was noticed that Au-Al intermetallic compounds were formed in the non-reacted Al bond area and grew outward from the bond pad. More intermetallic compounds were formed through the entire Al bond pad as the thermal aging process continued. This extended formation of the intermetallic compounds was also observed during the investigation of lifted balls at longer aging times. It was found that the formation of intermetallic compounds expanded into the entire bond pad and the intermetallic areas were larger than the actual bond areas, as shown in Figures 44(f) and 47(d).

The phenomena, observed in the standard wirebonds at 150°C were also seen in the wirebonds at 175°C, as shown in Figures 56 through 59. As aging time increased, more intermetallic compounds formed in the non-reacted Al bond pad region, which was outside of the initial bond area. In some cases the intermetallic compounds even grew outward from the non-reacted Al bond pad region. As a result, more intermetallic compounds were found around the ball bond periphery. At 175°C aging temperature, the Al metal in the bond pad was consumed more than it was at 150°C.

The cross-section micrographs for the encapsulated wirebonds are shown in Figures 60 through 68. As was observed in the case of standard wirebonds, it was found that a significant amount of intermetallic compounds were formed in the encapsulated wirebonds, aged at room temperature for 2,000 hours, as shown in Figure 60. When thermal aging began, more intermetallic compounds formed in the Al bond pad and started growing outward from the bond pad, as can be seen in Figures 61 through 64 for 150°C aging temperature and Figures 65 through 68 for 175°C aging temperature. As observed in the standard wirebonds, the Al metal in the bond pad was consumed more when the encapsulated wirebonds were aged at 175°C than 150°C. The growth of intermetallic compounds outward from the bond pad can be easily observed in the micrographs shown in Figures 67 and 68, for encapsulated wirebonds aged at 175°C for 1,500 and 2,000 hours, respectively.

Worth noticing in Figures 51(a) through 68(a) was the presence of a purple region at the periphery of the ball bond. This area was specifically pointed out in Figure 65(a). This purple colored region was always present in the cross-sections of both types of wirebonds, regardless of aging temperature and time. This purple region was specifically found at the edge of intermetallic region in the Al bond pad. Based on earlier studies,[3,12] this purple region is most probably the Al-rich intermetallic compound, $AuAl_2$.

Overall, same observations were made for both standard and encapsulated wirebonds, aged at 150°C and 175°C, based on the micrographs of cross-sectioned samples, as shown in Figures 51 through 68. Intermetallic compounds formed across the bond interface and grew laterally into the non-reacted Al region in the bond pad, which

was outside of the bond periphery. Once intermetallic compounds formed in the Al bond pad, they started growing outward from the bond pad. The purple region also appeared around the bond perimeter in all samples and is thought to be the Al-rich intermetallic phase, $AuAl_2$.

5.3.2.2 Measurement of Intermetallic Layer Thickness

Based on the micrographs, as shown in Figures 51 through 68, the intermetallic layer thickness was measured at the various aging times. A significant amount of the intermetallic compounds was observed in both types of wirebonds, which had been aged at room temperature for 2,000 hours. This observation agrees with earlier studies[10,11] that indicated a significant amount of intermetallic compounds formed at room temperature. It was also noticed that the Al metal of the bond pad was not completely consumed in both types of wirebonds when aged at room temperature, as can be seen in Figures 51(a), 51(b), 60(a), and 60(b). As summarized in Table 14, more Au and Al were transformed into the intermetallic compounds in standard wirebonds than in encapsulated wirebonds, based on the thickness of the intermetallic layer.

Table 14. Intermetallic phase growth after aging at room temperature for 2,000 hours.

Wirebonds	Average Intermetallic Thickness (μm)	Standard Deviation
Standard	5.31	0.67
Encapsulated	3.61	0.40

The total intermetallic layer thicknesses for the two different aging temperatures, 150°C and 175°C, were measured and are plotted, as a function of the square root of aging time, in Figures 69 through 72. Variations in the intermetallic layer thickness, for

standard wirebonds at the two aging temperatures, are shown in Figure 69. The intermetallic layer thickness slowly increased with aging time at both temperatures. Even though the mean thickness values for standard wirebonds at 175°C were greater than the values for standard wirebonds at 150°C, wide variations in the thickness indicated that the two sets of thickness data were not significantly different from each other. This observation was confirmed by a *t*-test performed at the 95% confidence level.
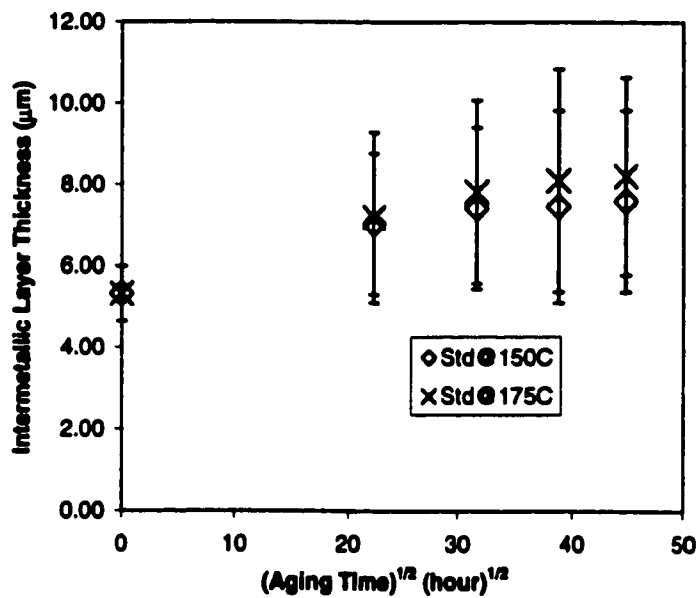
Figure 69. Intermetallic layer thickness as a function of square root of aging time for standard wirebonds.

The intermetallic layer thicknesses measured from encapsulated wirebonds at the two aging temperatures are shown in Figure 70. As was the case with the standard wirebonds, the intermetallic layer thickness for the encapsulated wirebonds also increased with aging time at 150°C and at 175°C. While the mean thickness values were greater for the encapsulated wirebonds aged at 175°C, they were not statistically different

from the mean thicknesses for the samples aged at 150°C, based on *t*-tests at the 95%

confidence level.

The intermetallic layer thicknesses for standard and encapsulated wirebonds were

compared to each other, as shown in Figures 71 and 72. At both aging temperatures, the

standard wirebonds had greater intermetallic thicknesses, regardless of aging time.

However, the wide variations in the intermetallic layer thickness indicated that both sets

of data were not statistically different.
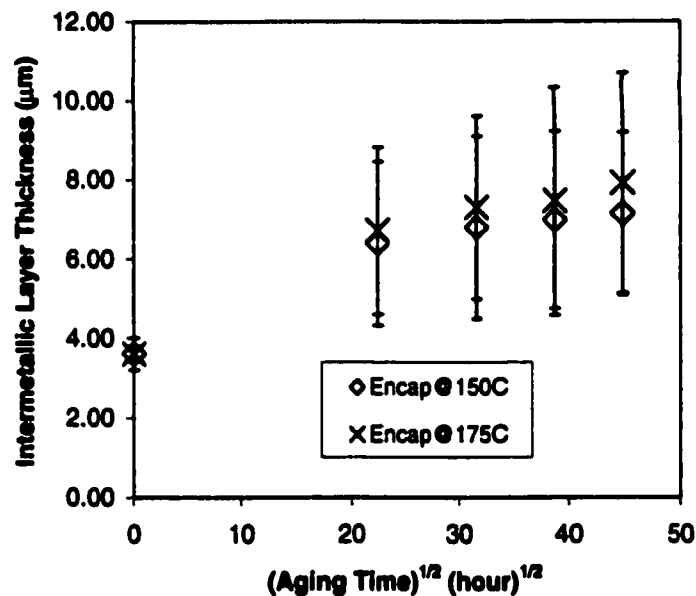
Figure 70. Intermetallic layer thickness as a function of square root of aging time for encapsulated wirebonds at the two temperatures.

Overall, it was found that the intermetallic compound formation and growth in

both types of wirebonds, at the two aging temperatures, followed the parabolic rate law,

represented by Equation (1). The growth of the intermetallic layers did not vary with

wirebonding technique at the aging temperatures employed. The effect of temperature,

150°C and 175°C, on the intermetallic layer growth was also not found. Wide variations
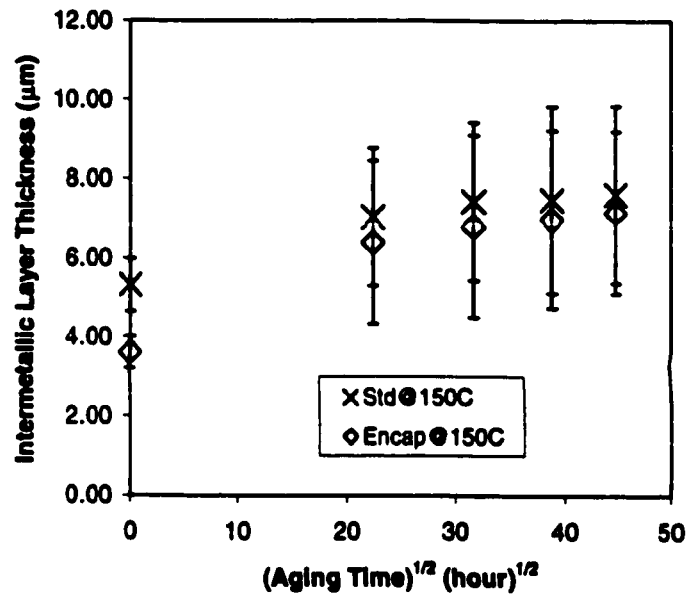
Figure 71. Intermetallic layer thickness as a function of square root of aging time for standard and encapsulated wirebonds at 150°C.
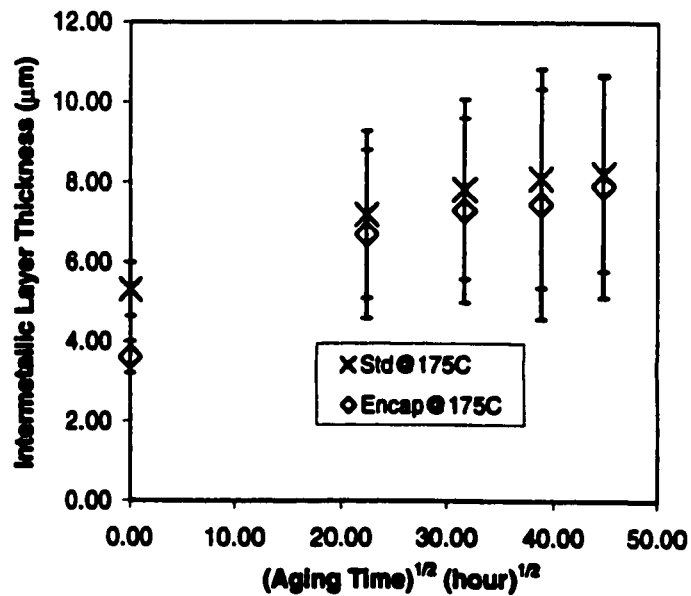
Figure 72. Intermetallic layer thickness as a function of square root of aging time for standard and encapsulated wirebonds at 175°C.

in the intermetallic layer thickness were observed in both standard and encapsulated wirebonds, which were heat treated at two temperatures. However, the prolonged aging at room temperature yielded greater intermetallic layer thicknesses for the standard wirebonds than the thicknesses for the encapsulated wirebonds. The thickness values for both types of wirebonds were found to be statistically different from each other.

Based on the plots of average total intermetallic layer thickness as a function of the square root of aging time for two different aging temperatures, as shown in Figures 69 and 70, the activation energies for the intermetallic layer growth in standard and encapsulated wirebonds were obtained. Detailed calculations for the activation energies are provided in the Appendix. For the calculation of activation energies, the intermetallic thickness data for 0 hour were excluded. The slopes of these curves, which connect the intermetallic layer thickness data for standard and encapsulated wirebonds at the two temperatures, yielded growth rate constants, as shown in Figures 73 and 74. The growth rate constants for standard wirebonds aged at 150°C and 175°C were determined to be 0.0241 μm/(hr)$^{1/2}$ and 0.0459 μm/(hr)$^{1/2}$, respectively, as shown in Figure 73. The growth rates obtained for encapsulated wirebonds at 150°C and 175°C were 0.0335 μm/(hr)$^{1/2}$ and 0.051 μm/(hr)$^{1/2}$, respectively, as shown in Figure 74.

The growth rate constants obtained for both types of wirebonds at the two aging temperatures were plotted as ln(growth rate) vs reciprocal aging temperature, 1/T, based on Equation (4), which was derived from the Arrhenius rate equation, Equation (2).

$$\ln(\text{growth rate}) = \ln C + (-E/RT)(1/T) \qquad (4)$$
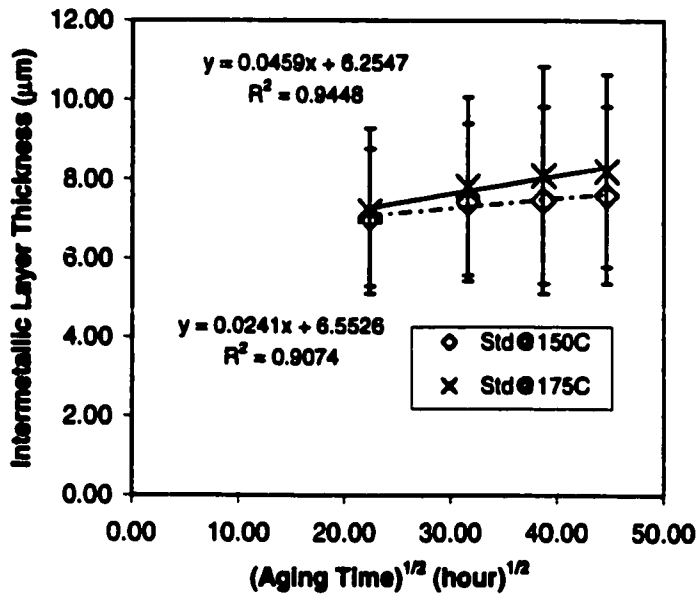
Figure 73. The intermetallic growth rate for standard wirebonds at two temperatures, 150°C and 175°C, as a function of the square root of aging time.
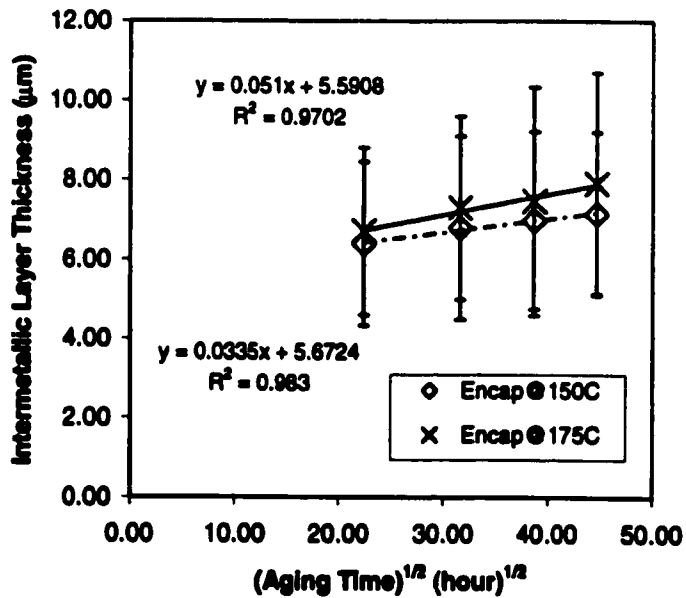
Figure 74. The intermetallic growth rate for encapsulated wirebonds at two temperatures, 150°C and 175°C, as a function of the square root of aging time.

The corresponding plots for the standard and encapsulated wirebonds are shown in Figures 75 and 76, respectively. From Figure 75 for standard wirebonds, -4.89×10^3 and 7.82 were obtained as the slope and y-intercept, respectively. From Figure 76 for encapsulated wirebonds, -3.19×10^3 and 4.14 were obtained as the slope and y-intercept, respectively. Based on Figure 75 for standard wirebonds and Equation (4), an Arrhenius relationship was obtained as follows:

$$\text{Growth rate} = 2.50 \times 10^3 \exp(-9,711/RT) \, \mu m/(hr)^{1/2} \tag{5}$$

Based on Figure 76, another Arrhenius equation was obtained for encapsulated wirebonds as follows:

$$\text{Growth rate} = 62.7 \exp(-6,196/RT) \, \mu m/(hr)^{1/2} \tag{6}$$

As shown in Equations (5) and (6), thermal activation energies for the growth of Au-Al intermetallic compounds in standard and encapsulated wirebonds were found to be 9.71 kcal/mol and 6.20 kcal/mol, respectively. The encapsulated wirebonds had lower activation energies at the two temperatures, 150°C and 175°C, compared to the standard wirebonds. These values in kcal/mol were converted to eV and compared with activation energies reported by other researchers[3,11,12,19,25,26,28] in Table 15.

As compared in Table 15, the activation energies obtained from current study are much smaller than others. Even though the experimental values were specifically compared to 0.56 eV, the activation energy reported by Charles et al. who employed thermosonic Au-Al bond for the study, the activation energies for both types of wirebonds were still small. These wide variations in activation energy could be due to
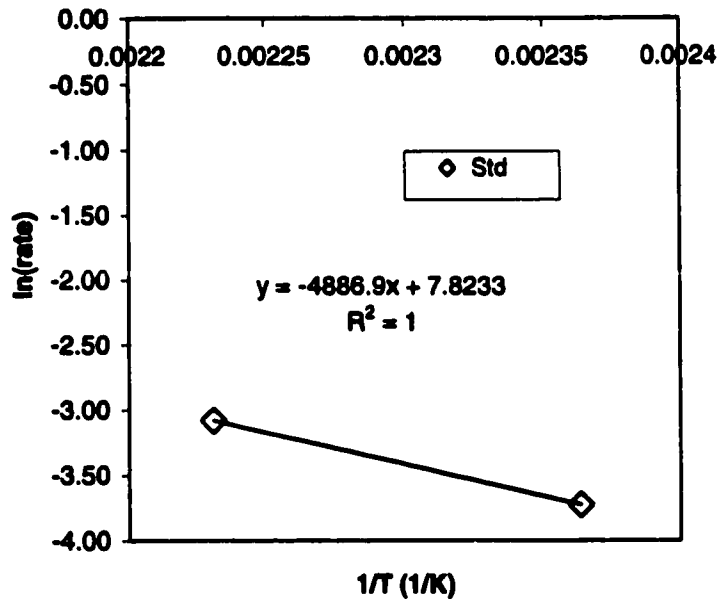
Figure 75. Arrhenius plot for the rate constant for standard wirebonds.
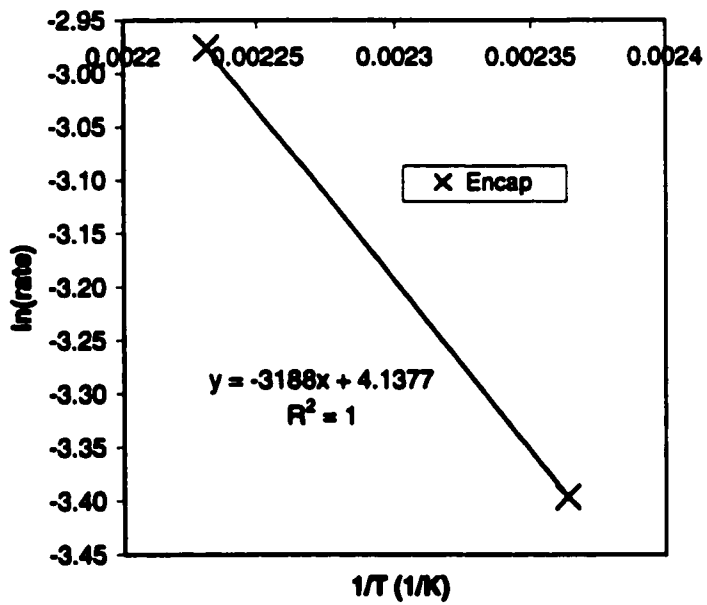
Figure 76. Arrhenius plot for the rate constant for encapsulated wirebonds.

the differences in bonding technique, properties of diffusion specimens, thermal aging conditions, and methodology employed for the measurement of activation energy.

Table 15. Thermal activation energies for the growth of Au-Al intermetallic compounds in standard and encapsulated wirebonds with activation energies reported in early studies.

Researcher	Specimen Type	Activation Energy (eV)
Current Study	Std: Thermosonic bond	0.42
	Encap: Thermosonic bond	0.27
Onuki and Koizumi[3]	Au-wire, Al-film (electrode)	1
Kashiwabara and Hattori[11]	Au-Al wire couples	0.78
Weaver and Brown[12]	Au-Al films	1
Philofsky[12]	Au-Al wire couples	0.69
Galli and Majni[19]	Au-Al films	1.2±0.1
Charles et al.[25]	Thermosonic Au-Al bond	0.56
Chen[26]	Ultrasonic Al-Au bond	0.55
Onishi and Fukumoto[24]	Au-wire, Al-film	0.88

Among these, it is thought that the method employed for the measurement of intermetallic layer thickness in this project most probably caused the wide variations in activation energy. As shown in Figures 73 and 74 for standard and encapsulated wirebonds, respectively, wide variations were found in the intermetallic layer thickness data. Cross-section micrographs for both types of wirebonds, as shown in Figure 51 through 68, also indicated that the thickness varied with location in the bond area. In spite of the wide variations in the thickness shown in the cross-section micrographs, only five spots in three locations of the bond area were randomly chosen and measured for the intermetallic layer thickness, as described earlier in Chapter 4. Even though the same locations across the bond interface were used for the thickness measurement, variations in the exact spots between samples can be expected to occur. In order to minimize

probable errors, which could arise during the intermetallic thickness measurement, the methodology employed for the measurement should be more controlled by increasing the number of spots and determining the specific locations for the measurement.

5.3.2.3 Analysis of the Bond Interface by Energy Dispersive X-ray (EDX)

The intermetallic regions between the Au ball and Al bond pad were analyzed employing EDX to determine the composition of layers across the interface. EDX results for standard wirebonds are shown in Figures 77 through 79. The results for standard wirebonds, which were stored at room temperature for 2,000 hours, are shown in Figure 77. EDX results for standard wirebonds, which were under thermal aging at 150°C for time periods up to 2,000 hours, are presented in Figures 78(a) through (d). The compositional changes in the standard wirebonds aged at 175°C are shown in Figures 79(a) through (d).

According to Figure 77, it was found that the Au-rich intermetallic compound formed across the interface. Based on earlier studies,[10,12,20] the composition of this Au-rich intermetallic phase was thought to be predominantly Au_5Al_2. At the region near the end of the Al bond pad, which was 10 µm distant from the starting point of the linescan, a higher Al peak was observed. This indicated that a significant amount of non-reacted Al was present in the bond pad.

In the case of standard wirebonds, which were heat treated at 150°C, there were shifts in the composition along with aging time, as shown in Figures 78(a) through (d). It was found that the Au-rich intermetallic compound was the dominant phase across the interface. Based on the compositional changes in Au and Al, as shown in Figures 78(a),

Au_4Al was thought to be the major intermetallic phase present at the bond interface for the standard wirebonds aged at 150°C for 500 hours.
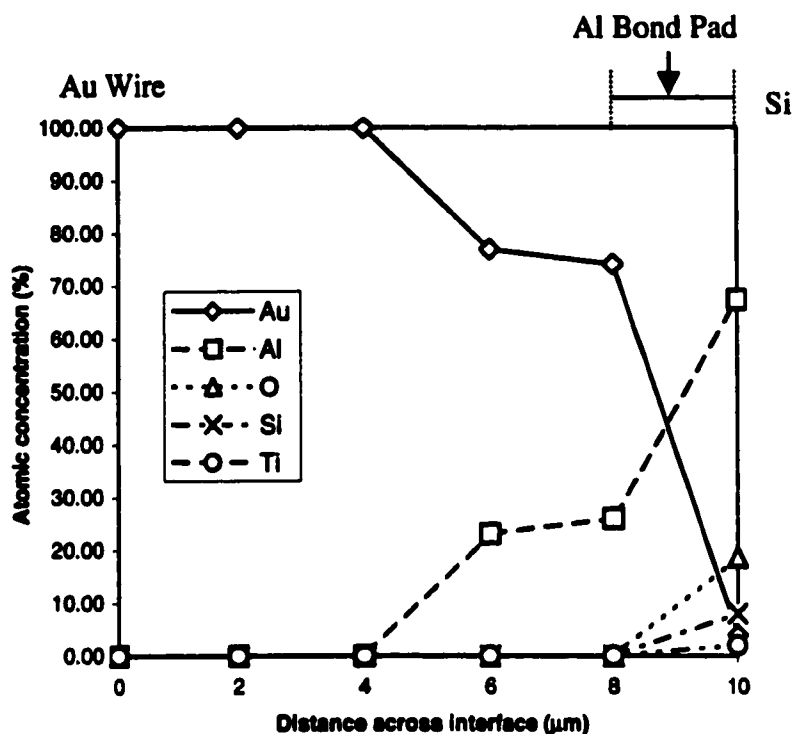
Figure 77. EDX results for standard wirebond aged at room temperature for 2,000 hours.

The intermetallic phases formed in the standard wirebonds after 1,000 hours of aging, as shown in Figure 78(b), were identified as the mixed phases of Au_5Al and Au_4Al. Au_4Al was expected to be present near the Au ball side, based on EDX results and Au-Al binary phase diagram,[9] as shown in Figure 3. It was thought that Au_5Al_2 would be present between Au_4Al and Al rich side at the bond interface.

After 1,500 hours of aging at 150°C, mixed phases of Au_5Al and Au_4Al were still present across the bond interface, as can be seen in Figure 78(c). When the aging time
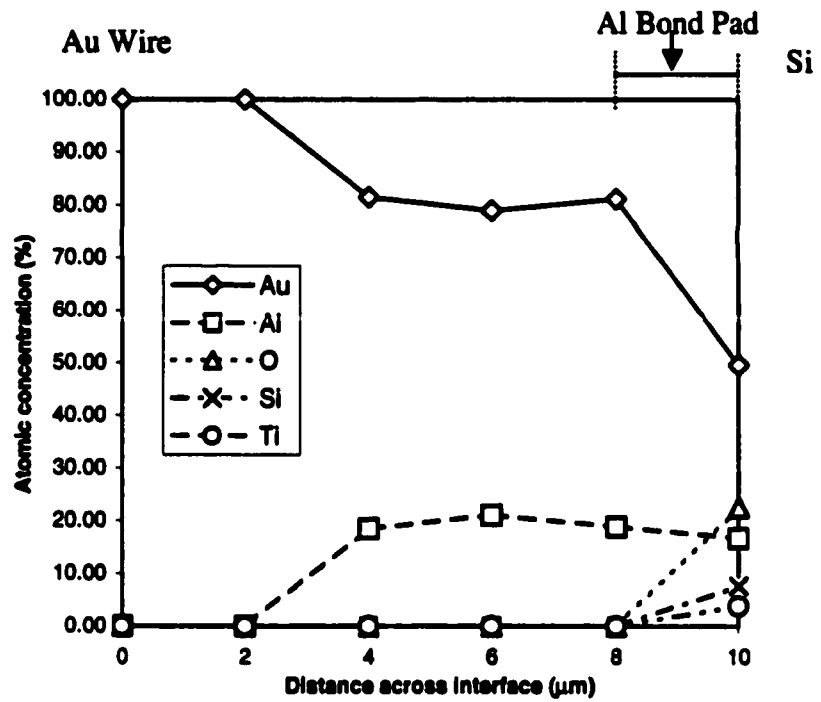
Figure 78(a). Standard wirebond aged at 150°C for 500 hours.
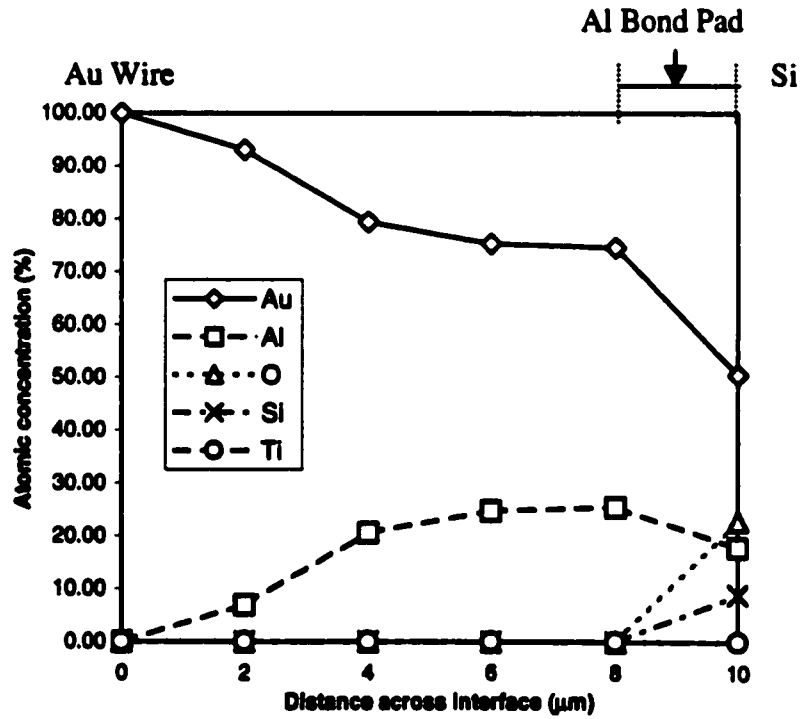
Figure 78(b). Standard wirebond aged at 150°C for 1,000 hours.
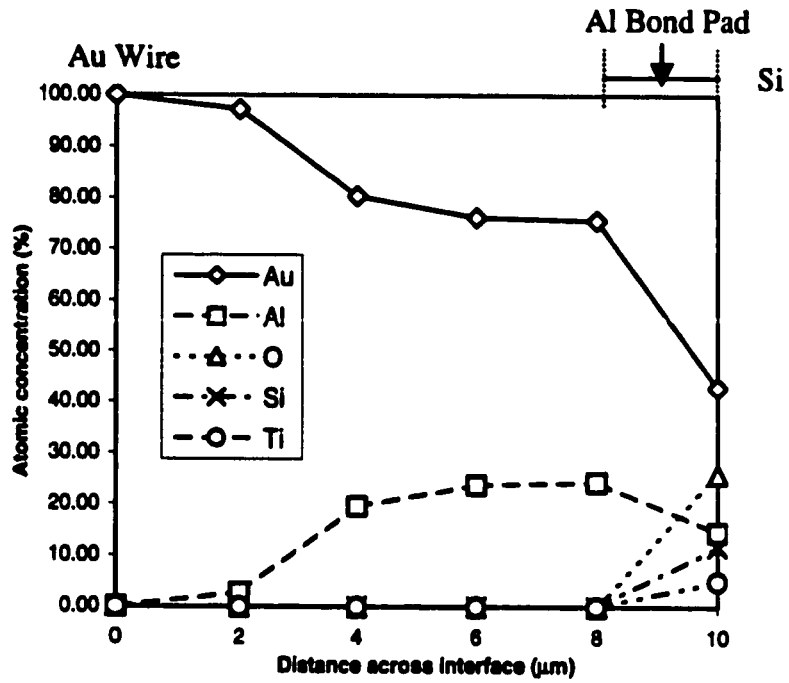
Figure 78(c). Standard wirebond aged at 150°C for 1,500 hours.
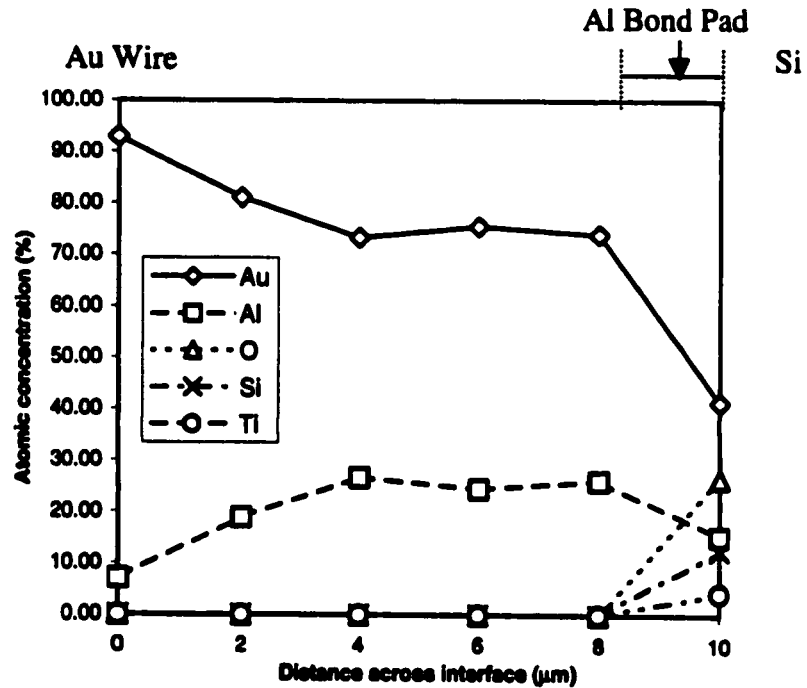
Figure 78(d). Standard wirebond aged at 150°C for 2,000 hours.

Figure 78. EDX results for standard wirebonds aged at 150°C for various times: (a) 500 hours, (b) 1,000 hours, (c) 1,500 hours, and (d) 2,000 hours.

exceeded 2,000 hours, Au_5Al_2 was thought to be the primary intermetallic phase present across the bond interface for standard wirebonds. However, mixed phases of Au solid solution and Au_4Al were expected near the Au ball region, which is 8 μm distant from the bottom of the Al bond. The distance across the bond interface, between 0 and 2 μm in Figure 78(d), corresponds to the region with mixed phases of Au_4Al and Au solid solution. It was thought that the presence of mixed Au_4Al and Au solid solution, in this particular interface region, was caused by increased Au diffusion from the Au ball side. Once the thermal aging time exceeded 1,500 hours, more Au from the Au ball region seemed to diffuse into the intermetallic region across the interface. Compositional changes, in the primary intermetallic phases for the standard wirebonds, indicated that more Al diffused from the bond pad as thermal aging proceeded. For example, the major intermetallic phase for the 500 hour aging time, Au_4Al, was changed to the mixed phases of Au_4Al and Au_5Al_2 for the 1,000 and 1,500 hour aging times. After 2,000 hours of aging, Au_5Al_2 became the dominant phase across the bond interface.

EDX results for the standard wirebonds, which were thermally aged at 175°C, are presented in Figures 79(a) through (d). As shown in Figure 79(a), the primary intermetallic phase consisting of the bond interface region, after 500 hours of aging, is Au_4Al. The same observation was made in the standard wirebonds, which were aged for 1,000 hours at the given temperature, as shown in Figure 79(b). However, some compositional changes were noticed in the standard wirebonds, when aged for 1,500 and 2,000 hours, as shown in Figures 79(c) and (d), respectively. According to Figure 79(c), the primary intermetallic phase across the bond interface was expected to be the mixed
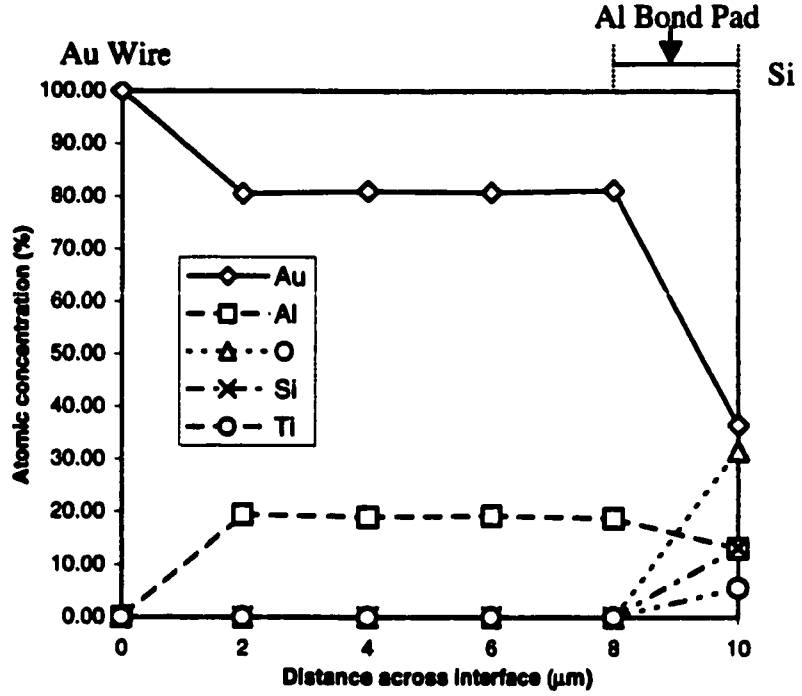
Figure 79(a). Standard wirebond aged at 175°C for 500 hours.
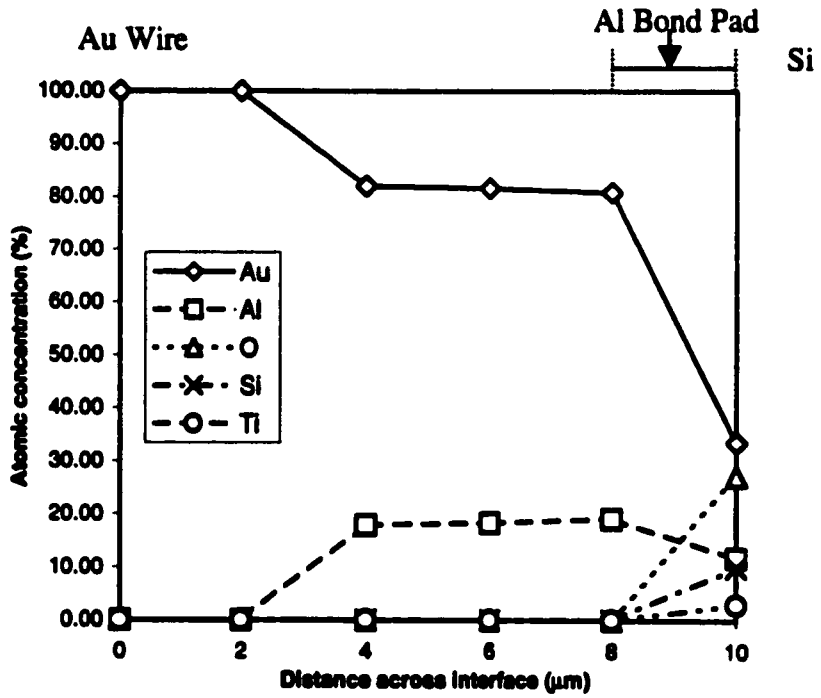
Figure 79(b). Standard wirebond aged at 175°C for 1,000 hours.
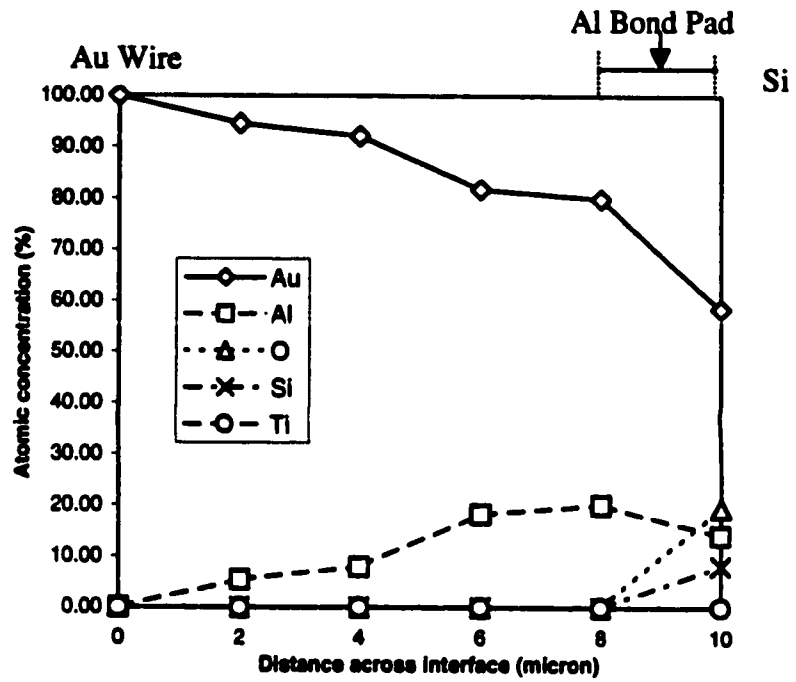
Figure 79(C). Standard wirebond aged at 175°C for 1,500 hours.
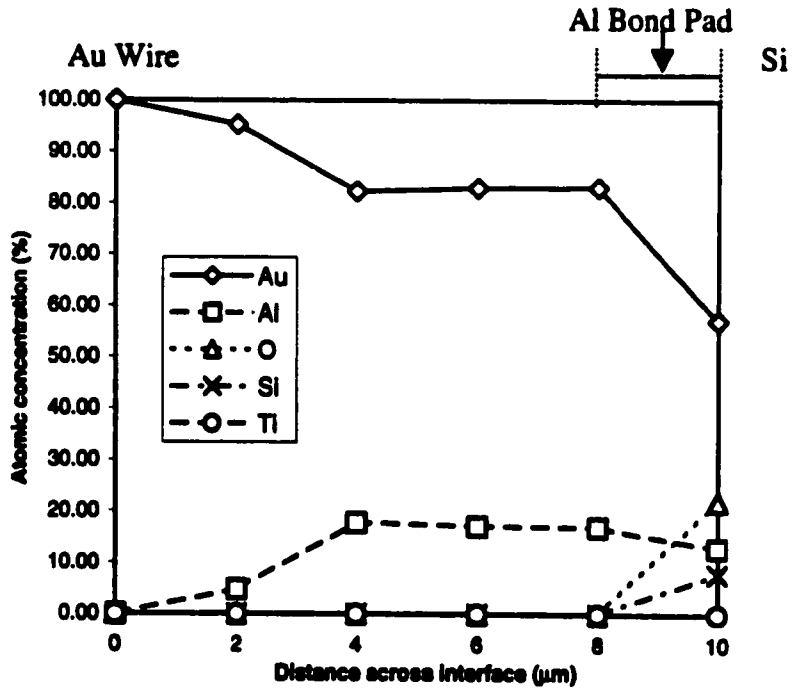
Figure 79(d). Standard wirebond aged at 175°C for 2,000 hours.

Figure 79. EXD results for standard wirebonds aged at 175°C for various times: (a) 500 hours, (b) 1000 hours, (c) 1500 hours, and (d) 2000 hours.

phases of Au_4Al and Au solid solution. As discussed earlier for the standard wirebonds aged at 150°C, this might be due to the diffusion of Au into the Au-rich intermetallic region. When thermal aging at 175°C exceeded 2,000 hours, the Au-rich intermetallic compound, Au_4Al, was mixed more with Au solid solution, as can be seen in Figure 79(d). Under this thermal aging condition, mixed phases of Au_4Al and Au solid solution were thought to be the major intermetallic phases at the bond interface. Overall, the results agreed well with the diffusion behaviors expected from the phase diagram shown in Figure 3.[9]

EDX results for the encapsulated wirebonds are shown in Figures 80 through 82. The compositional changes across the interface for the wirebonds, which were stored at room temperature for 2,000 hours, are shown in Figure 80. Based on EDX results, the Au-rich intermetallic compounds were expected to dominate the bond interface. The probable intermetallic compounds present in the region were thought to be the mixed phases of Au_4Al and Au_5Al. High concentrations of Al were found near the Al bond pad. This is indicative of non-reacted Al present on the bond pad. This can be visually confirmed by examining the cross-section micrographs shown in Figures 60(a) and (b).

The effect of thermal aging at 150°C on the intermetallic compound growth in encapsulated wirebonds can be seen in Figures 81(a) through (d). According to EDX results for all aging times, the Au-rich intermetallic compounds were expected to be the primary phases present at the interface. When encapsulated wirebonds were aged at this temperature for 500 hours, Au_4Al was identified as the major intermetallic phase present across the bond interface, as shown in Figure 81(a). When thermal aging reached 1,000

hours, the mixed phases of Au_4Al and Au_5Al were found to be present at the interface, as can be seen in Figure 81(b). The same observation was made when aged for 1,500 hours, as shown in Figure 81(c). After aging for 2,000 hours, Au_5Al_2 was found to be stable across the interface, as shown in Figure 81(d). The mixed phases of Au_5Al_2, Au_4Al, and Au solid solution were also expected in the bond region near the Au ball. This might be due to the diffusion of Au into the intermetallic compound area across the bond interface.
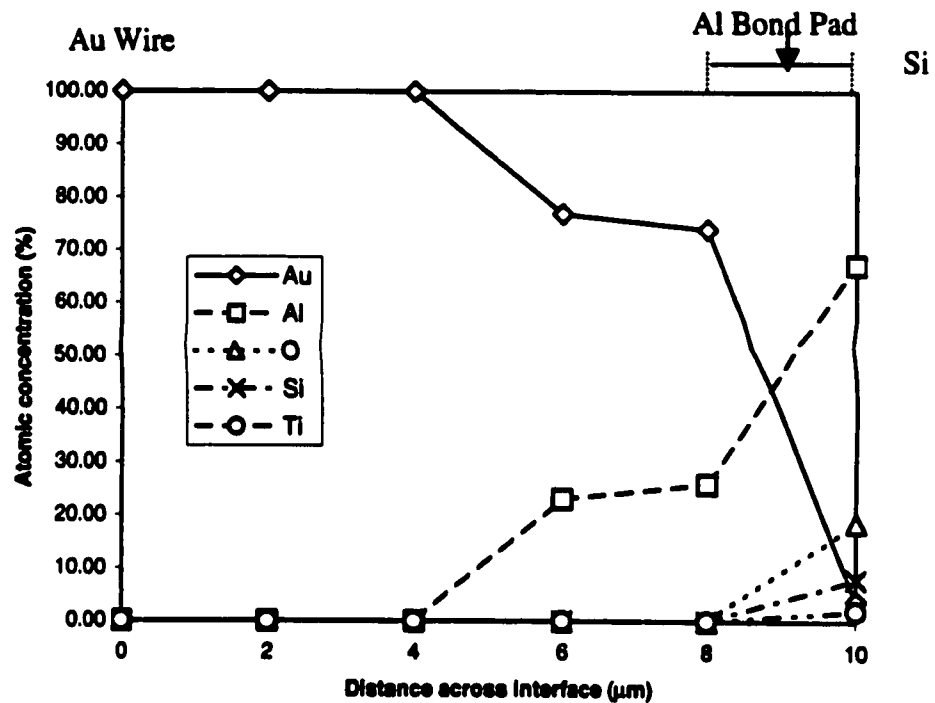
Figure 80. EDX results for encapsulated wirebond, which was aged at room temperature for 2,000 hours.
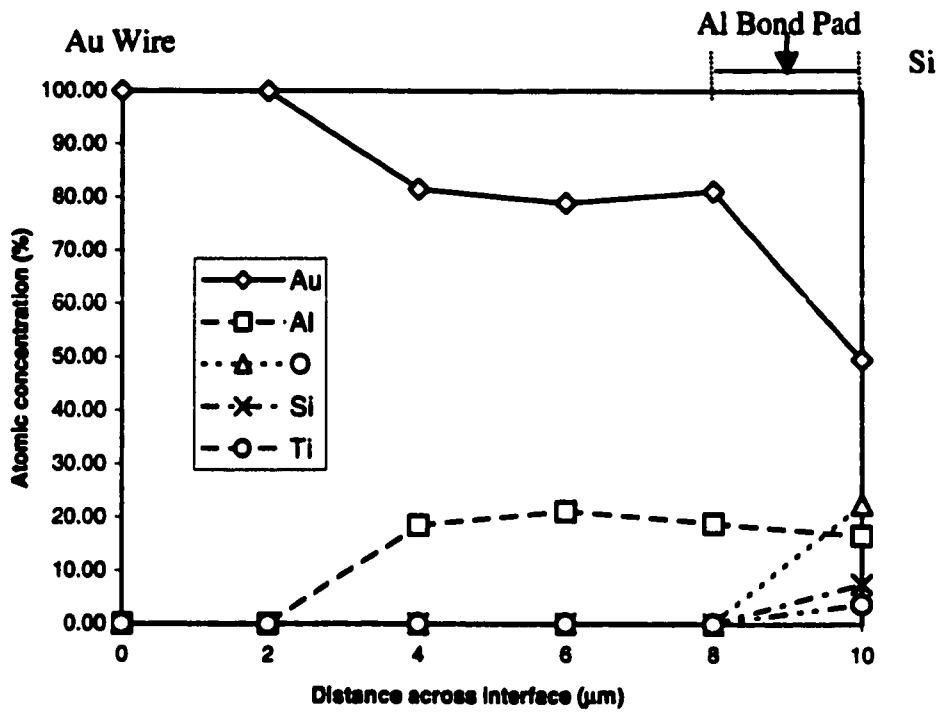
Figure 81(a). Encapsulated wirebond aged at 150°C for 500 hours.
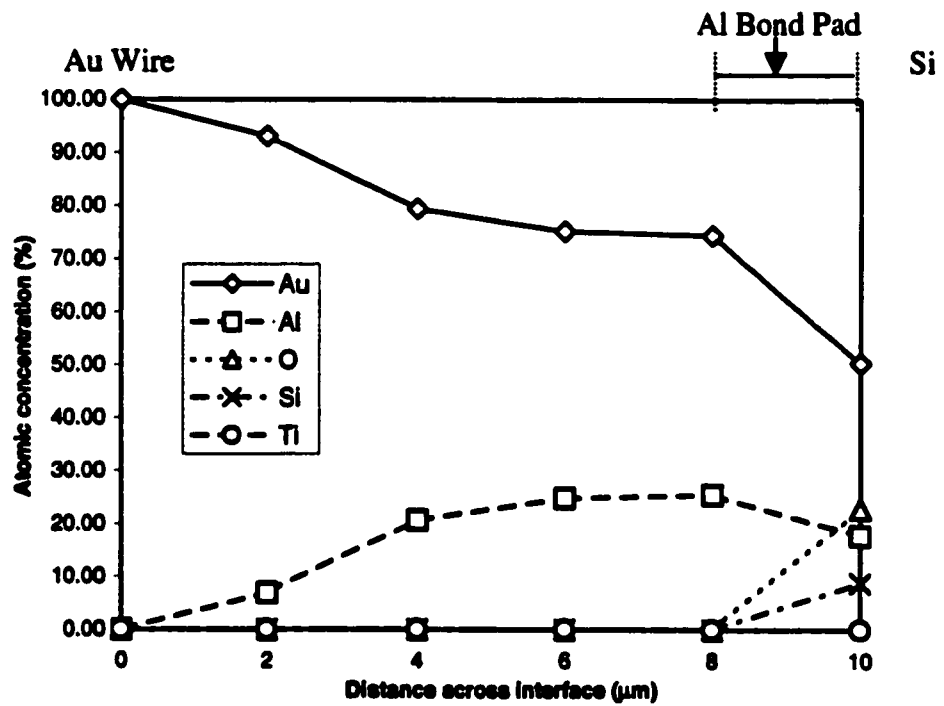
Figure 81(b). Encapsulated wirebond aged at 150°C for 1,000 hours.
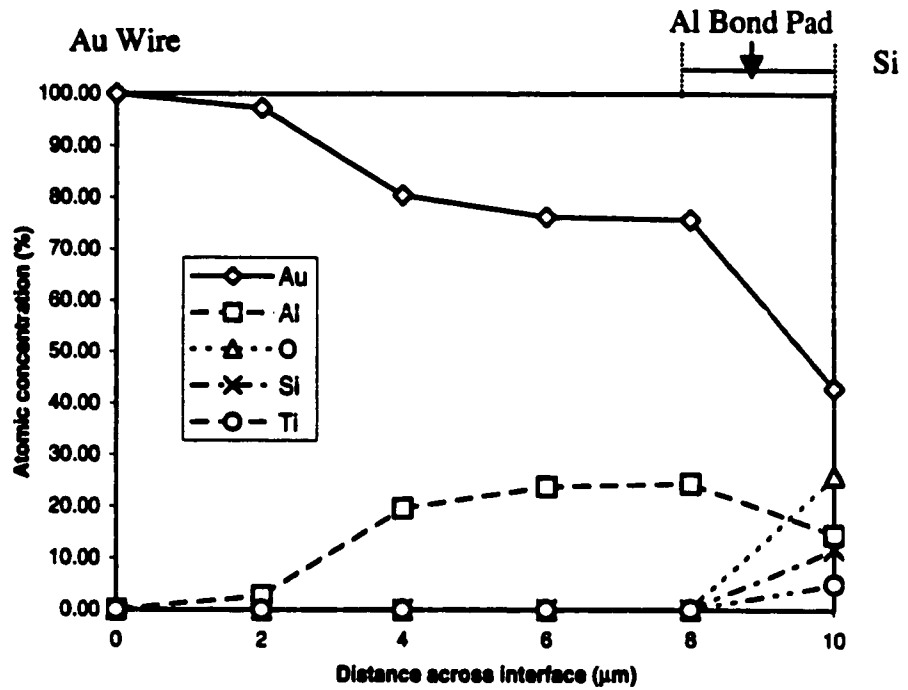
Figure 81(c). Encapsulated wirebond aged at 150°C for 1,000 hours.
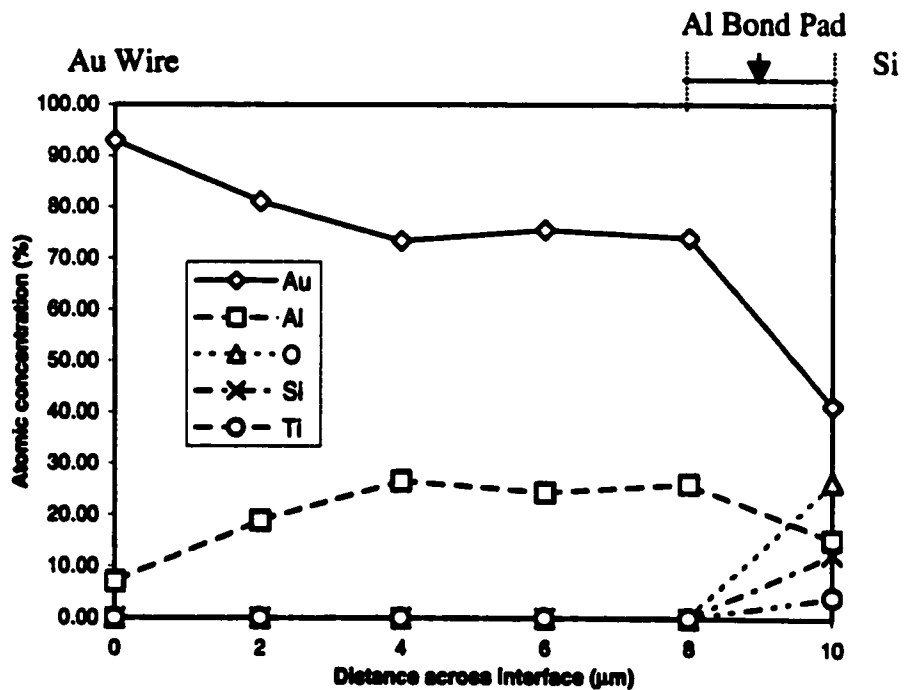
Figure 81(d). Encapsulated wirebond aged at 150°C for 2,000 hours.

Figure 81. EDX results for encapsulated wirebonds aged at 150°C for various aging times: (a) 500 hours, (b) 1,000 hours, (c) 1,500 hours, and (d) 2,000 hours.

145

The composition of the intermetallic layers present at the bond interface was also determined for encapsulated wirebonds, aged at 175°C, as shown in Figures 82(a) through (d). The primary intermetallic phase covering the interface was identified as Au_4Al. As shown in Figures 82(a) through (c), this Au-rich phase stabilized as thermal aging proceeded. At longer aging times, such as 2,000 hours, Au was thought to diffuse into the intermetallic region and yield high percentages in the atomic concentration. As shown in Figure 82(d), the mixed phases of Au_4Al and Au solid solution were expected at the bond interface near the Au ball region. The mixed phases of Au_4Al and Au_5Al_2 were also expected at the bond interface near the Al bond pad.

Overall, it was observed that the interface between the Au wire ball and the Al bond pad was composed of Au-rich intermetallic compounds, regardless of wirebonding technique, aging temperature, and aging time. As aging time increased, the Au_5Al_2 phase transformed to the more Au-rich intermetallic phase, Au_4Al. This phase stabilized as thermal aging continued. The diffusion of Au into the intermetallic region was also noticed as aging time increased. When 150°C was employed as aging temperature, mixed phases of Au_4Al and Au_5Al_2 were dominant in both standard and encapsulated wirebonds at longer aging times. However, when 175°C was used as aging temperature, mixed phases of Au_4Al and Au solid solution were the primary intermetallic compounds present across the bond interface at longer aging times, such as 2,000 hours.

During the examination of cross-section micrographs for standard and encapsulated wirebonds, purple regions around the bond perimeter, as pointed out in Figure 65, were found in all samples, regardless of aging temperature, aging time, and the
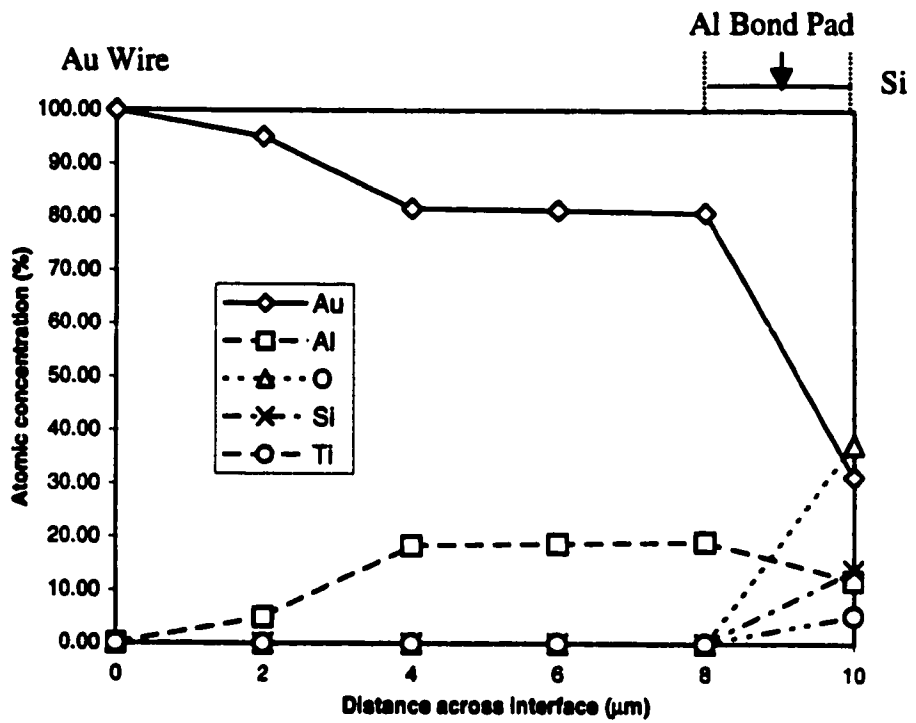
Figure 82(a). Encapsulated wirebond aged at 175°C for 500 hours.
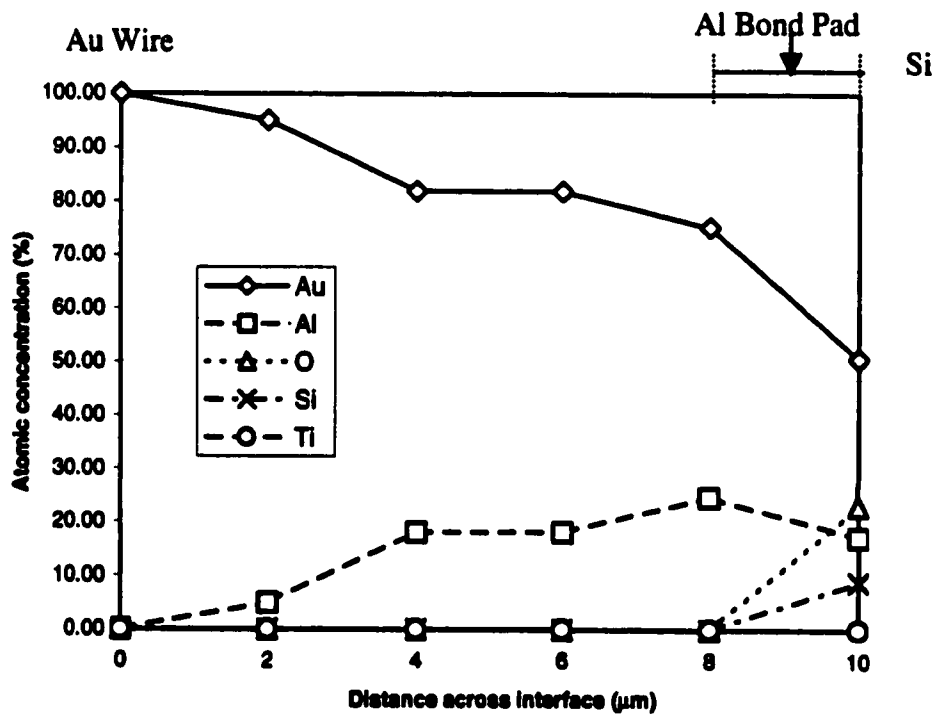
Figure 82(b). Encapsulated wirebond aged at 175°C for 1,000 hours.

147
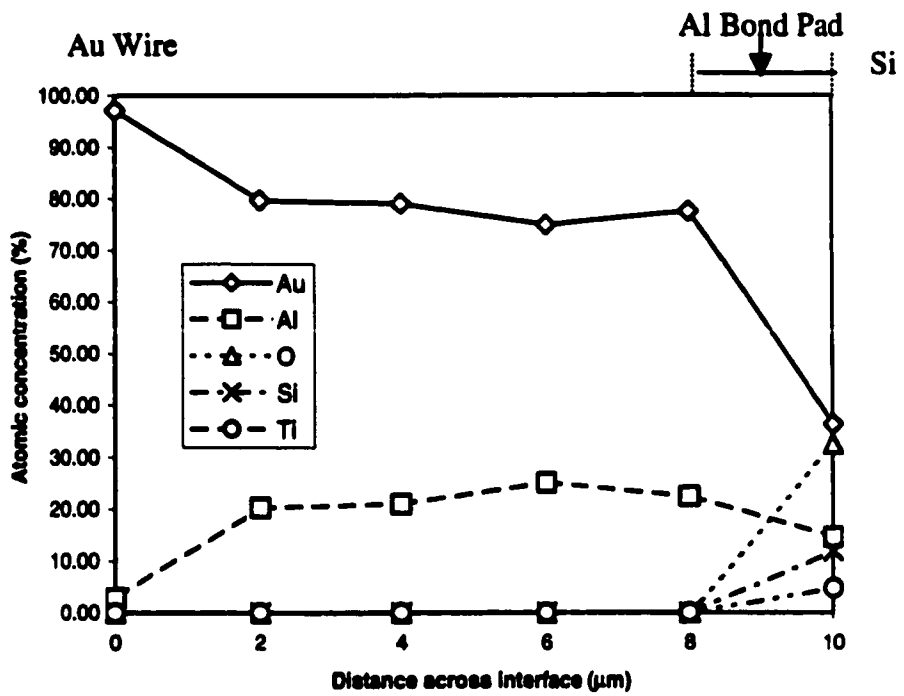
Figure 82(c). Encapsulated wirebond aged at 175°C for 1,500 hours.
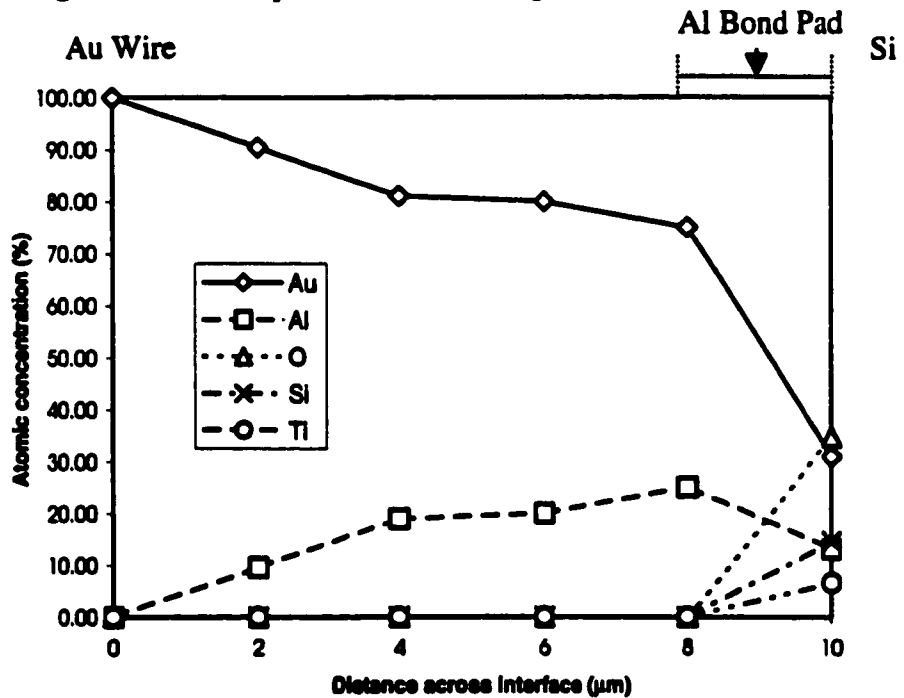
Figure 82(d). Encapsulated wirebond aged at 175°C for 2,000 hours.

Figure 82. EDX results for encapsulated wirebonds aged at 175°C for various times: (a) 500 hours, (b) 1,000 hours, (c) 1,500 hours, and (d) 2,000 hours.

type of wirebonding. These purple regions were identified using EDX. The results obtained from EDX analyses are shown in Figures 83 through 86 for both types of wirebonds, aged at 150°C and 175°C.

The purple regions of the standard wirebonds, which were stored at room temperature for 2,000 hours, were identified as an Au-rich intermetallic phase, as shown in Figure 83, at 0 hour. Based on the stoichiometry obtained from EDX analysis, this Au-rich phase is most probably Au_2Al. According to EDX results for the standard wirebonds aged at 150°C for 500, 1,500 and 2,000 hours, as shown in Figure 83, the purple regions were identified as the Al-rich intermetallic phase. This Al-rich intermetallic phase is most probably $AuAl_2$, comparing to the phase diagram shown in Figure 3.[9] However, the Au-rich phase was detected at 1,000 hours. At aging times of 500 and 1,000 hours, a significant amount of oxygen was detected. This might be due to an artifact introduced by the polishing of the cross-sectioned sample, or some aluminum was present as an oxide in this region. However, the main reason can be found in the sampling process for the EDX analysis on the purple region. Since spots for EDX analysis were randomly chosen within the purple regions, elements from slightly different areas could have been picked up and some variations resulted. However, further detailed analysis was not pursued to confirm the probable reasons causing the deviations in the results between samples, since it was beyond the scope of this project. Overall, it was found that the intermetallic region consisted of $AuAl_2$, based on the stoichiometry obtained from EDX analyses and literature.[12,25]

149
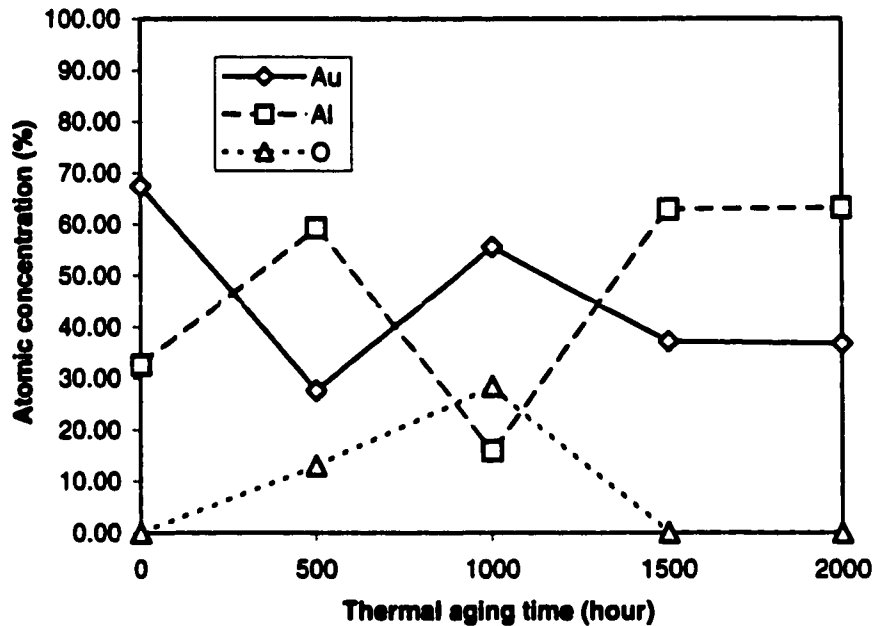
Figure 83. EDX results for the purple region of standard wirebonds aged at room temperature and 150°C for various times.

The purple regions in standard wirebonds at 175°C were also identified as the Al-rich intermetallic phase, as shown in Figure 84. As was observed in the case of standard wirebonds at 150°C, oxygen was detected after thermal aging for 1,000 and 2,000 hours. Based on EDX results, the Al-rich intermetallic compound, $AuAl_2$, was to be the intermetallic compound present at the interface region near the bond periphery.

EDX analysis on encapsulated wirebonds, aged at room temperature for 2,000 hours, revealed the presence of Al-rich intermetallic phase in the purple region, as shown in Figure 85. The purple regions observed in the encapsulated wirebonds, aged at 150°C for various times up to 2,000 hours, were also identified as the Al-rich intermetallic phase, based on EDX results. This Al-rich intermetallic phase is most probably $AuAl_2$,

based on Au-Al binary phase diagram.[9] This intermetallic phase was found to be present at the perimeter of ball bonds at all aging times.
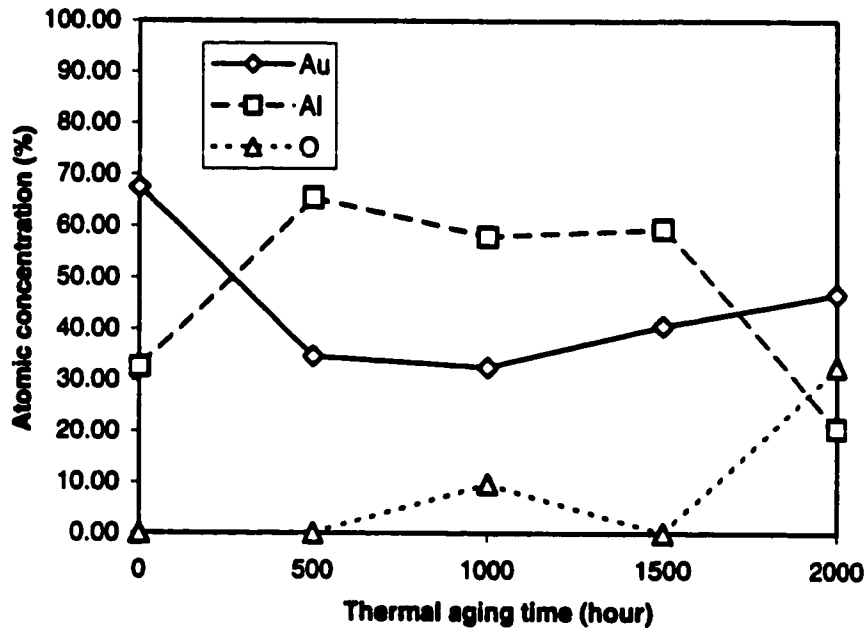
Figure 84. EDX results for the purple region of standard wirebonds aged at room temperature and 175°C for various times.

Similar EDX results were also obtained for the purple regions of the encapsulated wirebonds, which were aged at 175°C for up to 2,000 hours, as shown in Figure 86. When thermal aging was continued until 1,500 hours at the given temperature, the purple regions were identified as the Al-rich intermetallic phase, $AuAl_2$. However, EDX results at 2,000 hours indicated the presence of the Au-rich intermetallic phase in the region. This Au-rich intermetallic phase was identified as Au_5Al_2, based on the stoichiometry obtained from EDX results. It was thought that the deviation in the analysis results for the purple regions was most probably due to the randomized sampling for EDX analysis.
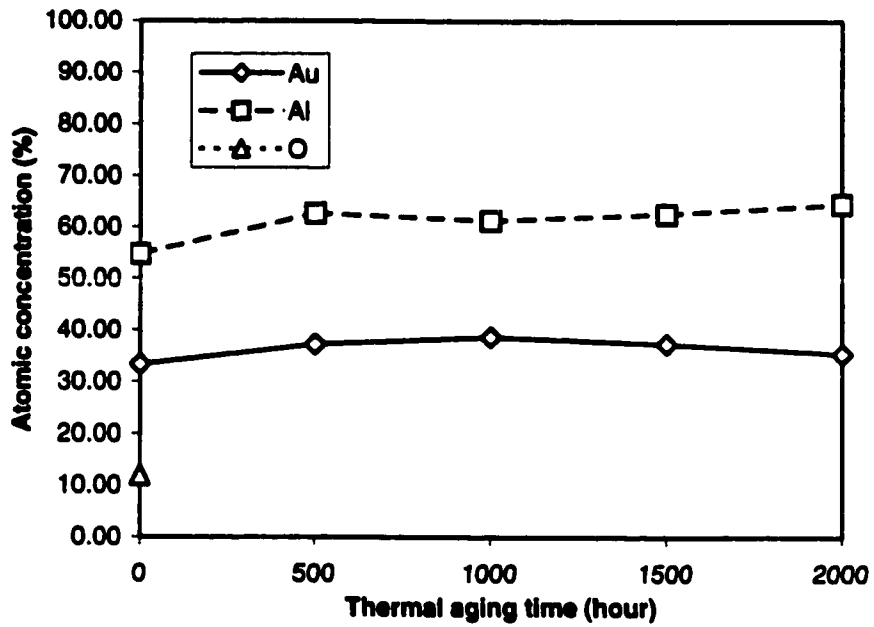
Figure 85. EDX results for the purple region of encapsulated wirebonds aged at room temperature and 150°C for various times.
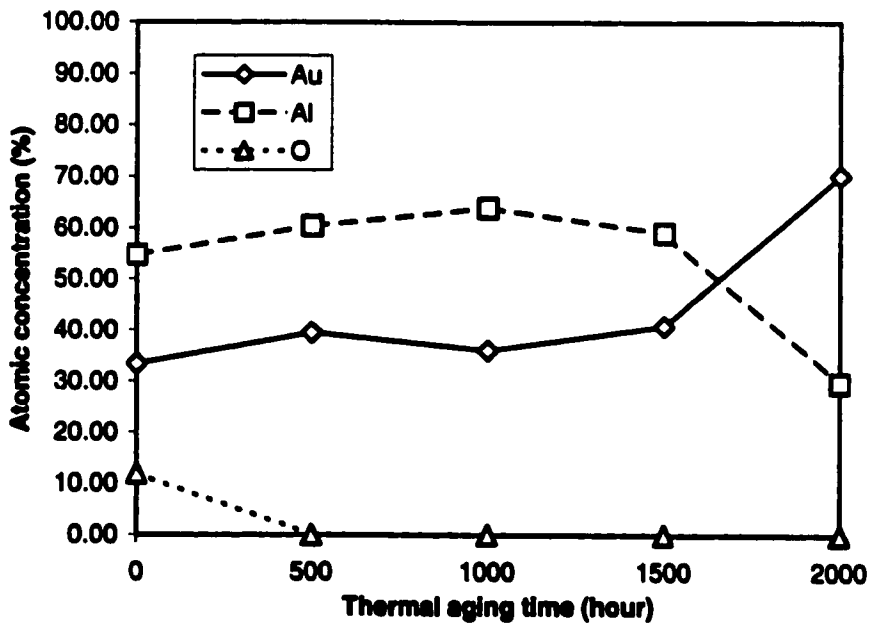
Figure 86. EDX results for the purple region of encapsulated wirebonds aged at room temperature and 175°C for various times.

Overall, the purple regions present in both types of wirebonds were identified as the Al-rich intermetallic phase, $AuAl_2$. This phase was found to be present in all samples and stayed stable at the two aging temperatures of 150°C and 175°C. This phase was not transformed into any other intermetallic phase even though prolonged thermal aging was employed. In addition, it was found that this phase could even form at room temperature when extended aging times, i.e., 2,000 hours, was employed. These observations confirmed the results obtained by other researchers.[3,10,12]

5.3.2.4 Investigation of Kirkendall Voids and Microcracks

The cross-section micrographs for standard and encapsulated wirebonds under various thermal aging conditions, as shown in Figures 51 through 68, were examined to investigate the presence of Kirkendall voids and microcracks in all samples. Both types of wirebonds, aged at room temperature for 2,000 hours, showed neither Kirkendall voids nor microcracks. Thermal aging at 150°C and 175°C did not induce the formation of Kirkendall voids and microcracks in both types of wirebonds, as can be seen in Figures 52 through 59 for the standard wirebonds and in Figures 60 through 68 for the encapsulated wirebonds. However, the cross-section micrographs of the encapsulated wirebonds, aged at 175°C for 1,500 hours, showed a significant amount of voids present on the entire ball bond, as shown in Figure 67. It was thought that these voids were formed during the bonding process. It should be also noted that the presence of voids in this sample was not related to Kirkendall voids or microcracks. However, the exact reason for the voids was not investigated since it was beyond the scope of this project.

Overall, no Kirkendall voids or microcracks were found in all wirebonds, regardless of the type of wirebonding technique, aging temperature and time.

5.3.3. Bond Pull Strength

The bond pull strengths of two sets of standard wirebonds, which were aged at 150°C and 175°C, were measured at the various thermal aging times. Variations in the average pull force and the standard deviation ($\pm\sigma$), along with thermal aging time, is shown in Figure 87. As aging time increased, the mean pull strengths of both sets of wirebonds at the two temperatures decreased. In general, the standard wirebonds aged at 150°C had greater pull strengths than those aged at 175°C, for aging times exceeding 250 hours. Wide variations between the pull forces were found at aging times longer than 500 hours. Student t-tests performed at the 95% confidence level showed that the pull forces for standard wirebonds at 150°C were not significantly different from the forces for the wirebonds aged at 175°C in the aging time interval up to 250 hours. However, the pull forces for both types of wirebonds were found to be statistically different from each when aged longer than 250 hours at the given temperature.

In both sets of standard wirebonds at 150°C and 175°C, all wire breaks occurred in the neck region right above the Au ball. This indicated that relatively strong bonds were made between the Au ball and the Al bond pad. This was also indicative of the absence of critical voiding or cracks at the bond interface. These observations were expected since the strength of the bond, made by forming a large diameter ball at the interface, was assumed to be much greater than the strength required to break the wire.[25]
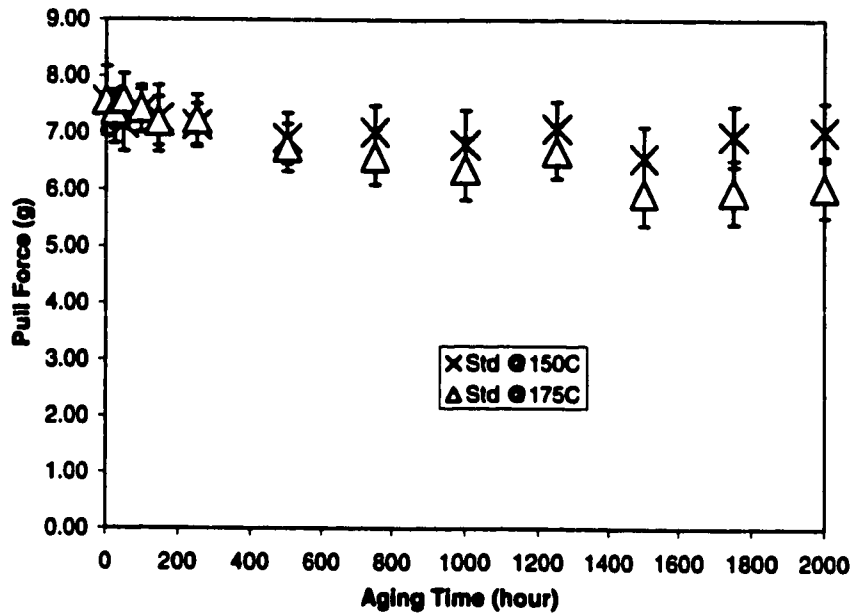
Figure 87. Pull force as a function of aging time for standard wirebonds at two temperatures, 150°C and 175°C.

Wire breaking in the neck region can be explained in terms of microstructural change that the Au wire undergoes during the bonding process. During the ball formation, the portion of the wire right above the ball is subjected to a high temperature close to the Au melting temperature. This portion of the Au wire is called the heat affected zone or HAZ.[3] Due to the rapid heat treatment for a short period of time, the wire in the HAZ undergoes recrystallization and grain growth, which makes the HAZ the weakest part of the bonding system, due to the larger grain structure than the rest of the wire. It has been also reported that this zone has a hardness about 20% lower than the original wire that is not under the influence of high temperature.[3] In addition, it is known that the grain growth is influenced by aging temperature and time.[5,7] At longer times and higher temperatures, larger grains result. Depending on the grain size, the

155

strength of the metal is altered. These observations were reflected in the variation of the pull forces for standard wirebonds at two aging temperatures. As shown in Figure 87, the average pull forces for standard wirebonds at 150°C were greater. Further, the pull forces slightly decreased with aging time at both temperatures.

The pull strengths of the encapsulated wirebonds aged at 150°C and 175°C were measured and the mean values were plotted as a function of thermal aging time in Figure 88. As was observed for the standard wirebonds, greater mean pull strengths were obtained from the encapsulated wirebonds aged at 150°C. As shown in Figure 88, the difference in aging temperature did not influence the pull forces significantly when the wirebonds were aged for time periods up to 96 hours. Fluctuations in the pull force were obtained in both sets of encapsulated wirebonds at two different aging temperatures, however, the mean pull strengths decreased slightly with aging time, regardless of aging temperature.

For a better understanding of the bond pull strength change in encapsulated wirebonds, the data presented in Figure 88 were sorted according to the failure mode described in Table 11. These are plotted, as a function of aging time, in Figures 89 and 90. Failure modes examined in encapsulated wirebonds at 150°C are shown in Figure 89(a). More than 90% of the wirebonds, at all aging times, displayed Mode 2 Failure, i.e., wire breaks at the neck. Mode 1 Failure, i.e., wire ball lifts, appeared after 96 hours of aging, but the frequency was below 10% for all aging times. As can be seen in Figure 89(a), the frequency of each failure mode fluctuates with the aging time and no specific trend can be found. This might have been caused by poor bonding rather than thermal

aging itself since none of the standard wirebonds aged at 150°C resulted in Mode 1

Failure, which is generally seen in wirebonds with insignificant amount of the

intermetallic compounds formed at the bond interface.
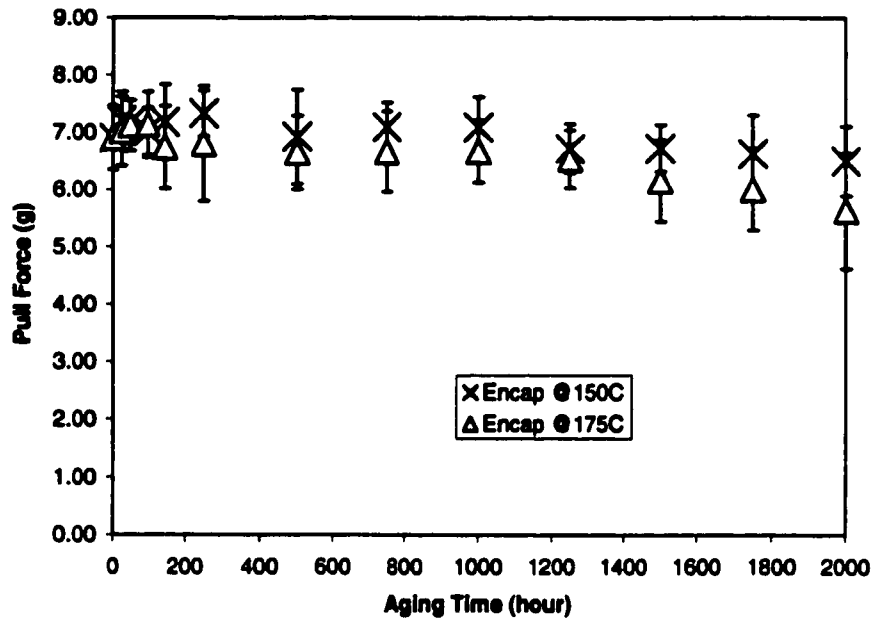
Figure 88. Pull force as a function of thermal aging time for encapsulated wirebonds at two temperatures, 150°C and 175°C.

The actual pull strengths measured for each failure mode are plotted in Figure

89(b). The average pull strength for Mode 2 Failure was found to vary only slightly with

aging time. As aging time increased, the mean strength decreased. However, variations

in the pull force were about the same at all aging times. Compared to Mode 2 Failure, the

mean pull strength of Mode 1 Failure fluctuated greatly, with wide variations. Wide
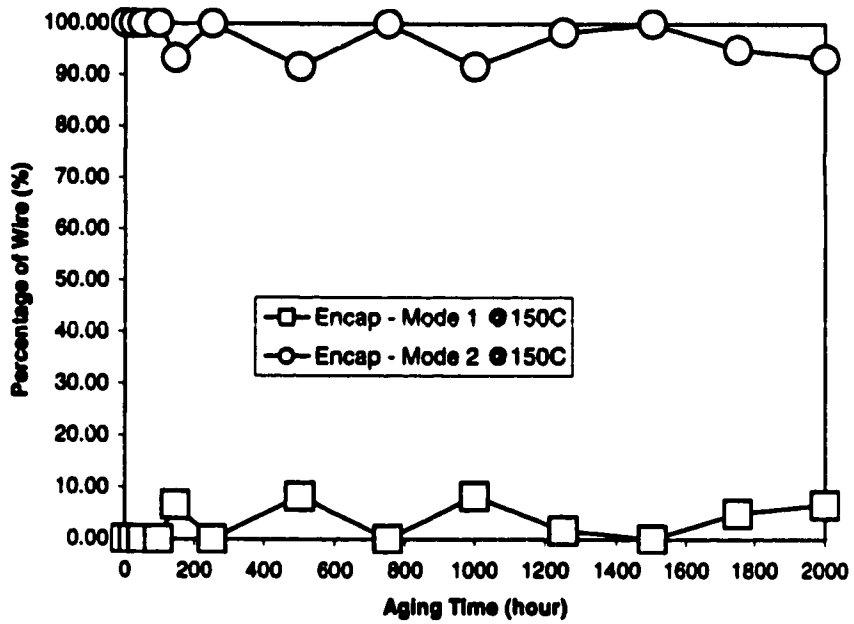
(a)
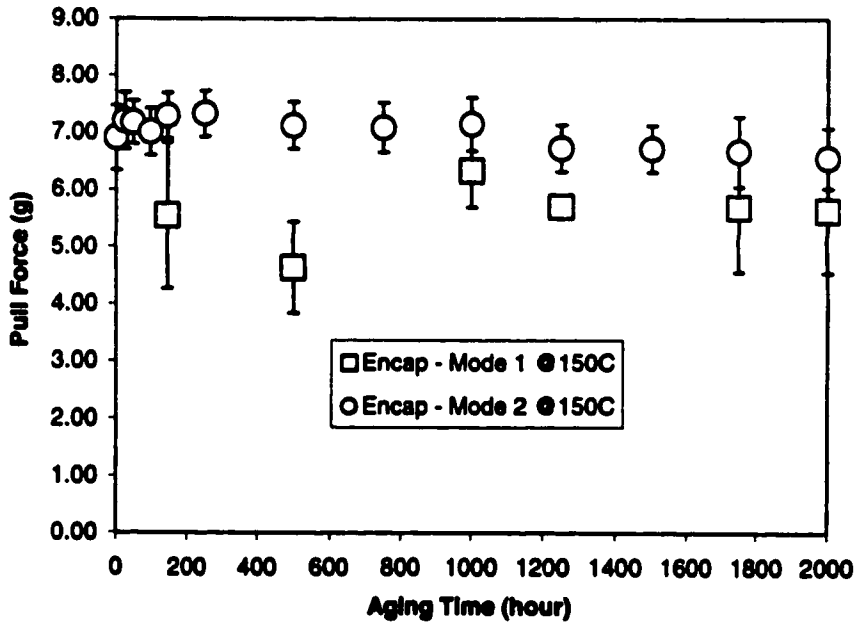
(b)

Figure 89. Failure mode of the bond pull test (a) and corresponding pull strength for each failure mode (b) as a function of thermal aging time for encapsulated wirebonds aged at 150°C.

variations in the pull force might be indicative of variations in the intermetallic compounds formed at the bond interface.

The pull strength data for encapsulated wirebonds aged at 175°C were sorted based on failure mode and plotted in Figures 90(a) and (b). As shown in Figure 90(a), Mode 2 Failure was more frequent than Mode 1 Failure. Mode 1 Failure, wire ball lifting, started to appear once thermal aging at 175°C began. The frequency of Mode 1 Failure increased as thermal aging proceeded. The average pull strengths for each failure mode at various aging times are shown in Figure 90(b). As was observed for encapsulated wirebonds aged at 150°C, the mean pull strength of Mode 2 Failure decreased with increase in aging time. Variations in the pull strength were about the same at all aging times. In the case of Mode 1 Failure, wide variations in the pull force were found. A general trend for Mode 1 Failure was not discernible due to the fluctuations in the pull force with aging time.

For the two aging temperatures, the average pull strengths of the standard and encapsulated wirebonds were plotted as a function of aging time and compared in Figures 91 and 92. Since standard wirebonds aged at 150°C showed only Mode 2 Failure, i.e., wire breaking at the neck region, the pull forces of encapsulated wirebonds for Mode 2 Failure were sorted out and plotted in Figure 92 for valid comparison. The mean pull forces for both standard and encapsulated wirebonds at 150°C fluctuated with aging time, as shown in Figure 91. At the beginning of thermal aging, the mean pull strengths of the
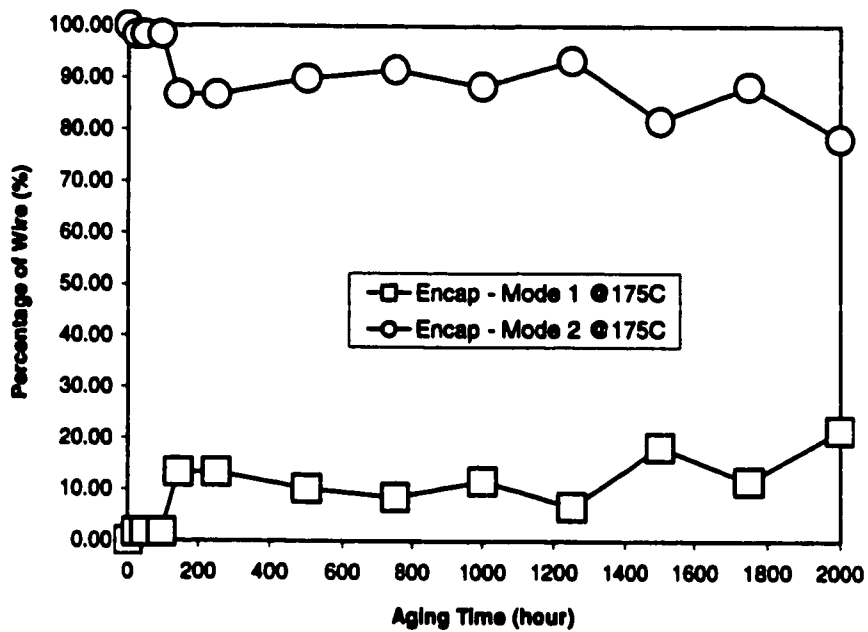
(a)
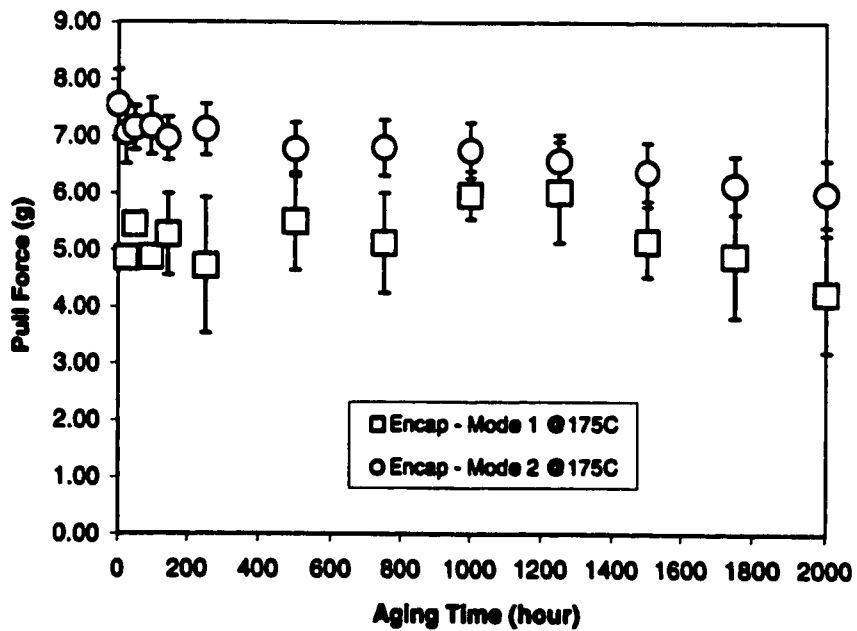
(b)

Figure 90. Failure mode of the bond pull test (a) and corresponding pull strength for each failure mode (b) as a function of thermal aging time for encapsulated wirebonds aged at 175°C.

standard wirebonds were greater than the strengths of encapsulated wirebonds. However, the mean values fluctuated statistically as the aging process continued. Overall, the pull force did not vary greatly with aging time in both types of wirebonds.
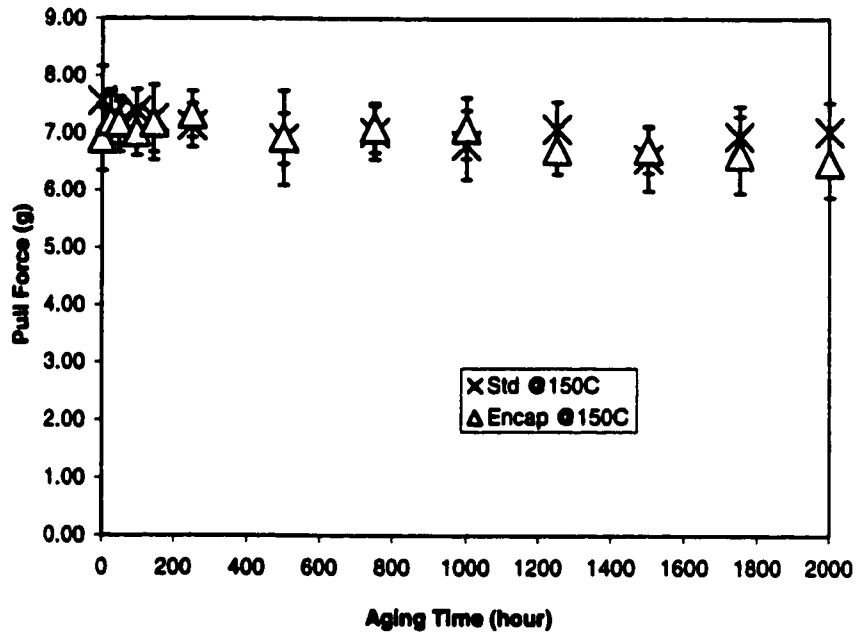
Figure 91. Bond pull force as a function of aging time for both standard and encapsulated wirebonds aged at 150°C.

In the case of standard and encapsulated wirebonds aged at 175°C, the mean pull strengths decreased slightly with aging time, as can be seen in Figure 92. As was observed with both types of wirebonds aged at 150°C, the pull strengths of both standard and encapsulated wirebonds aged at 175°C fluctuated with aging time. At the early stages of thermal aging, the mean pull forces for standard wirebonds were greater. However, after 250 hours of thermal aging, the mean forces of standard wirebonds began decreasing and reached the values smaller than the pull forces of encapsulated wirebonds

at each aging time. Variations in the pull forces for standard and encapsulated wirebonds were similar at all aging times.
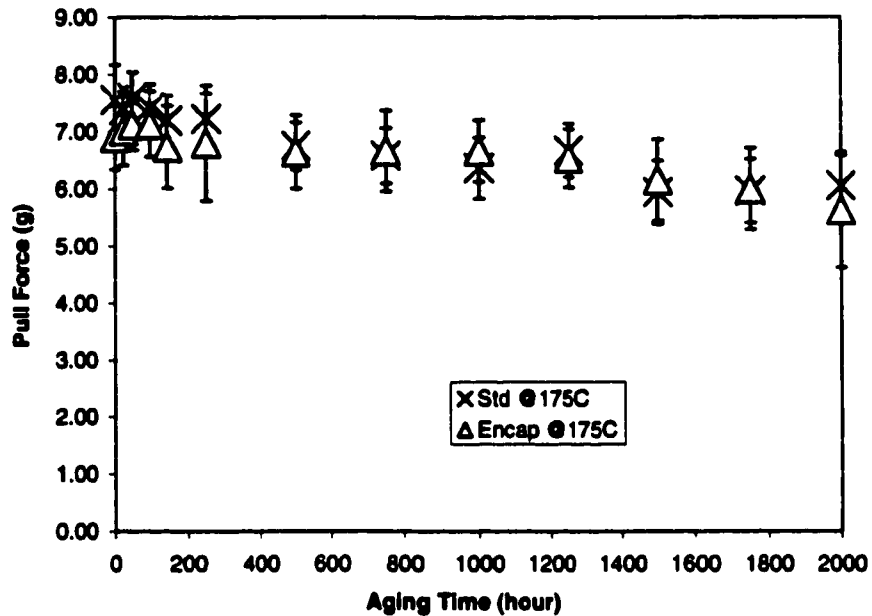
Figure 92. Bond pull force as a function of aging time for standard and encapsulated wirebonds aged at 175°C.

Overall, the mean pull strengths for standard and encapsulated wirebonds aged at 150°C did not vary greatly with aging time. Some fluctuations were observed in both sets of the pull strength data during the thermal aging. In the cases of standard and encapsulated wirebonds at 175°C, the mean pull strengths gradually decreased with aging time. This is indicative of microstructural changes occurring in the HAZ of the Au wire. In addition, it was found that the higher temperature, 175°C, had a greater influence on the microstructural change and further grain growth in the Au wire.

5.3.4 Ball Shear Strength

The results of the ball shear test for standard and encapsulated wirebonds are presented and compared to each other in Section 5.3.4.1. In Section 5.3.4.2, the specific shear failure modes, observed during the shear test for both types of wirebonds, are discussed. In Section 5.3.4.3, the shear strengths for the two types of wirebonds are discussed, as it related to the intermetallic layer thicknesses.

5.3.4.1 Ball Shear Strengths for Standard and Encapsulated Wirebonds

The ball shear force of the standard wirebonds was measured and converted to the shear stress by dividing it by the corresponding ball area. The mean shear stress values for standard wirebonds, which had been thermally aged at 150°C and 175°C, were plotted as a function of aging time in Figure 93. As can be seen in Figure 93, the shear strengths of the standard wirebonds, prior to thermal aging, were not zero. Since a significant amount of the intermetalllic compounds formed during the bonding process, as discussed in Section 5.3.1, some finite values of the shear strengths were expected from the wirebonds even though they were not thermally aged at a high temperature. The mean shear strengths of the standard wirebonds, aged at either temperature, increased with aging time. At the beginning of the thermal aging process, the shear strength increased rapidly with aging time. However, the increase in the shear strength slowed down as aging time exceeded 250 hours.

Overall, the average shear strengths of standard wirebonds at 175°C were greater than those obtained from the wirebonds at 150°C at every thermal aging time. ANOVA (analysis of variance) and Student t-tests performed on two sets of the shear strength data,

which were collected for each aging time, indicated that the shear strengths of standard wirebonds at 150°C were statistically different from the strengths of standard wirebonds at 175°C. This revealed that aging temperature influenced the bond strength, which is dependent on the formation and growth of the intermetallic compounds at the bond interface.
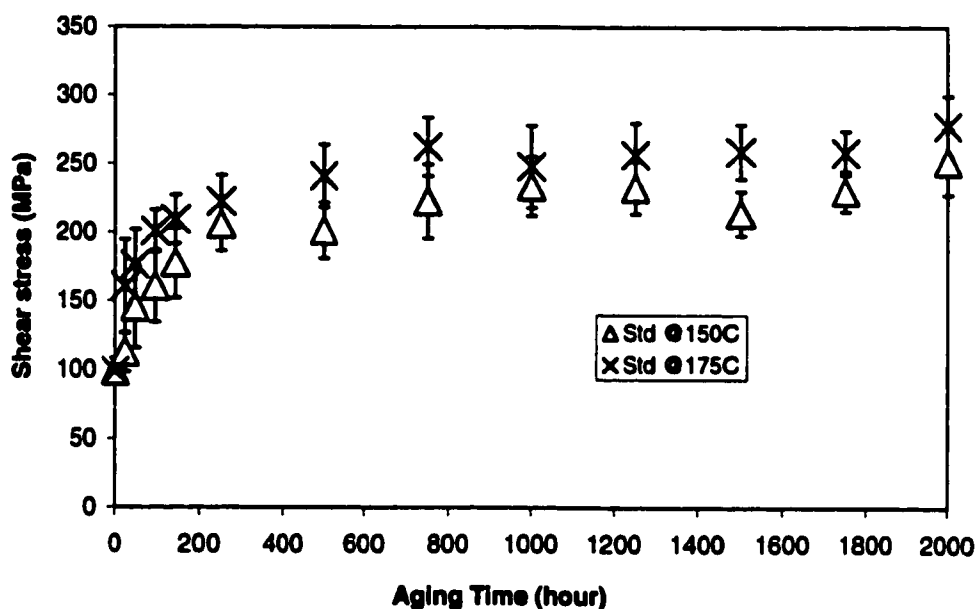
Figure 93. Ball shear strength as a function of aging time for standard wirebonds aged at two different temperatures, 150°C and 175°C.

The failure mode of the ball shear test was assigned to both sets of standard wirebonds aged at two temperatures, based on the criteria stated in Table 11. The frequency of each failure mode was plotted as a function of aging time in Figures 94(a) and (b). Standard wirebonds aged at 150°C yielded two major shear failure modes, which were ball lifting and shearing through the Au ball. These two modes corresponded to Mode 1 and 2 Failures, based on the standard failure modes used in industry as
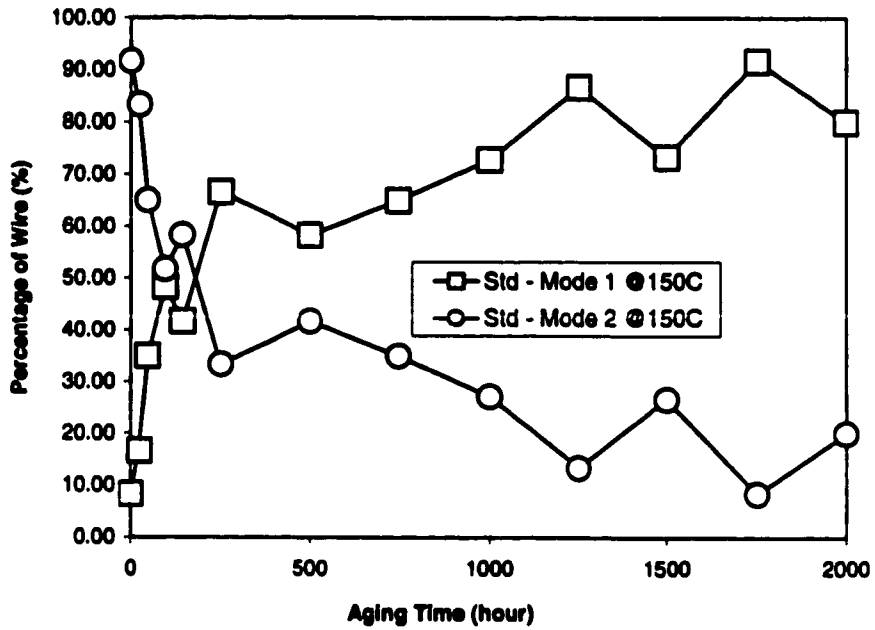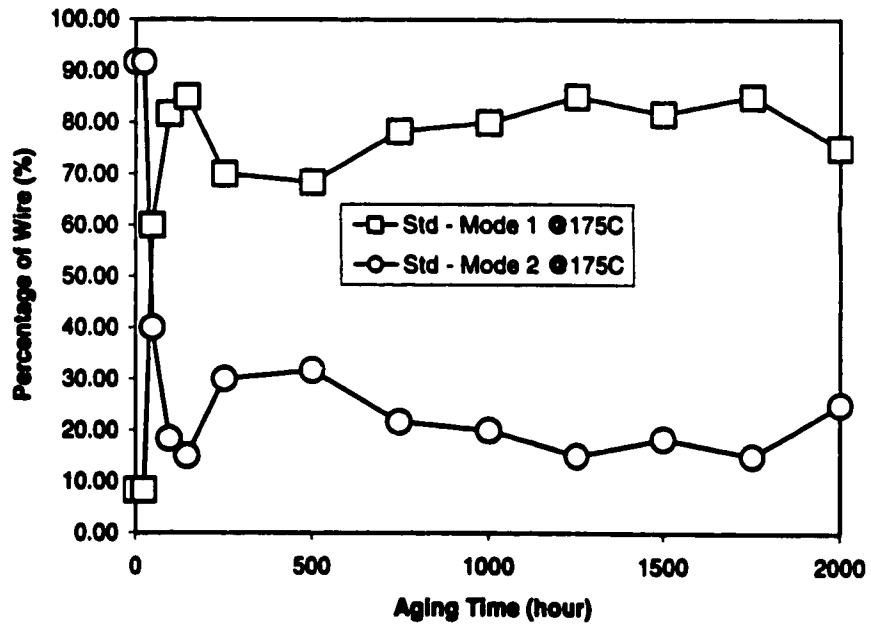
Figure 94. Failure mode of the ball shear test as a function of aging time for standard wirebonds aged at (a) 150°C and (b) 175°C.

described in Table 11. As shown in Figure 94(a) for standard wirebonds at 150°C, the frequency of Mode 1 Failure increased with aging time. In contrast, the frequency of Mode 2 Failure decreased as thermal aging proceeded. However, there were some fluctuations in the frequency along with aging time.

In the case of standard wirebonds aged at 175°C, the frequency of Mode 1 Failure gradually increased with aging time, as shown in Figure 94(b). Compared to standard wirebonds at 150°C, Mode 1 Failure was more frequent at the early stage of thermal aging. The frequency of Mode 2 Failure gradually decreased with aging time in an asymptotic manner. Similar to the case of standard wirebonds at 150°C, the frequencies of the two failure modes for standard wirebonds at 175°C fluctuated during the aging process. Overall, Mode 1 Failure was more frequent in both sets of standard wirebonds aged at 150°C and 175°C.

The average shear strengths of encapsulated wirebonds, aged at 150°C and 175°C, were also plotted as a function of aging time in Figure 95. As observed in standard wirebonds, the mean shear strength of encapsulated wirebonds rapidly increased at the beginning of thermal aging, at both temperatures. Some fluctuations in the average shear strength values were observed along with aging time, however, one standard deviation ($\pm\sigma$) scatter bands indicated that the shear strength slightly increased as thermal aging proceeded up to 2,000 hours. As shown in Figure 95, the mean shear strengths of encapsulated wirebonds aged at 175°C were greater than those for the wirebonds aged at 150°C at all aging times. Results from t-test at 95% confidence level and ANOVA (analysis of variance) revealed that two sets of the shear strength data for encapsulated

wirebonds were significantly different from each other at every aging time except 2,000 hours. At 2,000 hours aging time, there was a slight decrease in the shear strength of the wirebonds aged at 175°C, and a slight increase in the shear strength of these aged at 150°C. The higher aging temperature, 175°C, resulted in greater shear strengths. This was indicative of the effect of high temperature on the formation and growth of intermetallic compounds, which are directly related to bond quality.
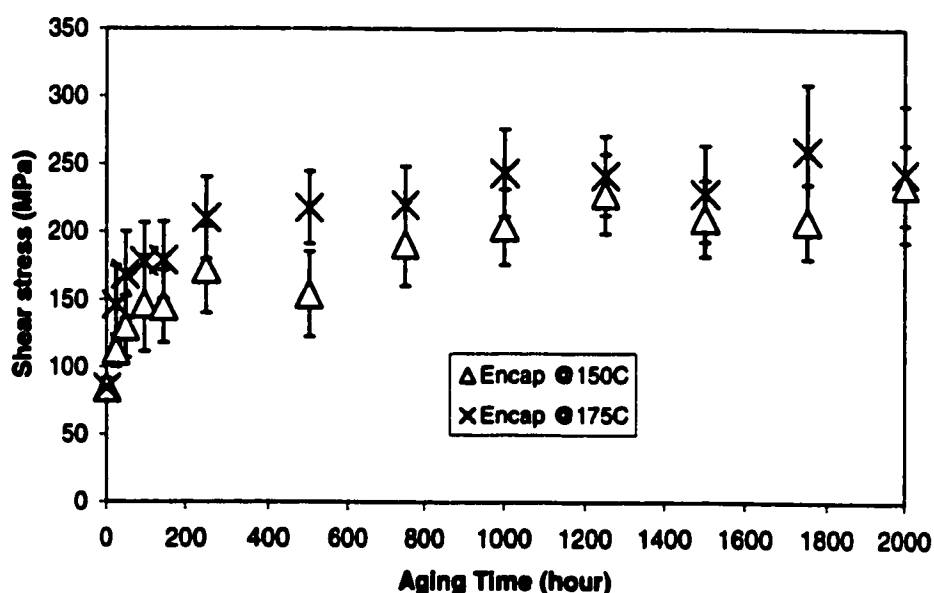
Figure 95. Shear strength as a function of aging time for encapsulated wirebonds aged at two different temperatures, 150°C and 175°C.

Failure modes of the ball shear test for encapsulated wirebonds were examined and assigned based on the criteria summarized in Table 11. As in the case of standard wirebonds, Mode 1 and 2 Failures were found for both sets of encapsulated wirebonds aged at 150°C and 175°C. The results are shown in Figures 96(a) and (b).
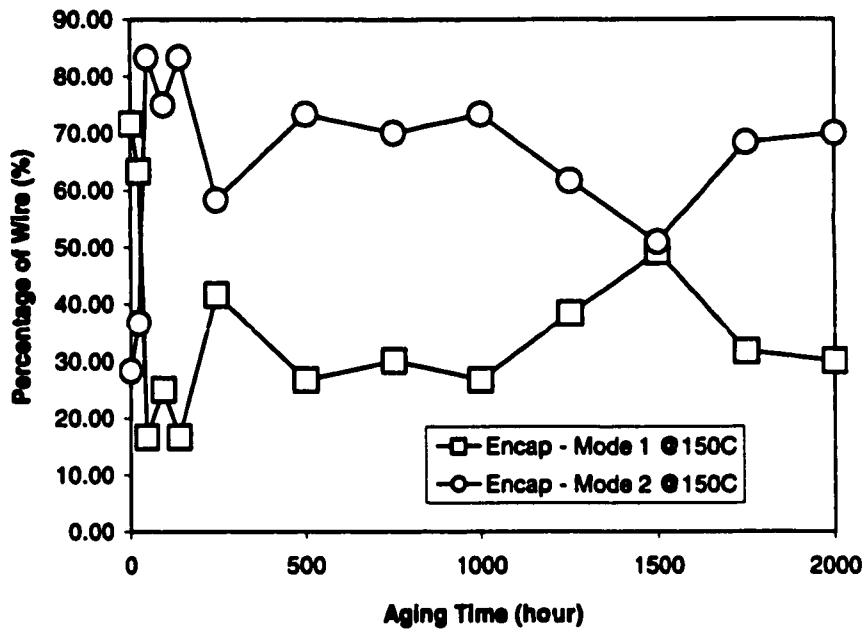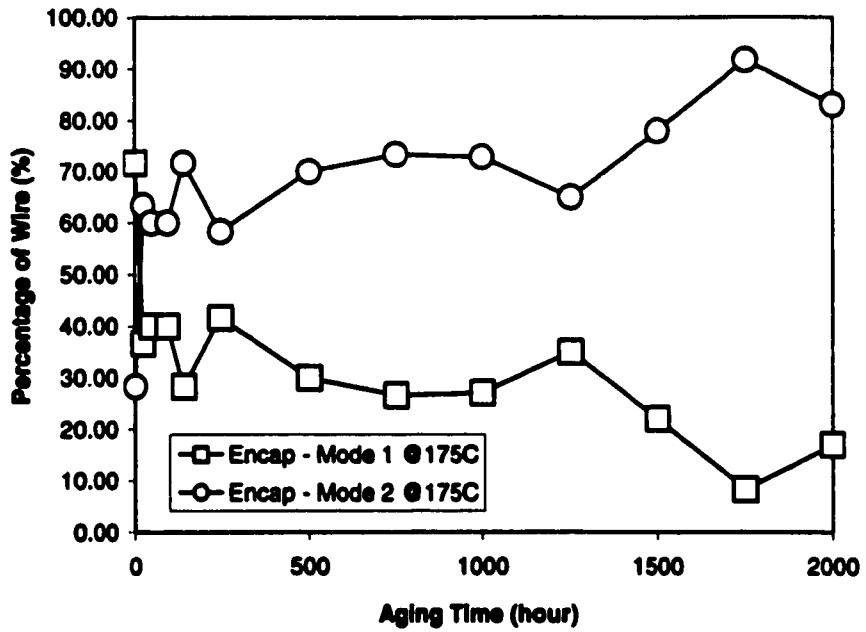
Figure 96. Failure mode of the ball shear test as a function of aging time for encapsulated wirebonds aged at (a) 150°C and (b) 175°C.

The frequencies of Mode 1 and 2 Failures observed in the wirebonds aged at 150°C fluctuated along with aging time, as shown in Figure 96(a). Mode 1 Failure was more frequent at the beginning of the shear test. However, the frequency decreased with increase in aging time. The frequency of Mode 2 Failure increased rapidly after 24 hours of aging and started decreasing after 144 hours. Since there were wide variations in the frequency, no general trend could be discerned.

In the case of encapsulated wirebonds aged at 175°C, the frequency of Mode 1 Failure decreased with aging time in general, as illustrated in Figure 96(b). In contrast, the frequency of Mode 2 Failure increased as thermal aging proceeded. Compared to the wirebonds at 150°C, these frequencies for Mode 1 and 2 Failures did not fluctuate greatly with aging time. Overall, Mode 2 Failure was observed more frequently in both sets of encapsulated wirebonds.

The shear strengths of standard and encapsulated wirebonds were also compared to each other at each aging temperature. For the comparison, the average shear strengths, with one standard deviation scatter bands, are plotted in Figures 97 and 98. For aging temperature of 150°C, standard wirebonds yielded greater shear strengths than encapsulated wirebonds. The shear strengths obtained from both types of wirebonds gradually increased as thermal aging process continued. More rapid changes in the shear strength were found at the beginning of thermal aging.

When 175°C was employed, a similar trend was observed. In both standard and encapsulated wirebonds, the shear strength increased with aging time, as shown in Figure 98. At aging times longer than 750 hours, the shear strength for standard wirebonds did
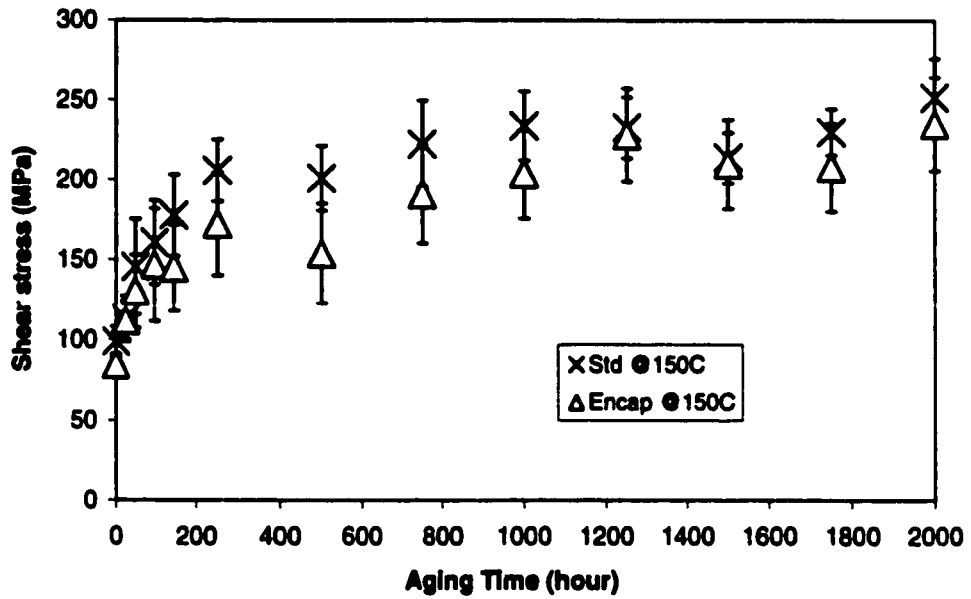
Figure 97. Comparison of the shear strengths between standard and encapsulated wirebonds aged at 150°C.
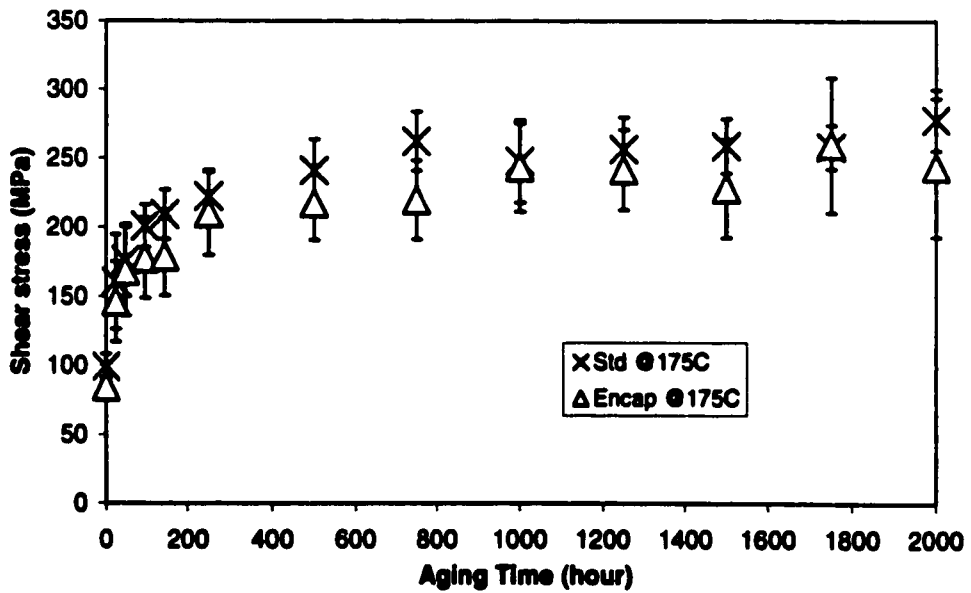
Figure 98. Comparison of the shear strengths between standard and encapsulated wirebonds aged at 175°C.

not vary greatly with aging time. However, the shear strengths for encapsulated wirebonds fluctuated statistically after passing 750 hours. The standard wirebonds had greater shear strengths.

5.3.4.2 Specific Shear Failure Modes

As discussed in Section 5.3.4.1, standard and encapsulated wirebonds at both thermal aging temperatures yielded two different ball shear failure modes, Failure Modes 1 and 2, based on Table 11. These failure modes were either ball lifting, i.e., shearing at the interface between Au ball and Al bond pad without leaving any Au residue on the bond pad, or ball shearing, i.e., shearing through the Au ball leaving Au residue on the bond pad. Since these standard failure modes do not give details about the exact shear planes related to the alloying reaction at the bond interface, the failure modes observed in standard and encapsulated wirebonds were sorted out based on the criteria described in Table 16. These criteria for the specific failure modes were based on the suggestion made by Selvaduray.[33]

Table 16. Specific ball shear failure modes based on the suggestion made by Selvaduray[33].

Shear Failure Mode	Residue on Al Bond Pad
A	Au only
B	Au + Intermetallic compounds
C	Intermetallic compounds only
D	Intermetallic compounds + Al
E	Al only

Representative micrographs for each failure mode, taken with an optical microscope, are shown in Figures 99 through 103. As shown in Figure 99, Mode A

Figure 99. Shear Mode A Failure.

Figure 100. Shear Mode B Failure.
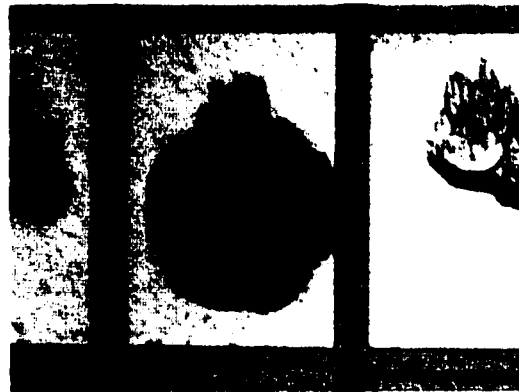
Figure 101. Shear Mode C Failure.

(a)
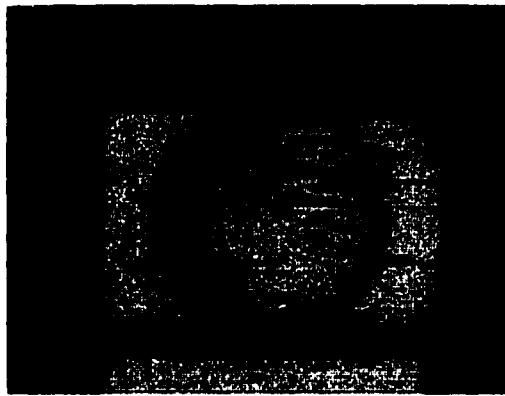
(b)
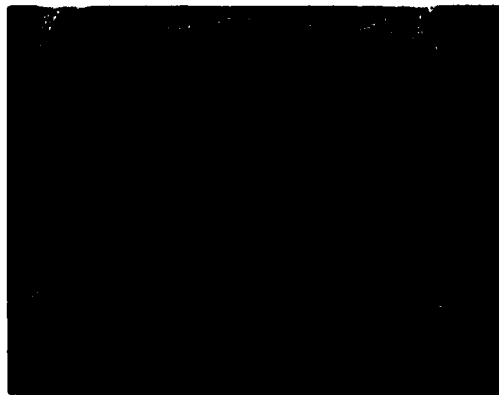
(c)

Figure 102. Shear Mode D Failure: (a) right after bonding and early stage of thermal aging, (b) after prolonged aging, and (c) corresponding SEM micrograph for (b) showing a depth difference.

(a)
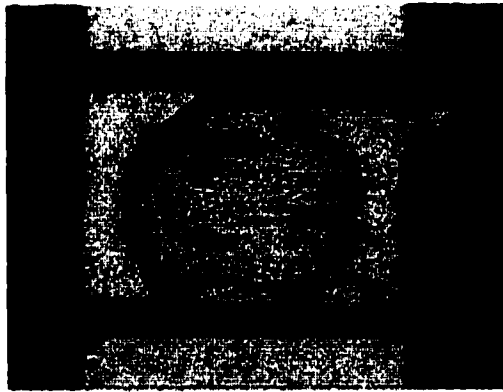
(b)
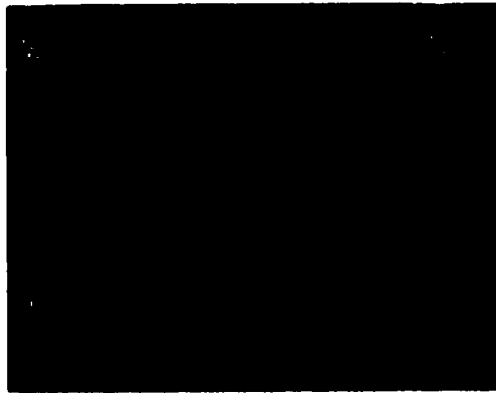
(c)

Figure 103. Shear Mode E Failure: (a) right after bonding and in early stage of thermal aging, (b) after prolonged aging, and (c) corresponding SEM micrograph for (b) showing a depth difference.

174

Failure was assigned when the shear occurred through the Au ball. This failure mode was easily distinguished due to the typical color of the Au ball. Figure 100 is the picture of Mode B Failure, showing the shear plane through mixed Au and the intermetallic phase. The intermetallic compounds in Figure 100 appeared in blackish color. They were assumed to be Au-Al intermetallic compounds due to the rough texture and color differentiated from both Al and Au. EDX analysis, performed on the dark region, confirmed the presence of the intermetallic compounds. Mode C Failure occurred when the ball bond was completely sheared through the intermetallic compounds at the bond interface. This failure mode, shown in Figure 101, was not observed during the shear test; however, it was found during the bond pull test of some degraded bonds, which specifically yielded Mode 1 Failure, i.e., ball lifting. Mode D Failure was assigned when the shear occurred through the plane of mixed Al and the intermetallic compounds. This failure mode is illustrated in Figures 102(a) through (c). As can be seen in Figures 102(a) through (c), a small amount of the intermetallic compounds was left on the Al bond pad after the shear test. The appearance of this failure mode could be either of Figure 102(a) or Figure 102(b) depending on when the ball was shear tested. When the wire ball was shear tested right after bonding or in early stage of thermal aging, the bond pad appeared similar to Figure 102(a). When the shear test was carried out on the balls after prolonged thermal aging, the bond pad was observed similar to Figure 102(b). The corresponding SEM micrograph for Figure 102(b), is shown in Figure 102(c). Comparison between Figures 102(b) and 102(c) revealed that there was a depth difference between Al bond pads of wirebonds, which were shear tested before and after longer hours of thermal

aging. This indicated that the actual shearing occurred through Al metal of the bond pad even when a significant amount of intermetallic compounds formed at the bond interface. However, Mode D Failure was not frequently observed in both types of wirebonds in this study. Mode E Failure indicates complete shearing through the interface of the Au ball and the Al metal of the bond pad without leaving Au and intermetallic compound residues on the bond pad. This failure mode was assigned when only Al was left on the bond pad after shearing the ball bond, as shown in Figures 103(a) through (c). This failure mode corresponds to Mode 1 Failure, which is used as the standard shear failure mode in the industry. However, Mode 1 Failure is more focused on the ball lifting, which occurs when there is a lack of intermetallic compounds formed at the bond interface or there exists bond degradation due to Kirkendall voids or cracks on the bond area.[3] This failure mode might be used more properly for the evaluation of bondability during the wire bonding process. Mode E Failure, as shown in Figure 103(a), is considered similar to Mode 1 Failure. Mode E Failure was observed in wirebonds, which were shear tested right after bonding or after thermal aging for a short period of time. However, the appearance of Al bond pads of wirebonds, which were shear tested after prolonged thermal aging, was slightly different, as shown in Figures 103(b) and (c). As noticed in the case of Mode D Failure, there was a depth difference in the Al metal of the bond pad. This indicated that the actual shearing occurred through non-reacted Al metal underneath the Au-Al ball bond. This was indicative of the strong link between the Au ball and the intermetallic compound layers. In addition, the weak link between the intermetallic layers and Al metal on the bottom of the bond pad was shown. It seemed

that this failure mode occurred even though a significant amount of the intermetallic compounds formed at the bond interface. Based on the criteria for the standard shear failure modes used in industry, as described in Table 11, Mode E and F Failures correspond to Mode 1 Failure. Mode A to C Failures seem to adequately fit in Mode 2 Failure.

Standard and encapsulated wirebonds, which were thermally aged at two different temperatures, 150°C and 175°C, for various times, were sorted out based on the specific shear failure modes A to E and plotted in Figures 104(a) through 107(a). The corresponding average shear strengths for each failure mode were also sorted out and plotted as a function of aging time in Figures 104(b) through 107(b).

As shown in Figure 104(a) for standard wirebonds aged at 150°C, four different specific failure modes were observed. Mode A Failure was the major failure mode obtained from standard wirebonds, which were shear tested right after bonding. The frequency of this failure mode started decreasing as aging proceeded. Mode A Failure disappeared after 144 hours of thermal aging. It was thought that this might have occurred due to the significant amount of the intermetallic compounds formed on the bond area. Mode B Failure appeared when standard wirebonds were thermally aged for 96 hours. The frequency of Mode B Failure increased with aging time. Mode C Failure, i.e., shearing through the intermetallic phase only, was not observed in standard wirebonds aged at 150°C, as examined in Figure 104(a). Mode D Failure appeared in the time interval between 500 and 1,250 hours. Mode E Failure was observed right after bonding and became more frequent as the thermal aging process continued. Prolonged
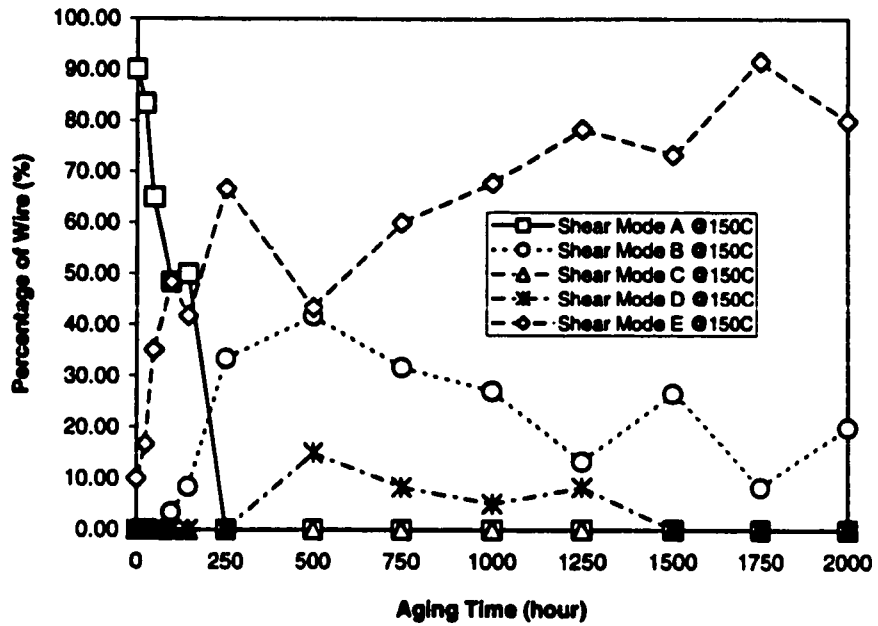
(a)
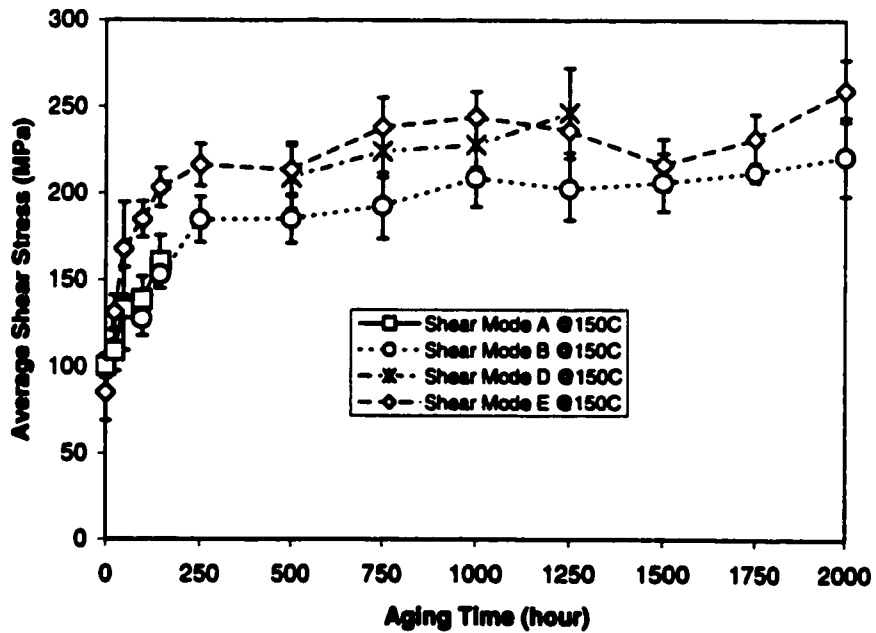
(b)

Figure 104. Frequency of shear failure mode (a) and corresponding shear strength for each mode (b) for standard wirebonds aged at 150°C for various times.

thermal aging at 150°C increased the frequency of Mode E Failure but decreased the frequency of Mode B Failure. Mode A Failure disappeared.

Overall, Mode B and E Failures were the primary shear modes observed in the standard wirebonds, aged at 150°C for longer than 250 hours. These failure modes were more obvious at longer aging times. At the early stage of thermal aging between 0 hour, i.e., right after bonding, and 96 hours, Mode A Failure was found to be the major shear failure mode.

The average shear strengths for each failure mode, observed in standard wirebonds at 150°C, were obtained and plotted as a function of aging time in Figure 104(b). The shear strengths for all failure modes increased with aging time. Mode E Failure had the highest strengths in general. However, immediately after bonding, it was found that the mean shear strength for Mode A Failure was greater than that for Mode E Failure. This indirectly indicated that Mode E Failure at this time point was due to ball lift, which is usually observed when there is very little intermetallic compound formation at the bond interface. Once thermal aging started, greater shear strengths were obtained from standard wirebonds, resulting in Mode E Failure rather than Mode A Failure.

A similar trend was found between Mode B and E Failures, at longer aging times. The mean shear strengths corresponding to Mode E Failure were still greater than the strengths for Mode B Failure. It was found that Mode E Failure observed during thermal aging was not arisen from the ball lifting. Cross-sections of standard wirebonds during the thermal aging, as shown in Figures 78(a) through (d), support this observation, since there was a significant amount of the intermetallic compounds formed at the bond

interface. As compared between Figures 103(a) and (b), the appearance of Mode E Failure, from standard wirebonds right after bonding, was different from that of the wirebonds which were thermally aged at 150°C. There was a depth difference in the Al bond pad. As discussed earlier, EDX analysis confirmed that Al was not completely consumed after 2,000 hours of thermal aging. Based on this observation, it was thought that the actual shear occurred through the Al metal under the ball bond since Al was the weakest link in the bond and Au was the next.[16]

As seen in Figures 102(a) through (c), Mode D Failure with a small amount of the intermetallic phases was very similar to Mode E Failure, in the appearance of the bond pad after shearing. However, the average shear strengths for Mode D Failure were somewhat lower than those for Mode E Failure, as shown in Figure 102(b). Overall, the shear strength for Mode E Failure was the greatest, followed by Mode D Failure, and Mode A and B Failures, in that order.

When standard wirebonds were aged at 175°C and shear tested, four different failure modes were observed, as shown in Figure 105(a). As was the case with the standard wirebonds aged at 150°C, Mode E Failure was the most frequent. The frequency of this failure mode increased with aging time. Compared to the standard wirebonds aged at 150°C, the wirebonds aged at 175°C had higher frequency of Mode E Failure.

The frequency of Mode A Failure started decreasing, and disappeared after 48 hours. Mode B Failure became less frequent as thermal aging proceeded. None of the

wirebonds displayed Mode C Failure. Mode D Failure occurred rather infrequently after 250 hours of aging.

The corresponding average shear strengths of each failure mode for standard wirebonds aged at 175°C are shown in Figure 105(b). The overall trend was very similar to the trend observed in standard wirebonds aged at 150°C. The average shear strength for Mode E Failure was the greatest at all aging times. As aging proceeded, this strength gradually increased. It was found that Failure Mode E was not caused by the lack of the intermetallic compounds present at the bond interface. This might be related to the non-reacted Al metal remaining in the bond pad since a significant amount of intermetallic compounds formed, as was reported in Sections 5.3.2.2 and 5.3.2.3. EDX analysis carried out for Mode E Failure also confirmed the presence of Al on the bond pad after shear.

In the case of Mode D Failure, the average shear strengths were not significantly different from those for Mode E Failure. The strength for Mode D Failure also increased with aging time. The average shear strengths for Mode A and B Failures were less than those for Mode D and E Failures. As aging time increased, the shear strength values for Mode A and B Failures gradually increased. However, the average strengths for Mode A Failure were less than the strengths for Mode B Failure at the beginning of thermal aging at 175°C. When the aging time exceeded 24 hours, the shear strengths for both failure modes were found not to be statistically different.

The specific failure mode changes in encapsulated wirebonds aged at 150°C can be seen in Figure 106(a). The frequency of Mode A Failure increased up to 48 hour
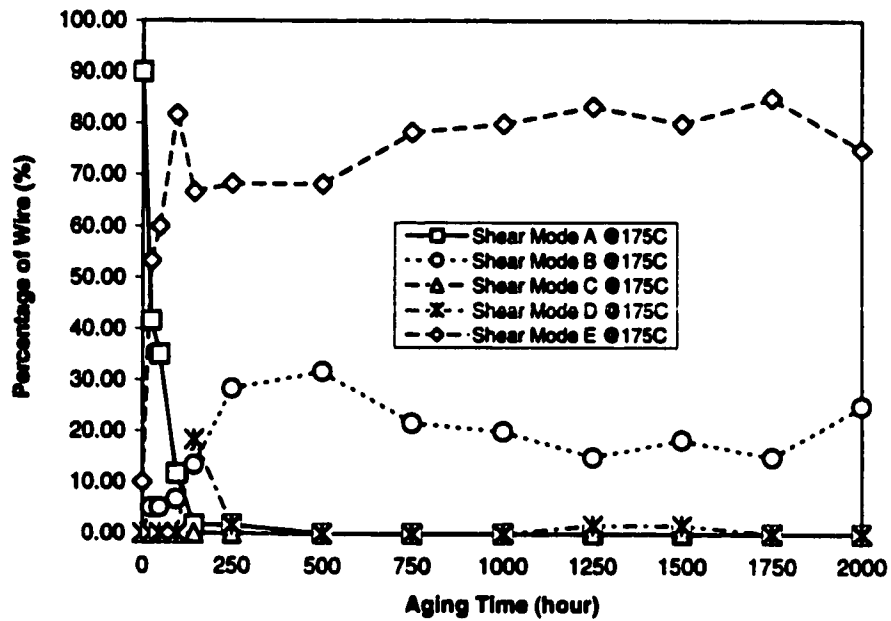
(a)
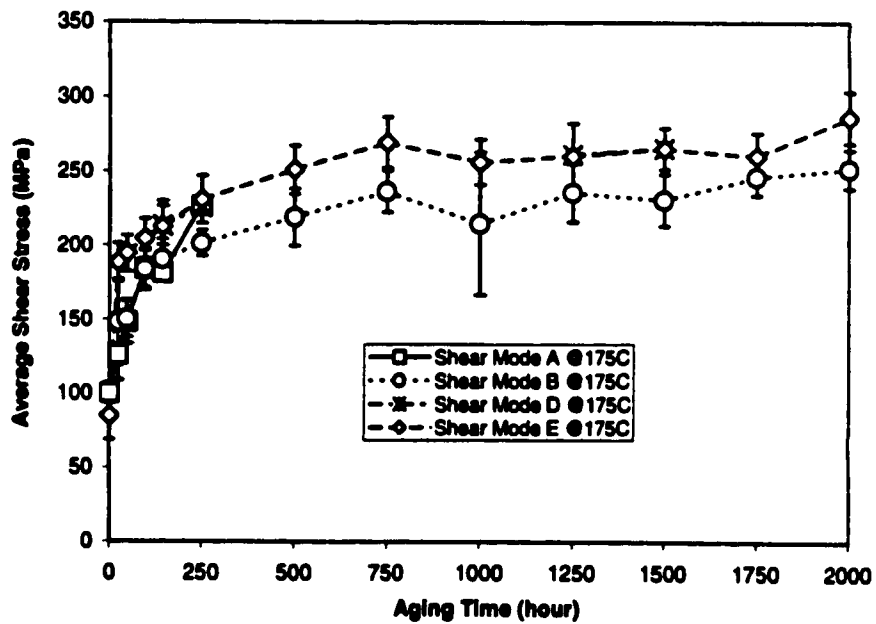
(b)

Figure 105. Frequency of shear failure mode (a) and the corresponding shear strengths for each failure mode (b) for standard wirebonds aged at 175°C for various times.

aging time points and started decreasing and finally disappeared after 250 hours of aging. This failure mode was the most frequent when aging time was 48 hours. In general, Mode B Failure was the most frequently observed in encapsulated wirebonds during the aging process at 150°C. This was not the case for the standard wirebonds, which had Mode E Failure as the most frequent failure mode. The frequency of Mode B Failure increased with aging time. Mode C Failure, i.e., shearing through the intermetallic compounds, was not observed at all. Mode D Failure was seldom seen. Mode E Failure consisted of 100% of the failure modes observed in encapsulated wirebonds right after bonding. The frequency of Mode E Failure decreased when aged for up to 48 hours and started increasing as thermal aging continued. It is thought that ball lifting caused the frequency drop shown in the early stage of thermal aging. This indicated insufficient amount of the intermetallic compounds formed at the bond interface. Mode E Failure, observed in the latter stage of thermal aging, might be due to the non-consumed Al metal, which remained underneath the ball bond in the bond pad.

The average shear strengths corresponding to each failure mode, for encapsulated wirebonds at 150°C, are shown in Figure 106(b). As was observed for standard wirebonds at both temperatures, encapsulated wirebonds with Mode E Failure showed the greatest shear strengths along with aging time. However, at 24 hour time point, the average strength for Mode E Failure was less than that for Mode A Failure. This confirmed that Mode E Failure was caused by ball lifting at this time point. The average shear strengths for Mode A and B Failures increased with aging time. The strengths were
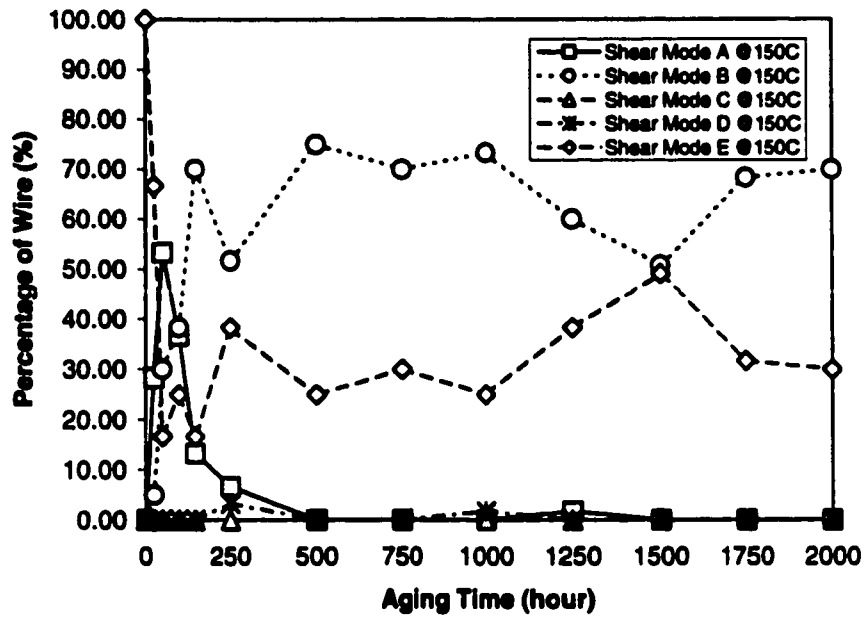
(a)

(b)

Figure 106. Frequency of shear failure mode (a) and the corresponding shear strengths for each failure mode (b) for encapsulated wirebonds aged at 150°C for various times.

not significantly different from those for Mode B Failure when aged for longer than 24 hours. In the case of Mode D Failure, it was found that the average shear strengths were not statistically different from the strengths for Mode E Failure, as can be seen in Figure 106(b).

The frequency of the specific shear failure modes and corresponding average shear strengths for encapsulated wirebonds aged at 175°C are shown in Figures 107(a) and (b). Mode B Failure was the most frequent failure mode similar to encapsulated wirebonds aged at 150°C. Mode A Failure appeared at the 24 hour time point and started decreasing with aging time. After 96 hours of aging, Mode A Failure completely disappeared. The frequency of Mode B Failure increased with aging time. Mode C Failure was not observed at all in the wirebonds. As observed in other sets of wirebonds discussed previously, Mode D Failure occurred occasionally, but was not frequent in general. The frequency of Mode E Failure dropped from 100% to approximately 13% upon the thermal aging at 175°C. This drop was more rapid compared to the frequency change observed in encapsulated wirebonds at 150°C, as shown in Figure 106(a). This might be due to the significant amount of the intermetallic compounds that are expected to be formed at the bond interface. This was confirmed by the data obtained from the lifted balls shown in Figure 50. As aging time increased, the frequency of Mode E Failure increased up to 250 hour time points and started decreasing as thermal aging proceeded.

Overall, the mean shear strengths for all failure modes, observed in encapsulated wirebonds at 175°C, increased with aging time, as shown in Figure 107(b). Compared to
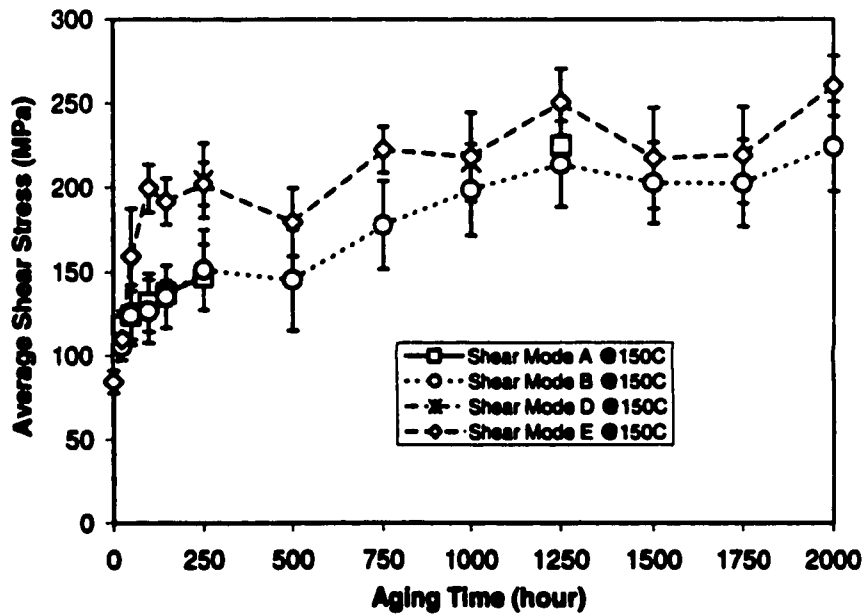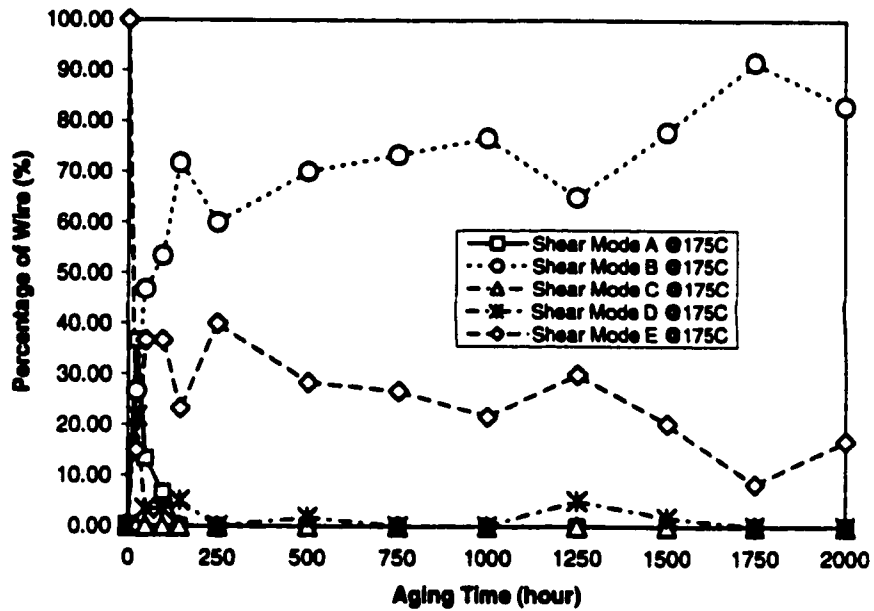
Figure 107. Frequency of shear failure mode (a) and the corresponding shear strengths for each failure mode (b) for encapsulated wirebonds aged at 175°C for various times.
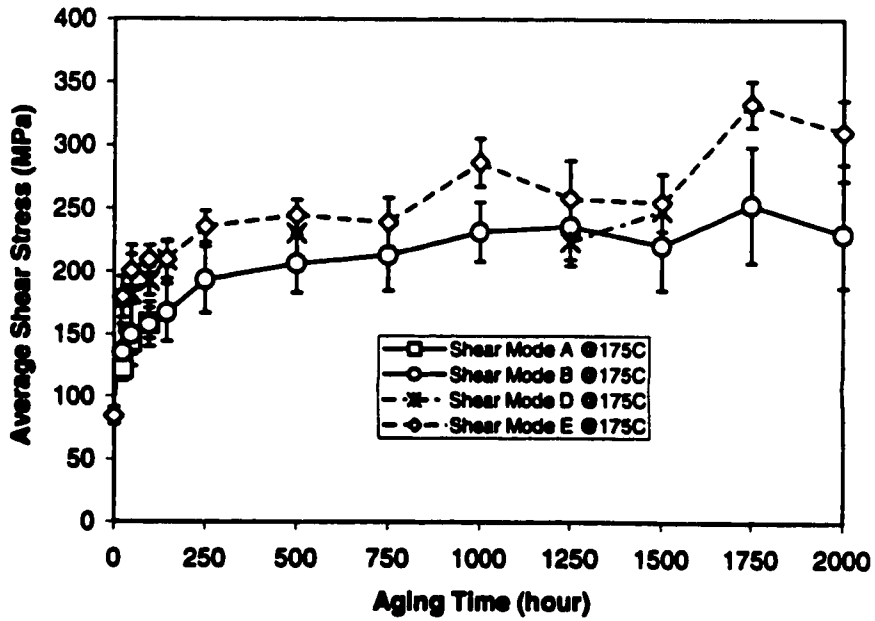
encapsulated wirebonds at 150°C, the mean shear strengths were greater at 175°C. The shear strengths for Mode A and B Failures were not significantly different from each other when the wirebonds were aged for time periods up to 96 hours. The average shear strength for Mode B Failure gradually increased with aging time. The strengths for Mode D Failure were found to be similar to those for Mode E Failure. Mode E Failure yielded the greatest shear strengths at all aging times. Even though the frequency of Mode E Failure was lower than that of Mode B Failure along with aging time, the average shear strengths for Mode E Failure were greater than those for Mode B Failure. Further, the average shear strengths for Mode E Failure increased as thermal aging continued.

So far, the specific shear failure modes and corresponding shear strengths were discussed for both standard and encapsulated wirebonds aged at two temperatures, 150°C and 175°C. Some general trends were found in standard wirebonds aged at the two aging temperatures. Mode A Failure appeared at the beginning of thermal aging. The frequency of Mode A Failure started decreasing with aging time. This failure mode disappeared after 250 hours of aging. Mode B Failure was the second most frequent shear failure mode observed in both sets of standard wirebonds at the two different temperatures. Mode B Failure became less frequent as aging time increased. Mode C Failure was not found at all. Mode D Failure was found at various aging times. However, no general trend could be observed due to the fluctuation observed in the low frequency. Mode E Failure was the most frequent during the aging processes and the frequency gradually increased with aging time.

Some variations in the frequencies of Mode B and E Failures were observed in encapsulated wirebonds, which were aged at the two different temperatures. Mode B Failure was the most frequent regardless of aging temperature. The frequency of Mode B Failure started increasing once thermal aging started. In the case of Mode E Failure, the frequency rapidly decreased and started increasing when thermal aging proceeded. The exact reason causing the deviations in the frequencies between Mode B and E Failures for standard and encapsulated wirebonds were not investigated. For Mode A, C, and D Failures, the trends shown in standard wirebonds were also observed in encapsulated wirebonds aged at 150°C and 175°C.

Regardless of aging temperature and the frequency for each failure mode, the same trends in the shear strength were obtained for both standard and encapsulated wirebonds. The average shear strength for Mode E Failure was the greatest once thermal aging started. The shear strengths for Mode D Failure were not significantly different from the strengths for Mode E Failure. It was also found that the strengths for Mode A and B Failures were not statistically different from each other.

5.3.4.3 Relationship between Shear Strength and Intermetallic Layer Thickness

Previous studies[22,23,25] indicated that the formation of a strong Au-Al bond was related to the intermetallic layers present at the bond interface. It was also reported that increase in the intermetallic bond area, thickness of the intermetallic layers, and consumption of the Al from the bond pad improved the shear strength.[22] Therefore, it was assumed that the shear strength of the ball bonds, which were under high temperature

heat treatment, would be proportional to the intermetallic layer thickness, the intermetallic ball area, or a combination of two.[25]

In order to investigate the relationship between the shear strength and the thickness of intermetallic layers formed at the bond interface, the shear strengths obtained for both standard and encapsulated wirebonds at the two aging temperatures were plotted as a function of the intermetallic layer thickness. The results for both standard and encapsulated wirebonds at two different aging temperatures, 150°C and 175°C, are shown in Figures 108 and 109, respectively. The data used for the plots were obtained from both types of wirebonds, which were thermally aged for various times, i.e., 500, 1000, 1500, and 2,000 hours. In addition, the shear strengths measured right after bonding and the intermetallic thickness obtained from both types of wirebonds aged at room temperature, were paired and plotted as the first points in Figures 108 and 109.

As shown in Figures 108(a) and (b) for standard wirebonds at 150°C and 175°C, respectively, the shear strength was proportional to the intermetallic layer thickness. The same observation was made for encapsulated wirebonds aged at 150°C and 175°C, as shown in Figures 109(a) and (b), respectively. It was found that the shear strength increased as the thickness of the intermetallic layers increased.

Based on the observation made on the figures, it was confirmed that increased thickness of the intermetallic layers gave greater shear strength. Further, it was thought that the change in the shear strength was diffusion controlled. Therefore, it was assumed that the shear strength would be proportional to the square root of aging time, $\sqrt{t}$, based
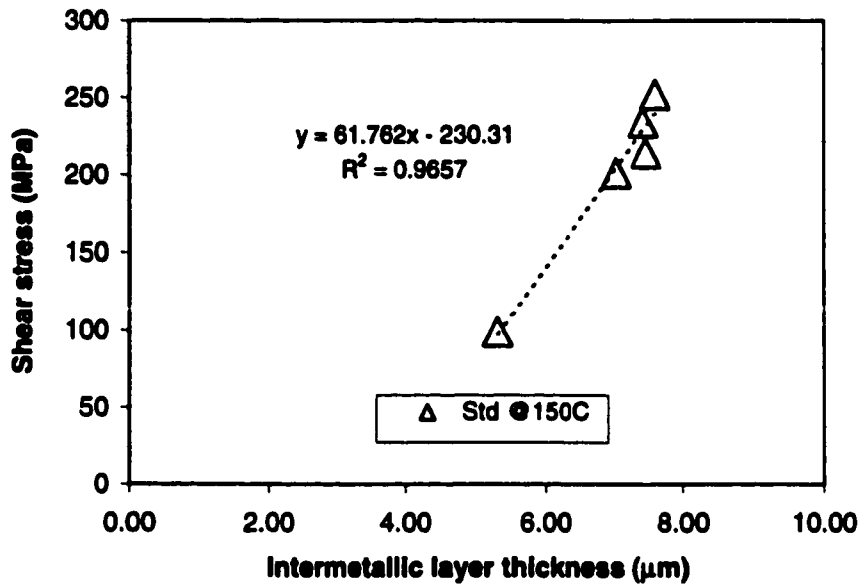
(a)
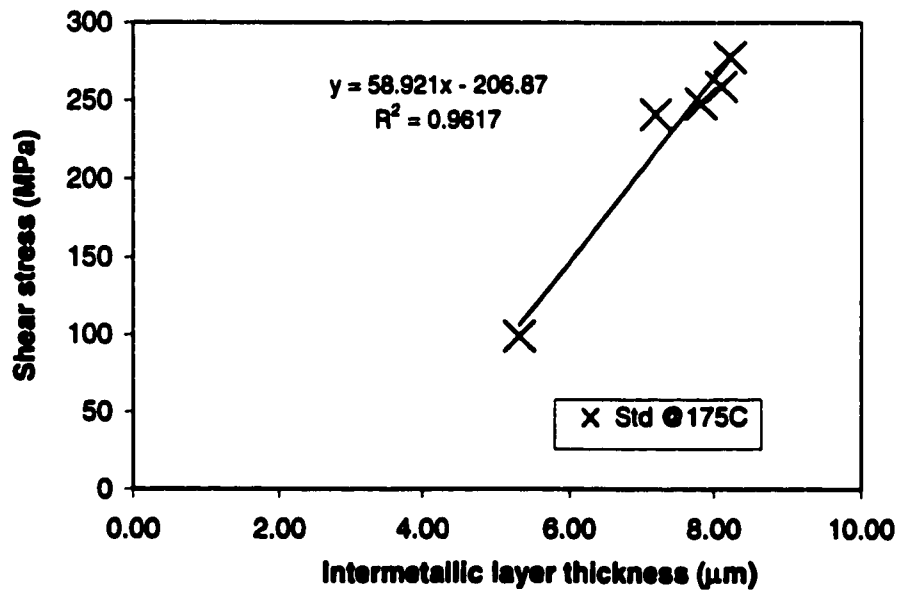
(b)

Figure 108. Shear strength as a function of intermetallic layer thickness for standard wirebonds aged at (a) 150°C and (b) 175°C.

(a)

(b)

Figure 109. Shear strength as a function of intermetallic layer thickness for encapsulated wirebonds aged at (a) 150°C and (b) 175°C.

on the diffusion equation,[5] $x = (Dt)^{1/2}$. However, no further investigation was carried out

to confirm the assumption, since it was beyond the scope of this project.
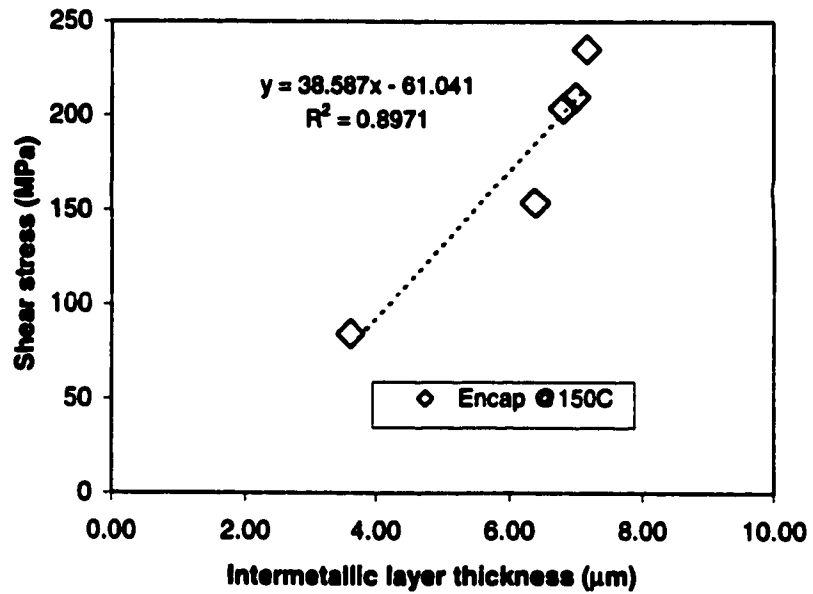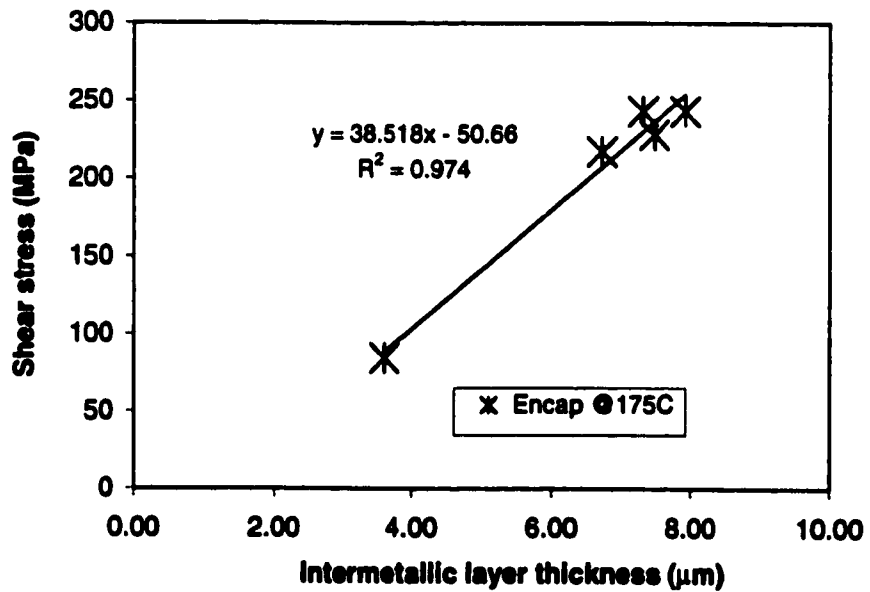
CHAPTER 6

Conclusion

This study has detailed the formation and growth of Au-Al intermetallic compounds in thermosonic Au wire - Al metallization wirebonding systems as related to the bond reliability merits for ultra fine pitch devices. The specimens used for the study were prepared by varying the bonding and thermal aging conditions.

Results of preliminary studies showed that bonding temperature and thermal aging temperature do have significant effects on the formation and growth of intermetallic compounds at the bond interface. It was also found that encapsulated wirebonds were comparable to standard wirebonds, based on the results obtained from mechanical strength measurements and metallographic examination.

From the extensive study, Experiment 5, it was found that the bond qualities for standard and encapsulated wirebonds were comparable to each other under prolonged thermal aging at 150°C and 175°C. Standard wirebonds were found to have a little faster lateral diffusion rate of Au-Al at the bond interface. The intermetallic layer thicknesses measured for both types of wirebonds were not statistically different. Activation energies for the growth of Au-Al intermetallic compounds in standard and encapsulated wirebonds were obtained as 9.71 kcal/mol (0.42 eV) and 6.20 kcal/mol (0.27 eV), respectively, based on the average intermetallic layer thicknesses. These activation energy values were much smaller than the values reported in the literature. EDX analyses done on the bond interface revealed that the Au-rich intermetallic phases were present across the interface regardless of the kind of wirebonding technique, aging temperature, and aging

time. The purple region observed around the bond periphery was identified as the Al-rich intermetallic phase, $AuAl_2$. These results were in good agreement with the results reported by previous researchers. Metallographic examinations employing cross-sectioning revealed that neither Kirkendall voids nor microcracks were present in all samples, regardless of aging temperature, time and the type of wirebonding technique. The pull strengths for both types of wirebonds decreased slightly with aging time, in an asymptotic manner. This observation was more obvious at the 175°C aging temperature. The shear strength was found to increase with aging time. In general, the shear strengths for standard wirebonds were greater than the strengths for encapsulated wirebonds.

Overall, temperature and time applied for thermal aging influenced the performance of wirebonds regardless of the kind of wirebonding technique. The formation and growth of the intermetallic compounds in Au-Al wirebonding systems are diffusion controlled.

CHAPTER 7

Recommendations for Future Research

The following studies are recommended to further improve the understanding of the formation and growth of Au-Al intermetallic compounds in both standard and encapsulated wireboding systems.

1) Store the wirebonds at two aging temperatures for various times. The time interval should be narrowed down for the early stage of intermetallic compound formation. Perform cross-section and measure the intermetallic layer thickness for the investigation of the diffusion kinetics.

2) Perform EDX on the bond interface increasing the number of linescans. This allows more detailed information about the specific intermetallic compounds, which are spread in various regions across the bond interface.

3) Etch the Al bond pad after the shear test and perform EDX on the etched bond pad to investigate the possible intermetallic phase which causes the bond failure during the shear test.

4) Increase the thermal aging time to longer than 2,000 hours at the two temperatures to investigate when both standard and encapsulated wirebonds start failing in the bond pull and ball shear tests in case lifetime of the wirebonded devices exceeds 2,000 hours.

Investigation into the above listed areas should provide insight into the formation and growth of Au-Al intermetallic compounds as related to the bond reliability in two

types of wirebonding systems. In addition, this might be helpful in clearly determining

which wirebonding technique works better for ultra fine pitch devices.

CHAPTER 8

References

1. Tummala, R., Rumaszewski, E., and Klopfenstein, A., Microelectronics Packaging Handbook, Part 2, Chapman & Hall, (1997), pp. 25-56.

2. ASM International, Electronic Materials Handbook, volume 1: Packaging, ASM, (1989), pp. 224-236.

3. Harman, G., Wire Bonding in Microelectronics Materials, Processes, Reliability, and Yield, McGraw-Hill Publishers, second edition, (1997), pp. 11-30, 67-107, 115-129.

4. Song, J., Prabhu A., Singh, I., Nguyen, L., and Selvaduray, G., "Wirebond Integrity for Ultra Fine Pitch Devices", Int. Symp. On Microelectronics (IMAPS '99), Chicago, October 26-28 (1999).

5. Reed-Hill, R. and Abbaschian, R., Physical Metallurgy Principles, PWS Publishing Company, third edition, (1994), p. 272.

6. Shewmon, P., Diffusion in Solids, McGraw-Hill, New York, (1963), pp. 40-83, 115-135.

7. Porter, D.A. and Easterling, K.E., Phase Transformations in Metals and Alloys, Chapman & Hall, second edition, (1992), pp. 27, 60-106.

8. DeHoff, R., Thermodynamics in Materials Science, McGraw-Hill, New York, (1993), pp. 160-203.

9. Hansen, M., The Constitution of Binary Phase Diagrams, McGraw-Hill Publishers, second edition, (1958), pp. 68-70.

10. Majni, G., Nobili, C., Ottaviani, G., and Costato, M., "Gold-Aluminum Thin-Film Interactions and Compound Formation", Journal of Applied Physics, Vol. 52, No. 6, (June 1981), pp. 4047-4054.

11. Kashiwabara, M. and Hattori, S., "Formation of Al-Au intermetallic compounds and resistance increase for ultrasonic Al wire bonding", Rev. Elec. Commun. Lab., Vol. 17, No. 9, (September 1969), pp. 1001-1013.

12. Philofsky, E., "Intermetallic Formation in Gold-Aluminum Systems", Solid State Electronics, Vol. 13, No. 10, (October 1970), pp. 1391-1399.

13. Bernstein, L., Semicond. Prod., Vol. 34 (1959).

14. Selikson, B. and Longo, T.A., Proceedings IEEE , Vol. 52, (1964), p. 1683.

15. Cunningham, J.A., Solid-State Electronics, Vol. 8, (1965), p. 735.

16. Blech, I.A. and Sello, H., Journal of the Electrochemical Society, Vol. 113, (1966), p. 1052.

17. Browning, G.V., Colteryahn, L.E., and Cummings, D.G., Physics of Failure in Electronics, Vol. 4, RADC (1964), p. 428.

18. Sinha, A. K., "Intermetallic Compound Formation in Au-Al Bonding System", Journal of Electochemical Society India, Vol. 26, No. 2, (April 1977), pp. 15-18.

19. Galli, E., Majni, G., Nobili, C., and Ottaviani, G., "Gold-aluminum intermetallic compound formation", Electrocomponent Science and Technology, Vol. 6, No. 3-4, (August 1980), pp. 147-150.

20. Campisano, S. U., Chang, C. T., Giudice, A. L. O., and Rimini, E., "Ion-beam mixing in Au-Al thin film bilayers", Proceedings of the Third International Conference on Ion Beam Modification of Materials, Grenoble, France, September 6-10, (1982), pp. 139-145.

21. Kato, H., "Formation of intermetallic compounds in Al thin films vapor-deposited on Au plate", Japanese Journal of Applied Physics, Part 1, Vol. 26, No. 10, (October 1987), pp. 1786-1790.

22. Ramsey, T., Alfaro, C., and Dowell, H., "Metallurgy's Part in Gold Ball Bonding", Semiconductor International, Vol. 14, No. 5, (April 1991), pp. 98-102.

23. Carrass, A. and Jaecklin, V.P., "Analytical Methods to Characterise the Interconnection Quality of Gold Ball Bonds", Proceedings of EuPac'96, 2nd European Conference on Electronic Packaging Technology and 8th International Conference on Interconnection Technology in Electronics, Essen, Germany, (January 31-February 2, 1996), pp. 135-139.

24. Trigwell, S., Selvaduray, G., and Singh, A., "Effects of Intermetallic Compound Formation on the Electrical Performance of Wirebonded Interconnets", The International Journal of Microcircuits and Electronic Packaging, Vol. 19, No. 1, (First Quarter 1996), pp. 14-21.

25. Charles, H. K. and Clatterbaugh, G. V., "Ball Bond Shearing – A Complement to the Wire Bond Pull Test", Proceedings of International Microelectronics Symposium, November, (1983), pp. 171-186.

26. Chen, G. K. C., "On the Physics of Purple-Plague Formation, and the Observation of Purple Plague in Ultrasonically-Joined Gold-Aluminum Bonds", IEEE Transactions on Parts, Materials and Packaging, Vol. PMP-3, No. 4, (December 1967), pp. 149-153.

27. Gerling, W., "Electrical and Physical Characterization of Gold-Ball Bonds on Aluminum Layers", IEEE ECC, New Orleans, Louisiana, May 14-16, (1984), pp. 13-20.

28. Azamawari, K., Shimada, Y., Shibayama, Y., Maki, N., and Matsumoto, H., "Au-Al bond degradation mechanism and the analysis with infrared microscope", International Symposium for Testing and Failure Analysis (ISTFA), Los Angeles, November 6-10, (1989), pp. 15-19.

29. Kato, H., "Volume change due to intermetallic compound formation at the Al-Au bond in semiconductor devices", Japanese Journal of Applied Physics, Part 1, Vol. 25, No. 6, (June 1986), pp. 934-935.

30. JEDEC Standards, JESD22-B116

31. MIL-STD-883E Method 2011.7, (March 1989).

32. National Semiconductor Corporation, "Failure Analysis Specification for Metal Etch", Santa Clara, California, (1991).

33. Selvaduray, G., Professor, Department of Chemical and Materials Engineering, San Jose State University, San Jose, California, Personal Communication, (November 1999).

APPENDIX

Calculation of Thermal Activation Energy

In order to determine the thermal activation energy for the growth of Au-Al intermetallic compounds in standard and encapsulated wirebonds, Arrhenius rate equation, Equation (2), was used.

$$K = C \exp(-E/kT) \tag{2}$$

where K is the growth rate constant, C is a constant, E is the activation energy for the intermetallic compound growth, k is Boltzmann's constant (R/N_a, where R is gas constant and N_a is Avogardro's number), and T is the absolute temperature in K. Changing from atomic to molar quantities enables this equation to be written as follows.

$$K = C \exp(-E/RT) \tag{a}$$

Equation (a) can be rewritten changing the both sides of Equation (a) to log, and written as

$$\ln(K) = \ln(C) + (-E/R)(1/T) \tag{b}$$

According to Equation (b), activation energy, E, can be obtained by plotting ln(K) as a function of (1/T). The slope, obtained from the graph of ln(K) as a function of (1/T), equals to (-E/R). Multiplying the slope by (-R) gives E.

From Figure 73, the graph of intermetallic layer thickness as a function of the square root of aging time for standard wirebonds, the growth rates are found to be 0.0241 $\mu m/(hr)^{1/2}$ and 0.0459 $\mu m/(hr)^{1/2}$ for 150°C and 175°C, respectively. These growth rates, K, and thermal aging temperatures, T, are plugged in Equation (b). ln(K) values are plotted as a function of (1/T), as shown in Figure 75. From Figure 75, -4.89 × 10^3 and

7.82 are obtained as the slope and y-intercept, respectively. Multiplying the slope, -4.89 × 10^3, by (-R), -8.31 J/mol/K, results in 40.6 kJ/mol as activation energy. This energy value is converted to 9.71 kcal/mol and 0.422 eV, using conversion factors (1 J = 4.184 cal and 1 eV = 1.6 × 10^{-19} J). According to Equation (b), ln(C) equals to the y-intercept, 7.82. Therefore, C = exp (7.82) = 2.50 × 10^3. Substituting E and C values into Equation (a) yields an Arrhenius relationship for standard wirebonds aged at 150°C and 175°C. Therefore, the Arrhenius rate equation is written as follows.

$$\text{Growth rate, } K = 2.50 \times 10^3 \exp(-9,711/RT) \ \mu m/(hr)^{1/2} \qquad (4)$$

Following the same steps used for standard wirebonds, an Arrhenius rate equation for encapsulated wirebonds, aged at 150°C and 175°C, is obtained as follows.

$$\text{Growth rate, } K = 62.7 \exp(-6,196/RT) \ \mu m/(hr)^{1/2} \qquad (5)$$